UNIVERSITY OF THESSALY
DEPARTMENT OF MECHANICAL ENGINEERING

M. Sc. Thesis

On the motion of charged particles subject to random forces and fields

SARANTIS PANTAZIS

Submitted for the partial fulfilment of the requirements
for the M. Sc. Degree in Mechanical Engineering
2009

The approval of this Postgraduate Thesis by the Department of Mechanical Engineering of the University of Thessaly does not imply acceptance of the author's opinions. (Law 5343/32, article 202, paragraph 2). The views and opinions expressed herein do not necessarily reflect those of the European Commission.

Approved by the members of the examining committee:

First Examiner (Supervisor)	Prof. Dimitris Valougeorgis Department of Mechanical Engineering, University of Thessaly
Second Examiner	Associate Prof. Nikolaos Andritsos Department of Mechanical Engineering, University of Thessaly
Third Examiner	Prof. Giorgos Liberopoulos Department of Mechanical Engineering, University of Thessaly
Fourth Examiner	Prof. Costas Papadimitriou Department of Mechanical Engineering, University of Thessaly
Fifth Examiner	Associate Prof. Nikos Pelecasis Department of Mechanical Engineering, University of Thessaly

Acknowledgements

During the writing of this thesis, I have received a great deal of guidance and encouragement by Prof. Dimitris Valougeorgis and Prof. Alkis Grecos. This work would not be possible without their invaluable suggestions and eagerness to help me. Furthermore, I would like to thank the other members of the examining committee, Professors N. Andritsos, N. Pelekasis, C. Papadimitriou and G. Liberopoulos, for their suggestions and constructive criticism. Moreover, many colleagues contributed over the last months with bits of support. In particular I am very thankful to Serafeim Misdanitis for being there to help and cheer me up, even in the most adverse days. I would also like to express my gratitude to Natasa for her unlimited patience and understanding during the past year and for sharing with me a part of her life. Finally, I am grateful to my family for believing in me and for being a source of inspiration and strength. This work has been funded by the Association EURATOM-Hellenic Republic. This support is highly acknowledged.

Sarantis Pantazis

On the motion of charged particles subject to random forces and fields

Sarantis Pantazis
University of Thessaly, Department of Mechanical Engineering, 2009
Association EURATOM – Hellenic Republic

Supervisor: Prof. Dimitris Valougeorgis

Abstract

In plasma physics, it is often necessary to study the motion of a charged particle in a magnetic field, modelling the effect of collisions by additive random forces. Following Langevin, the force is taken to be the sum of a friction term, proportional to the velocity, and a fluctuating component referred to as "noise". This stochastic term is assumed to be a Gaussian stationary process with vanishing mean and a covariance matrix characterized by correlation times which may vanish ("white noise") or be finite (e.g. "coloured noise"). This problem, for the case of a uniform field, leads to two systems of equations, one for the 1D longitudinal motion along the direction of the field and another for the 2D transverse motion perpendicular to it. These two systems can be studied independently. Because of the linearity of the equations, formal solutions are written and expressions for the expectation values of powers of the position and/or the velocity of the particle are obtained. For white noise, the problem has been studied analytically and numerically. However, the case of a stochastic term with finite correlation time has not been considered in detail.

Here, the influence of non-white noises is studied and numerical simulations based on two different approaches are presented. In the first approach, by adding an

equation for the evolution of the stochastic term, the problem is reduced essentially to that of white noise. However, this technique is not to be adopted in general since it can only reproduce specific kinds of noise. In the second approach the forcing term is modelled by a Fourier series with random, uniformly distributed, phases and may be considered as more general. Simulations with the latter method are presented for a random force with the correlation function of coloured, Gaussian or Lorentzian noise. To judge the extracted accuracy from the computational approaches, the numerical results have also been compared with available analytical solutions. In addition, an extensive parametric study has been performed with respect to various involved parameters including the correlation time and the friction coefficient.

This numerical investigation serves for validating and benchmarking purposes of the implemented computational schemes and will be used in more complex problems. The problem of motion of a charged particle inside a space dependent electric field has also been investigated. The governing system of equations is non-linear and can only be solved numerically using the Fourier series approach because the explicit form of the field is not available. Results show good qualitative agreement with benchmark problems.

In the future, random motion in electromagnetic fields and inhomogeneous magnetic fields will also be considered.

Contents

Nomenclature

$\mathbf{B}(r,t)$	magnetic field
c	stochastic force component strength
$E(r,t)$	electric field
$F(t)$	force imposed on the particle
m	particle mass
N	number of Fourier series terms
$N(t)$	sample values from a normal distribution $N(0,1)$
N_R	number of simulations
p	stochastic electric field strength
q	electric charge
$r(t)$	particle position vector $[x, y, z]$
$R_{AB}(t,s)$	correlation function of A and B
$S_A(\omega)$	spectral energy density of A
T	total time
$V(t)$	particle velocity vector $[u, v, w]$

Greek symbols

γ	friction factor
$\Delta\omega$	frequency step
ε	correlation time
$\xi(t)$	stochastic force vector $[\xi_x, \xi_y, \xi_z]$
λ	correlation length
σ_A	standard deviation of A
σ_A^2	variance of A
Φ_n	random angle, uniformly distributed in $[0, 2\pi]$
Ω	cyclotron frequency
ω_{max}	maximum value of frequency considered

Chapter 1 – Introduction and Literature Review

Any realistic model of a real-world phenomenon must take into account possible random fluctuations. Randomness (also referred to as "noise") should be integrated into the calculation of any important quantity since an inherent variation is exhibited, prohibiting accurate estimation. This behaviour is modelled by stochastic differential equations.

One of the first to observe stochastic motion was Robert Brown in 1827. He noticed that particles contained in pollen move irregularly inside a fluid. His initial thought was that pollen was "alive" but this hypothesis was quickly rejected after repeating the experiment with coal dust. The theory of Brownian motion was later established by Einstein [1, 2], and verified experimentally by Perrin [3]. Similar results were obtained by von Smoluchowski [4] using the random walk approach. The use of equations of motion subject to random forces was introduced by Langevin [5] and his work is a concrete basis of Brownian motion. It led to an extensive use of stochastic differential equations in problems of physics and engineering.

The formulation developed by Langevin is the starting point for the study of particle motion, which in the general case is governed by the following equations

$$\frac{d\boldsymbol{r}(t)}{dt} = \boldsymbol{V}(t) \tag{1.1}$$

$$m\frac{d\boldsymbol{V}(t)}{dt} = q\left[\boldsymbol{E}(\boldsymbol{r},t) + \boldsymbol{V}(t)\times\mathbf{B}(\boldsymbol{r},t)\right] + \boldsymbol{F}(t) \tag{1.2}$$

$$\boldsymbol{F}(t) = -m\gamma\boldsymbol{V}(t) + mc\xi(t) \tag{1.3}$$

In the above expressions, the main unknowns are $\boldsymbol{r}(t) = \left(x(t), y(t), z(t)\right)$ and $\boldsymbol{V}(t) = \left(u(t), v(t), w(t)\right)$, representing the particle position and velocity, respectively, while $\boldsymbol{F}(t) = \left(F_x(t), F_y(t), F_z(t)\right)$ is the force vector and $\xi(t) = \left(\xi_x(t), \xi_y(t), \xi_z(t)\right)$ the stochastic force component. We investigate motion inside time and space dependent magnetic or electric fields, denoted by $\mathbf{B}(\boldsymbol{r},t)$ and $\boldsymbol{E}(\boldsymbol{r},t)$. The constants q, γ and c symbolize the particle's electric charge, the friction factor and the strength of the random force, respectively. The equations are derived from their deterministic counterparts with

the addition of a force $\boldsymbol{F}(t)$ exerted by the surrounding molecules, composed of a friction component and a stochastic part. Furthermore, a random force may also stem from a stochastic component of the magnetic/electric field.

In the following chapters, two cases will be considered: the motion of a charged particle in a stationary, uniform magnetic field $\mathbf{B}(\boldsymbol{r},t)=B_0\boldsymbol{e}_x$ under the influence of friction and random forces, and that of frictionless, one-dimensional motion in a spatially dependent stochastic electric field $E(x,t)=E(x)$ with the properties

$$\langle E(x)\rangle = 0 \tag{1.4}$$

$$\langle E(x)E(x+y)\rangle = \frac{p^2}{\lambda\sqrt{\pi}}e^{-\frac{y^2}{\lambda^2}} \tag{1.5}$$

where p, λ are constants.

The stochastic term can have many qualities. It is frequently assumed to be a Gaussian stationary process with vanishing mean and a covariance matrix characterized by correlation times which may vanish ("white noise" [6, 7]) or be finite (e.g. "coloured noise" [8, 9]). This noise can either be additive (as shown in equation 1.3) or multiplicative [10] or even a combination of the previously mentioned types [11, 12]. There also exist non-Gaussian noises.

The appropriate type of noise depends on the application. The common properties of the noise term are

(i) $\langle \boldsymbol{\xi}(t)\rangle = 0$ and (1.6)

(ii) $\langle \xi_i(t)\xi_i(t+\tau)\rangle = \phi(|\tau|)$ (1.7)

with $i = x, y$ or z, and $\phi(|\tau|)$ is chosen so that $\int_{-\infty}^{\infty}\phi(|\tau|)d\tau = 1$. The following types of noise and their corresponding correlation functions will be used in this work:

White noise : $\phi(|\tau|) = \delta(|\tau|)$ (1.8)

Coloured noise : $\phi(|\tau|) = (2\varepsilon)^{-1}\exp(-|\tau|/\varepsilon)$ (1.9)

Gaussian noise : $\phi(|\tau|) = (\varepsilon\sqrt{\pi})^{-1}\exp(-\tau^2/\varepsilon^2)$ (1.10)

Lorentzian noise : $$\phi(|\tau|) = \varepsilon\left[\pi\left(\tau^2 + \varepsilon^2\right)\right]^{-1} \qquad (1.11)$$

The parameter ε is called correlation time and it indicates that the correlation of the stochastic force at time t with another instance of the force in the time interval $[t-\varepsilon, t+\varepsilon]$ is not negligible. It can be seen that, as $\varepsilon \to 0$ all noises approach the white noise, while for $\varepsilon \to \infty$ the noise vanishes. In Figure 1.1 the correlation function of each noise (except white) is plotted for two values of the ε parameter. There are significant differences among them, especially near zero τ and for large correlation times ε (the Lorentzian noise is spread over a larger area while coloured noise has a steeper curve).

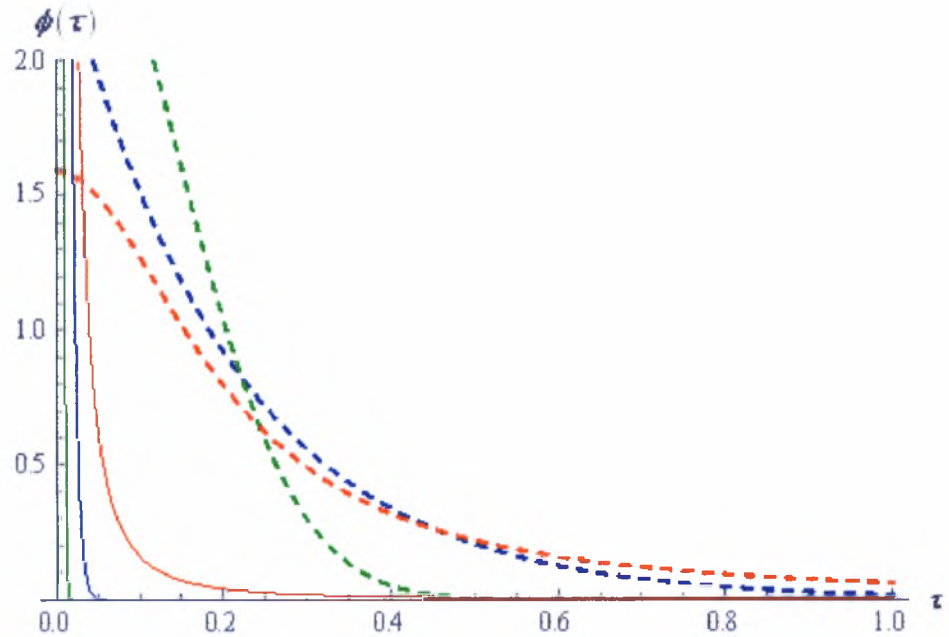

Figure 1.1: Correlation functions of coloured (blue), Gaussian (green) and Lorentzian (red) noise at two correlation times (dashed: $\varepsilon = 0.2$, continuous: $\varepsilon = 0.005$).

A simplified version of stochastic motion is often described in literature using the "random walk" example [13], shown in Figure 1.2. Imagine a particle, which can either move left or right for a distance equal to Δx. If motion to each direction has the same probability and $x_0 = 0$, it follows that the mean displacement is zero. Its position after N steps will be

$$x_N = \Delta x_1 + \Delta x_2 + \ldots + \Delta x_N = \sum_{i=1}^{N} \Delta x_i \qquad (1.12)$$

where $\Delta x_i = \pm \Delta x$ depending on the direction of motion, and the squared length of the trajectory will be

$$x_N^2 = N(\Delta x)^2 + \sum_{j=1,k=1,j\neq k}^{N} \Delta x_j \Delta x_k \qquad (1.13)$$

When (1.13) is averaged and due to the fact that the steps are independent from each other, it gives

$$\langle x^2 \rangle = N(\Delta x)^2 \qquad (1.14)$$

Therefore, since $\Delta x = \upsilon \tau$, where υ is the particle velocity and τ the travelling time, we obtain

$$\langle x^2 \rangle = \frac{t}{\tau} \cdot (\upsilon \cdot \tau \cdot \Delta x) = D \cdot t \qquad (1.15)$$

where t is the total time ($t = N\tau$) and $D = \upsilon \Delta x$ is a constant. It is important to note that $\langle x^2 \rangle$ is proportional to time t. We can reach the same conclusion in three dimensions or for non-fixed Δx (in this case, knowledge of the probability distribution for the increments is necessary).

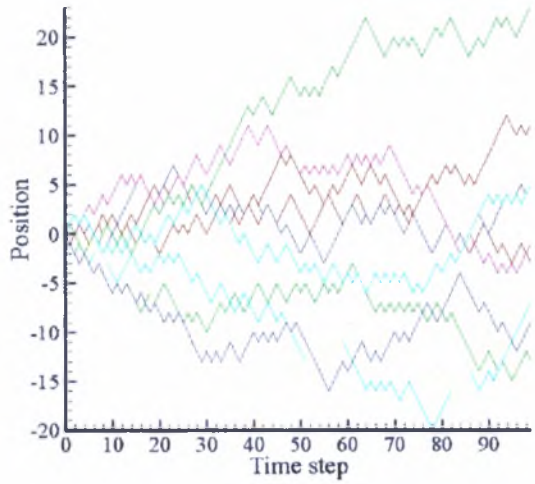

Figure 1.2: Realizations of the random walk example.

The dependence of the mean square displacement on time is a vital factor of the diffusion process. Therefore, assuming that

$$\langle r^2 \rangle \sim t^a \qquad (1.16)$$

where $\vec{r}$ is the position of the particle, diffusion is classified via the superscript a. The value $a=1$ corresponds to normal diffusion, while all other cases are termed anomalous. When $a>1$ or $a<1$, superdiffusive or subdiffusive processes take place, respectively. The special case $a=2$ is called ballistic diffusion. An important difference between normal and anomalous diffusion is shown in Figure 1.3. In the case of anomalous diffusion, the trajectory consists of long "free flight" paths and local "trapping" of the particle in certain areas of the flow domain, in contrast to the more homogeneous motion appearing during normal diffusion.

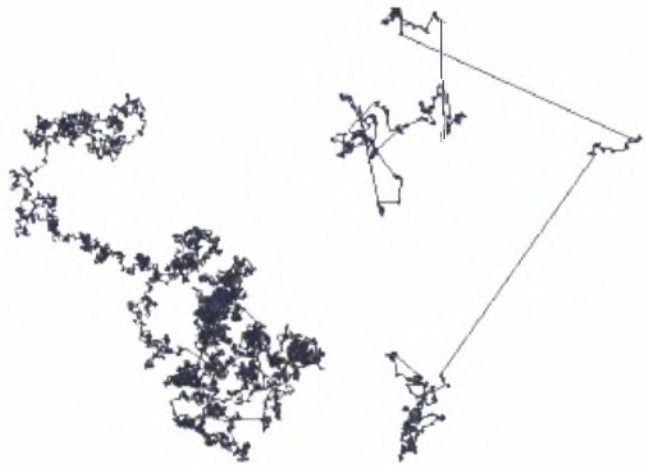

Figure 1.3: Trajectories in conditions of normal (left) or anomalous diffusion (right).

Another way of investigation of stochastic motion is through the Fokker-Planck equation (FPE) [14]. This is a partial differential equation which can be used to estimate the probability that a particle will be located at a position x at time t. This probability can be calculated using the *Chapman-Kolmogorov* equation

$$P(x,t)=\int_{-\infty}^{\infty} P(x-\Delta x,t-\Delta t)\,q(\Delta x,x-\Delta x)\,dx \tag{1.17}$$

where $q(\Delta x,x-\Delta x)$ is the probability that the particle will move for Δx when it is located in $x-\Delta x$. Therefore, equation (1.17) denotes the probability that the particle moves from $(x-\Delta x,t-\Delta t)$ to (x,t). If we expand both elements of the integrand in a Taylor series we obtain the FPE

$$\frac{\partial P(x,t)}{\partial t}=-\frac{\partial}{\partial x}\left[V(x)P(x,t)\right]+\frac{\partial^2}{\partial x^2}\left[D(x)P(x,t)\right] \tag{1.18}$$

where $V(x)$ is the mean velocity and $D(x)=\langle \Delta x^2 \rangle / (2\Delta t)$ is the diffusion coefficient. An important difference of this approach is the appearance of the drift term (first term of the right hand side in equation 1.18) and the spatial dependence of both the drift velocity and diffusion coefficient. Therefore, it can be applied in a wider range of problems. However, it is valid only in near-equilibrium situations. The Fokker-Planck equation has not been used in this work.

A significant amount of work has been accomplished on the theoretical aspects of stochastic differential equations and their numerical solution. In contrast to classical numerical analysis, here we differentiate between "strong" convergence (a simulation path is approached) and "weak" convergence (a bulk quantity, such as the mean value of position, is approached) [15, 16]. Some basic information on numerical simulation, as well as many details of the mathematics of Brownian motion, the Ornstein-Uhlenbeck process and the extraction of the spectral energy density function, are presented by Gillespie [17].

Similarly with classical numerical analysis, there are also algorithms of second order accuracy in time step [18], stochastic versions of Runge-Kutta algorithms [15, 19, 20] and implicit schemes [15]. Significant differences exist between them and their corresponding deterministic counterparts, which can not be applied in stochastic differential equations, and a lot of work has been performed in this field.

Alternatively, an integral algorithm is presented in [21, 22] for the generation of coloured noise. The authors consider it a substantial improvement since the time step can be larger than in first order algorithms and it is faster and more accurate.

Another method of calculation of the stochastic force is by a series obtained by Fourier transform [23]. In this approach there are important merits, such as the fact that the spectral energy density of the noise is only needed. Thus, it is a very general approach able to implement any kind of noise. In addition, the long "tails" are simulated, a larger time step can be used and the series is ergodic (reaching convergence sooner). Furthermore, it is one-dimensional (some noises may need more than one equations) and the amount of terms required does not depend on the discretization. The authors give more specific instructions about the numerical parameters in [24] and the method is used

again in [25, 26, 27] and compared with Fokker-Planck results. Due to its flexibility, this approach will be applied in the present work.

The force can also originate in the presence of a field that may have a stochastic component, which is the case for example when a charged particle moves inside a magnetic/electric field of a fusion reactor. This is a problem of increased interest during the past decades due to the applications in plasma confinement. The work of Lemons and Kaufmann [7] studies the motion of a particle in a uniform, stationary, non-stochastic magnetic field, while in [28] the magnetic field is composed of a constant and a stochastic perturbation component. Both articles include the influence of an additive white noise term. In [29] the influence of both stochastic magnetic and electric fields in a tokamak are studied assuming uniform average magnetic and electric fields with Gaussian fluctuations and using some experimental results. Plasma diffusion in the presence of a magnetic field is also examined [30] using the Fokker-Planck equation and explicit expressions are provided for the particle density and its moments.

Some work has also been performed in the measurement of stochastic magnetic fields in several tokamaks around the world (TEXTOR, Madison Symmetric Torus, ASDEX Upgrade). These data serve for the introduction of new models [31], the comparison with numerical simulations [32], or the determination of certain parameters, in order to numerically study fast MHD phenomena in a computationally efficient manner [33]. Finally, there are also studies concerning the topology of stochastic magnetic fields in tokamaks [34] and stellarators [35].

Stochastic electric fields, dependent both on time and position, have also been investigated in many works. The range of applicability of the quasilinear theory is investigated in [36] using the problem of stochastic acceleration of a charged particle in a random electric field. A comparison of quasilinear theory, resonance broadening theory and direct numerical integration of trajectories is performed in [37] and agreement is found at low amplitudes. Above a certain value, however, both theoretical formulations fail simultaneously. Ishihara et al [38, 39, 40] have also examined the turbulent motion of charged particles inside an electric field with stochastic fluctuations. They have mostly performed test particle experiments to determine the range of applicability of the quasi-

linear theory, investigated the long term behaviour of the diffusion coefficient and also considered non-Markovian effects.

Apart from the applications mentioned above, many more exist in mathematics, engineering and physical sciences, causing a considerable increase of interest on the solution of stochastic differential equations during the last decades. In particular, there are numerous applications in genetics, electric circuits, financial sciences, fatigue cracking [16], structural mechanics [16, 41], stability of helicopter/spacecraft/satellite [16, 27, 42] and more.

The main purpose of this work is to study diffusion of charged particles inside electromagnetic fields. In particular, we are interested in the magnetic confinement of the particles in a fusion reactor and therefore our goal is to study their motion perpendicular to the magnetic lines. Furthermore, the motion of charged particles in a fluctuating magnetic field, with or without an additive random force, is of considerable interest in plasma physics, see e.g. [43] and references cited there. For this purpose, numerical codes have been developed to simulate simple benchmarking cases and will be used in the future for the investigation of stochastic electromagnetic or inhomogeneous magnetic fields.

In Chapter 2, motion in a uniform magnetic field will be examined by the analytical solution of the governing equations. In Chapter 3, the motion under the influence of two types of noises will be investigated numerically, while in Chapter 4 a more general approach, suitable for the study of any noise or field, will be employed and benchmarked. The results will be analysed in Chapter 5. Finally, in Chapter 6 the case of motion inside a stochastic electric field will be examined.

Chapter 2 – Motion in a uniform magnetic field

2.1 Introduction

The equations describing the motion for a positively charged particle inside a uniform, homogeneous, stationary magnetic field and subject to a random force are

$$\frac{d\boldsymbol{r}(t)}{dt} = \boldsymbol{V}(t) \tag{2.1.1}$$

$$\frac{d\boldsymbol{V}(t)}{dt} = \Omega\left[\boldsymbol{V}(t) \times \boldsymbol{e_x}\right] + \boldsymbol{f}(t) \tag{2.1.2}$$

$$\boldsymbol{f}(t) = -\gamma \boldsymbol{V}(t) + c\boldsymbol{\xi}(t) \tag{2.1.3}$$

where $\boldsymbol{r} = [x, y, z]$, $\boldsymbol{V} = [u, v, w]$, $\boldsymbol{f} = \left[f_x, f_y, f_z\right]$ are the position, velocity, and force per unit mass and $\boldsymbol{e_x}$ is the unit vector in the x direction. These equations are derived from (1.1)-(1.3) after dividing with m and defining $\Omega = B_0 q / m$ as the cyclotron frequency, where m is the particle mass, q is the particle electric charge and B_0 the strength of the magnetic field. The constant c is the strength of the stochastic force and may obtain different values parallel and perpendicular to the magnetic field, while γ is a parameter related to the friction exerted by the surrounding molecules. This problem can be decomposed in two systems of equations, one for the longitudinal motion along the direction of the field and another for the two dimensional transverse motion. These two systems can studied independently due to the linearity of the problem.

The analytical expressions for the average and standard deviation of the position, velocity and force applied on the particle are some of the useful information we can acquire about the motion. The correlation function

$$R_{AB}(t, s) = \left\langle A(t)\, B(s) \right\rangle \tag{2.1.4}$$

is defined, where A, B can be substituted by any component of $\boldsymbol{r}$, $\boldsymbol{V}$ or $\boldsymbol{\xi}$ and $s = t + \tau$ with t the current time and τ an arbitrary time constant. The $\boldsymbol{\xi}$ correlations are preferred over $\boldsymbol{f}$ since the force contains the friction term as well and it is preferred to study only the noise term. These expressions will be used to benchmark the numerical

results and to perform numerical simulations, as well as provide further insights to the underlying physics.

2.2 Motion along the magnetic field

The motion of the particle in the x-coordinate is not affected by the magnetic field. The system of equations is

$$\frac{dx(t)}{dt} = u(t) \tag{2.2.1}$$

$$\frac{du(t)}{dt} = -\gamma u(t) + c\xi_x(t) \tag{2.2.2}$$

The general solution of (2.2.2) for the corresponding velocity component is

$$u(t) = u_0 e^{-\gamma t} + ce^{-\gamma t}\int_0^t e^{\gamma t'}\xi_x(t')dt' . \tag{2.2.3}$$

The position is calculated from (2.2.1) and is equal to

$$\begin{aligned} x(t) &= x_0 + \int_0^t u(t')dt' \\ &= x_0 + \int_0^t \left[u_0 e^{-\gamma t'} + c\int_0^{t'} e^{-\gamma(t'-t'')}\xi_x(t'')dt'' \right] dt' = \\ &= x_0 + \frac{u_0}{\gamma}\left(1-e^{-\gamma t}\right) + c\int_0^t\int_{t''}^t e^{-\gamma(t'-t'')}\xi_x(t'')dt'dt'' . \end{aligned}$$

After integrating once and changing t'' to t' we obtain

$$x(t) = x_0 + \frac{u_0}{\gamma}\left(1-e^{-\gamma t}\right) + \frac{c}{\gamma}\int_0^t \left(1-e^{-\gamma(t-t')}\right)\xi_x(t')dt' . \tag{2.2.4}$$

Since the term $\xi(t')$ is stochastic, we can only acquire information on the mean value and standard deviation of position and velocity. The mean value of each quantity is obtained by averaging (2.2.3) and (2.2.4) since $\langle \xi_x(t) \rangle = 0$

$$\langle u(t) \rangle = u_0 e^{-\gamma t} \tag{2.2.5}$$

$$\langle x(t) \rangle = x_0 + \frac{u_0}{\gamma}\left(1-e^{-\gamma t}\right). \tag{2.2.6}$$

Due to the linearity of the problem, it is enough to solve for zero initial conditions. Therefore, $x_0 = u_0 = 0$ is assumed for the rest of the calculations and we have

$$u(t) = ce^{-\gamma t}\int_0^t e^{\gamma t'}\xi_x(t')dt' \tag{2.2.7}$$

$$x(t) = \frac{c}{\gamma}\int_0^t\left(1-e^{-\gamma(t-t')}\right)\xi_x(t')dt' \tag{2.2.8}$$

We are also interested in the correlations including the particle position and velocity. These are obtained by multiplying (2.2.3) and (2.2.4) accordingly and then averaging. For example, the variance of velocity is

$$R_{uu}(t,s) = \langle u(t)u(s)\rangle = \left\langle ce^{-\gamma t}\int_0^t e^{\gamma t'}\left[ce^{-\gamma s}\int_0^s e^{\gamma s'}\xi(s')ds'\right]\xi(t')dt'\right\rangle$$

$$= c^2e^{-\gamma(t+s)}\int_0^t\int_0^s e^{\gamma(s'+t')}\langle\xi(s')\xi(t')\rangle ds'dt' =$$

$$= c^2e^{-\gamma(t+s)}\int_0^t\int_0^s e^{\gamma(s'+t')}\phi(|t'-s'|)ds'dt' \tag{2.2.9}$$

with $\phi(|t'-s'|)$ according to (1.8)-(1.11). The integral of (2.2.9) can be simplified after some transformations (see Appendix B). The result is

$$R_{uu}(t,s) = \frac{c^2}{2\gamma}\left\{e^{-\gamma(s-t)}\int_{-t}^{s-t} e^{\gamma t'}\phi(|t'|)dt' + e^{-\gamma(t-s)}\int_{-s}^{t-s} e^{\gamma t'}\phi(|t'|)dt'\right.$$

$$\left.-e^{-\gamma(t+s)}\left[\int_0^t e^{\gamma t'}\phi(|t'|)dt' + \int_0^s e^{\gamma t'}\phi(|t'|)dt'\right]\right\}. \tag{2.2.10}$$

This expression is valid for any non-negative t and s, while for $s = t$ we get

$$R_{uu}(t,t) = \frac{c^2}{\gamma}\left\{\int_0^t e^{-\gamma t'}\phi(t')dt' - e^{-2\gamma t}\int_0^t e^{\gamma t'}\phi(t')dt'\right\}. \tag{2.2.11}$$

Similarly, the correlations

$$R_{xu}(t,s) = \langle x(t)u(s)\rangle =$$

$$= \frac{c^2}{\gamma}\left\{e^{-\gamma s}\int_0^t\int_0^s e^{\gamma s'}\phi(|t'-s'|)ds'dt' - e^{-\gamma(t+s)}\int_0^t\int_0^s e^{\gamma(t'+s')}\phi(|t'-s'|)ds'dt'\right\} \tag{2.2.12}$$

$$R_{xx}(t,s)=\langle x(t)x(s)\rangle=$$

$$=\frac{c^2}{\gamma^2}\left\{\int_0^t\int_0^s\phi(|t'-s'|)ds'dt'-e^{-\gamma s}\int_0^t\int_0^s e^{\gamma s'}\phi(|t'-s'|)ds'dt'\right. \tag{2.2.13}$$

$$\left.-e^{-\gamma t}\int_0^t\int_0^s e^{\gamma t'}\phi(|t'-s'|)ds'dt'+e^{-\gamma(t+s)}\int_0^t\int_0^s e^{\gamma(t'+s')}\phi(|t'-s'|)ds'dt'\right\}$$

can be calculated. For $s=t$ we finally acquire

$$R_{xu}(t,t)=\frac{c^2}{\gamma^2}\left\{\int_0^t\phi(t')dt'+e^{-2\gamma t}\int_0^t e^{\gamma t'}\phi(t')dt'-e^{-\gamma t}\left[\int_0^t\phi(t')dt'+\int_0^t e^{\gamma t'}\phi(t')dt'\right]\right\} \tag{2.2.14}$$

$$R_{xx}(t,t)=\frac{c^2}{\gamma^3}\left\{2\left(\gamma t-1+e^{-\gamma t}\right)\int_0^t\phi(t')dt'-2\gamma\int_0^t t'\phi(t')dt'\right.$$

$$\left.+\left(2e^{-\gamma t}-e^{-2\gamma t}\right)\int_0^t e^{\gamma t'}\phi(t')dt'-\int_0^t e^{-\gamma t'}\phi(t')dt'\right\} \tag{2.2.15}$$

There is an alternative solution for the autocorrelation of position. It can be seen that

$$R_{xu}(t,t)=\langle x(t)u(t)\rangle=\left\langle x(t)\frac{dx(t)}{dt}\right\rangle=\frac{1}{2}\frac{d\langle x(t)x(t)\rangle}{dt}=\frac{1}{2}\frac{dR_{xx}(t,t)}{dt}$$

and therefore

$$R_{xx}(t,t)=2\int_0^t R_{xu}(t',t')dt'\,. \tag{2.2.16}$$

Based on the above closed form expressions, some results for the noises (1.8)-(1.11) are provided in Section 2.4.

2.3 Motion transversal to the magnetic field

The next step will be the solution in the two dimensions y and z, perpendicular to the magnetic field of frequency Ω in the direction of x. The governing equations are

$$\frac{d}{dt}\begin{bmatrix}y\\z\end{bmatrix}=\begin{bmatrix}v\\w\end{bmatrix} \tag{2.3.1}$$

$$\frac{d}{dt}\begin{bmatrix}v\\w\end{bmatrix}=\Omega\begin{bmatrix}0&1\\-1&0\end{bmatrix}\begin{bmatrix}v\\w\end{bmatrix}-\gamma\begin{bmatrix}v\\w\end{bmatrix}+c\begin{bmatrix}\xi_y\\\xi_z\end{bmatrix} \tag{2.3.2}$$

To calculate the mean values, we average (2.3.1) and (2.3.2) and as a result the noise terms are eliminated. The solution of the system is

$$\langle y(t)\rangle = \frac{1}{1+b^2}\left\{ y_0 + \frac{1}{\gamma}\left[v_0 + b\left(w_0 + \Omega y_0\right)\right] + \frac{e^{-\gamma t}}{\gamma}\left[\left(bv_0 - w_0\right)\sin\left(\Omega t\right) - \left(v_0 + bw_0\right)\cos\left(\Omega t\right)\right]\right\} \tag{2.3.3}$$

$$\langle z(t)\rangle = \frac{1}{1+b^2}\left\{ z_0 + \frac{1}{\gamma}\left[w_0 + b\left(-v_0 + \Omega z_0\right)\right] + \frac{e^{-\gamma t}}{\gamma}\left[\left(bv_0 - w_0\right)\cos\left(\Omega t\right) + \left(v_0 + bw_0\right)\sin\left(\Omega t\right)\right]\right\} \tag{2.3.4}$$

$$\langle v(t)\rangle = e^{-\gamma t}\left[v_0\cos\left(\Omega t\right) + w_0\sin\left(\Omega t\right)\right] \tag{2.3.5}$$

$$\langle w(t)\rangle = e^{-\gamma t}\left[w_0\cos\left(\Omega t\right) - v_0\sin\left(\Omega t\right)\right] \tag{2.3.6}$$

The deterministic solution for the position of the particle for a non-zero initial velocity is a spiral trajectory, as shown in Figure 2.1. Due to the linearity of the problem, calculations with a random force can be performed with the particle at rest in the beginning and the complete solution is obtained with superposition with the deterministic path for the appropriate initial velocity.

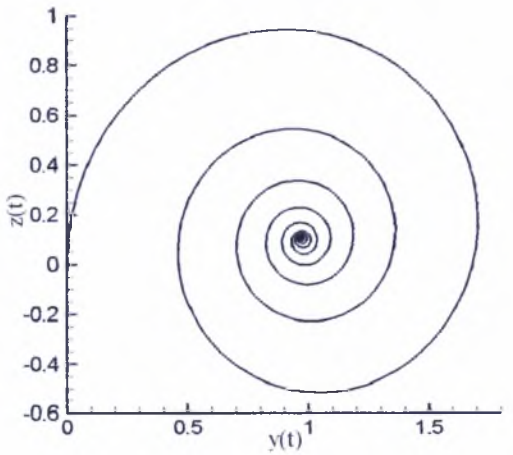

Figure 2.1: Deterministic trajectory for $c=1$, $\gamma=1$, $\Omega=10$ and $w(0)=10$.

For initial conditions equal to zero, the general solution is

$$\begin{bmatrix} y(t) \\ z(t) \end{bmatrix} = c\int_0^t\int_0^{t'} e^{(\Omega-\gamma)t''}\begin{bmatrix} \xi_y\left(t'-t''\right) \\ \xi_z\left(t'-t''\right) \end{bmatrix} dt''dt' \tag{2.3.7}$$

$$\begin{bmatrix} v(t) \\ w(t) \end{bmatrix} = c\int_0^t e^{(\Omega J-\gamma)(t-t')} \begin{bmatrix} \xi_y(t) \\ \xi_z(t) \end{bmatrix} dt' \tag{2.3.8}$$

Correlations can be calculated in the way shown in Section 2.2. The analytical derivation of the corresponding quantities is tedious and does not exhibit substantially different features in comparison to the one-dimensional problem, while the resulting expressions are more difficult to handle. It must be noted that for large times, the variance of position behaves asymptotically as

$$R_{yy}(t) = R_{zz}(t) \sim \frac{c^2}{\Omega^2+\gamma^2} t \tag{2.3.9}$$

in the case of white noise.

2.4 Analytical solutions for various noises along the magnetic field

We are interested in the extraction of analytical expressions for the estimation of the variance of position x and velocity u and the $x-u$ correlation at any given time for the specific noises (1.8)-(1.11). The behaviour of these quantities reveals important information about the nature of the motion. The equations extracted here will also be used to benchmark the numerical codes of Chapter 4.

At this stage the correlation function $\phi(t')$ can be substituted from (1.8-1.11) into (2.2.11), (2.2.14) and (2.2.15) and the integrals are either handled analytically (for white and coloured noise) or numerically (for Gaussian and Lorentzian noise). In the case of white noise, the expression

$$\int_0^t f(t')\delta(t')dt' = \frac{1}{2} f(0) \tag{2.4.1}$$

has been used. This is merely a convention, since Dirac's function may be derived by taking the limit $\varepsilon \to 0$ of a sequence of functions $\delta_\varepsilon(t')$, which can either be symmetric or not. The final expressions are

$$R_{uu}(t,t) = \frac{c^2}{2\gamma}\left(1-e^{-2\gamma t}\right) \tag{2.4.2}$$

$$R_{xu}(t,t)=\frac{c^2}{2\gamma^2}\left(1-e^{-\gamma t}\right)^2 \tag{2.4.3}$$

$$R_{xx}(t,t)=\frac{c^2}{2\gamma^3}\left[2\gamma t-3+4e^{-\gamma t}-e^{-2\gamma t}\right] \tag{2.4.4}$$

for white noise and

$$R_{uu}(t,t)=\frac{c^2}{2\gamma\left(a^2-1\right)}\left[a-1-2ae^{-(\gamma+1/\varepsilon)t}+(a+1)e^{-2\gamma t}\right] \tag{2.4.5}$$

$$R_{xu}(t,t)=\frac{c^2}{2\gamma^2}\left[1-e^{-t/\varepsilon}-e^{-\gamma t}+e^{-(\gamma+1/\varepsilon)t}\right.$$
$$\left.-\frac{1}{a-1}\left(e^{-t/\varepsilon}-e^{-\gamma t}\right)+\frac{1}{a-1}\left(e^{-(\gamma+1/\varepsilon)t}-e^{-2\gamma t}\right)\right] \tag{2.4.6}$$

$$R_{xx}(t,t)=\frac{c^2}{2\gamma^3\left(a^2-1\right)}\left\{2\gamma\left(a^2-1\right)t-2a^2e^{-\left(\gamma+\frac{1}{\varepsilon}\right)t}\right.$$
$$\left.+2a^2(1+a)e^{-\frac{t}{\varepsilon}}+2\left(a^2-a-2\right)e^{-\gamma t}+(a+1)e^{-2\gamma t}+\left[-2a^3-2a^2+a+3\right]\right\} \tag{2.4.7}$$

for coloured noise.

The expressions (2.4.2) to (2.4.7) are consistent with the remarks of Chapter 1, that is, the variance of position is proportional to the time after a short transitional period. Therefore, in long term conditions normal diffusion prevails, but we are also interested in short times. It is not trivial to determine how small this time interval is in the general case from the integrals of (2.2.11), (2.2.14) and (2.2.15). For that purpose, a graphical representation of three correlations, $R_{xx}(t,t)$, $R_{xu}(t,t)$ and $R_{uu}(t,t)$, for certain values of the parameters is given in Figures 2.2 and 2.3. Four noises and two values of ε, namely 10^{-3} and 10^{-1}, are considered for a short time interval. It is seen that for small ε the curves practically coincide. This is not unexpected, since equations (1.9) to (1.11) can describe white noise as the correlation time approaches zero. Where larger values are examined, the curves display small differences near the beginning of time, where the exponential terms are still not negligible. Overall, they are qualitatively similar and for larger times (more than 7 units) the long term behaviour is recovered ($R_{xx}(t,t)$ is proportional to time and $R_{uu}(t,t)$ is constant). We will also comment on the dependence of the results in terms of c and γ in Chapter 4, where a more detailed interpretation is attempted.

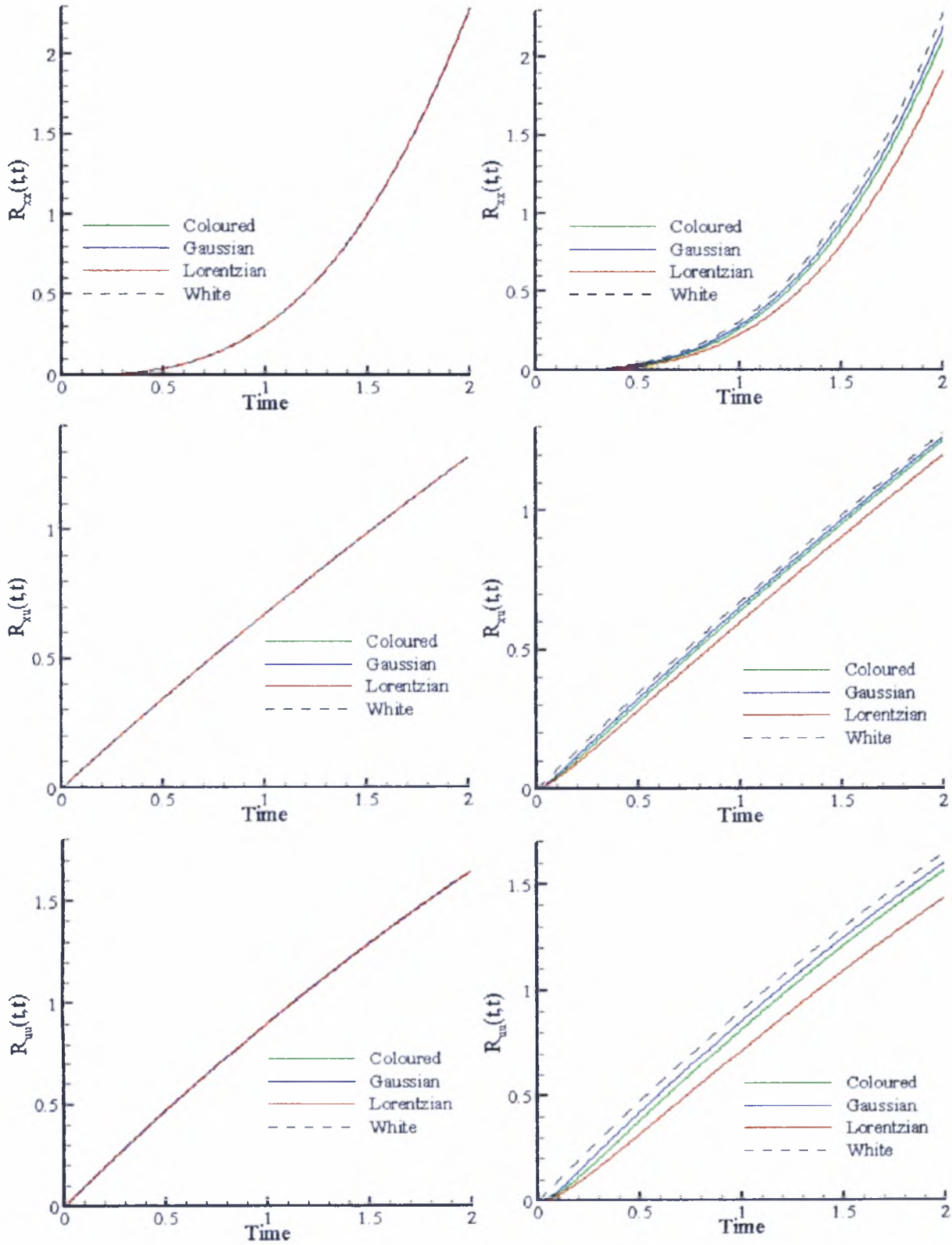

Figure 2.2: Comparison of $R_{xx}(t,t)$ (up), $R_{xu}(t,t)$ (middle) and $R_{uu}(t,t)$ (down) for various noises, with $c^2=1$, $\gamma=10^{-1}$, $\varepsilon=10^{-3}$ (left) and $\varepsilon=10^{-1}$ (right).

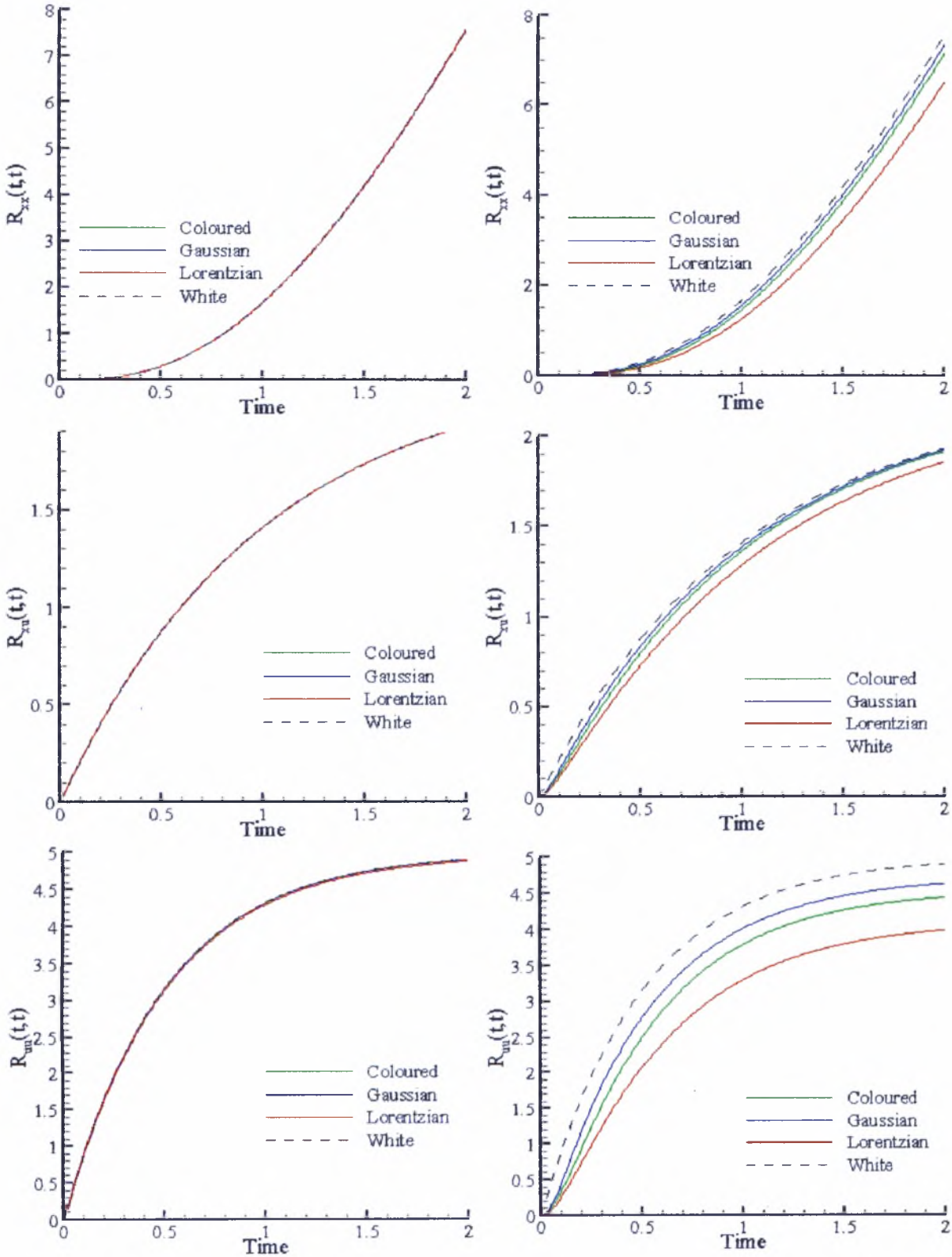

Figure 2.3: Comparison of $R_{xx}(t,t)$ (up), $R_{xu}(t,t)$ (middle) and $R_{uu}(t,t)$ (down) for various noises, with $c^2=10$, $\gamma=1$, $\varepsilon=10^{-3}$ (left) and $\varepsilon=10^{-1}$ (right).

Chapter 3 – Discretized form of the governing equations

3.1 General considerations

The discretized form of equations (2.1.1)-(2.1.3), obtained by substituting

$$dA \to \Delta A = A(t+\Delta t) - A(t) \tag{3.1.1}$$

where A is equal to any component of $\boldsymbol{r}$, V or ξ, is required to perform numerical calculations. The system depends on the type of stochastic force. The discretized governing equations are

$$x(t+\Delta t) = x(t) + u(t)\Delta t \tag{3.1.2}$$

$$y(t+\Delta t) = y(t) + v(t)\Delta t \tag{3.1.3}$$

$$z(t+\Delta t) = z(t) + w(t)\Delta t \tag{3.1.4}$$

$$u(t+\Delta t) = u(t) - \gamma u(t)\Delta t + c\xi_x(t)\Delta t \tag{3.1.5}$$

$$v(t+\Delta t) = v(t) + \left(-\gamma v(t) + w(t)\Omega\right)\Delta t + c\xi_y(t)\Delta t \tag{3.1.6}$$

$$w(t+\Delta t) = w(t) + \left(-\gamma w(t) - v(t)\Omega\right)\Delta t + c\xi_z(t)\Delta t \tag{3.1.7}$$

In the case of white noise, the $\xi_i(t)$ term with $i = x, y, z$ can be substituted by

$$\xi_i(t) = N(t)/\sqrt{\Delta t} \tag{3.1.8a}$$

with $N(t)$ denoting random values conforming to a normal distribution with zero mean and standard deviation unity $N(0,1)$. The explanation for this approximation is found in [44]. Additional equations can also be added to describe the evolution of the stochastic force if we are interested in simulating coloured noise [21]. The expressions

$$\xi_i(t+\Delta t) = \xi_i(t) - \frac{\xi_i(t)}{\varepsilon}\Delta t + \frac{\sqrt{\Delta t}}{\varepsilon}N(t) \tag{3.1.8b}$$

are included for each random force component, $i = x, y, z$. This is a common practice in the literature when coloured noise must be included. However, it must be noted that, unless the initial conditions are appropriate, that is $\xi(-\infty) = 0$, this is not the typical coloured noise described by (1.9). In this work, we have used zero initial conditions for

the stochastic force, i.e. $\xi(0)=0$, and therefore this is a special case of the Chapter 2 results. It must be noted that other noises, such as Gaussian or Lorentzian, can not be simulated this way since we can not extract an expression like (3.1.8) for the evolution of noise to close the system.

Since the majority of available random generators produce random numbers R uniformly distributed in $[0,1]$, an algorithm is required to obtain the appropriate noise. The most commonly used methods to obtain a non-uniform distribution are: i) the inverse-cumulative [45], ii) acceptance-rejection [45] and iii) Box-Mueller method [6]. The first one is unsuitable for this case because it can not reproduce a normal distribution. A description and comparison of the two latter methods is found in Appendix B. The Box-Mueller algorithm is preferred in this work due to its simplicity and relatively small computational cost.

The initial conditions are $r_i(0)=V_i(0)=\xi_i(0)=0$. Alternatively, the initial value of the force ξ_0 could be selected according to a Gaussian distribution [9, 21]

$$P(\xi_0)=\sqrt{\frac{\varepsilon}{2\pi}}e^{-\frac{\varepsilon\xi_0^2}{2}}. \tag{3.1.9}$$

This is achieved using again the Box-Mueller algorithm.

3.2 Analytical solution

The mean values of position and velocity are obtained by averaging the discretized equations of white noise (3.1.2)-(3.1.8a). For example, for (3.1.2) we write

$$\langle x(t+\Delta t)\rangle-\langle x(t)\rangle=\langle u(t)\rangle\Delta t$$

By dividing with Δt and taking the limit $\Delta t\to 0$ we obtain

$$\frac{d\langle x(t)\rangle}{dt}=\langle u(t)\rangle \tag{3.2.1}$$

and by repeating this procedure for the rest of the quantities we get

$$\frac{d\langle y(t)\rangle}{dt}=\langle v(t)\rangle \tag{3.2.2}$$

$$\frac{d\langle z(t)\rangle}{dt}=\langle w(t)\rangle \tag{3.2.3}$$

$$\frac{d\langle u(t)\rangle}{dt}=-\gamma\langle u(t)\rangle \tag{3.2.4}$$

$$\frac{d\langle v(t)\rangle}{dt}=-\gamma\langle v(t)\rangle+\langle w(t)\rangle\Omega \tag{3.2.5}$$

$$\frac{d\langle w(t)\rangle}{dt}=-\gamma\langle w(t)\rangle-\langle v(t)\rangle\Omega. \tag{3.2.6}$$

The solution of this system of first order o.d.e's is

$$\langle x(t)\rangle=x_0+\frac{u_0}{\gamma}\left(1-e^{-\gamma t}\right) \tag{3.2.7}$$

$$\begin{aligned}\langle y(t)\rangle=\frac{1}{1+b^2}\Bigg\{&y_0+\frac{1}{\gamma}\left[v_0+b\left(w_0+\Omega y_0\right)\right]\\&+\frac{e^{-\gamma t}}{\gamma}\left[\left(bv_0-w_0\right)\sin\left(\Omega t\right)-\left(v_0+bw_0\right)\cos\left(\Omega t\right)\right]\Bigg\}\end{aligned} \tag{3.2.8}$$

$$\begin{aligned}\langle z(t)\rangle=\frac{1}{1+b^2}\Bigg\{&z_0+\frac{1}{\gamma}\left[w_0+b\left(-v_0+\Omega z_0\right)\right]\\&+\frac{e^{-\gamma t}}{\gamma}\left[\left(bv_0-w_0\right)\cos\left(\Omega t\right)+\left(v_0+bw_0\right)\sin\left(\Omega t\right)\right]\Bigg\}\end{aligned} \tag{3.2.9}$$

$$\langle u(t)\rangle=u_0e^{-\gamma t} \tag{3.2.10}$$

$$\langle v(t)\rangle=e^{-\gamma t}\left[v_0\cos\left(\Omega t\right)+w_0\sin\left(\Omega t\right)\right] \tag{3.2.11}$$

$$\langle w(t)\rangle=e^{-\gamma t}\left[w_0\cos\left(\Omega t\right)-v_0\sin\left(\Omega t\right)\right] \tag{3.2.12}$$

These expressions are the same as those obtained in Chapter 2. Therefore, it is seen that the order of averaging and integrating the governing equations does not play a role.

It is well known that variances and covariances can be calculated using the expressions $\sigma_A^2(t)=\langle A^2(t)\rangle-\langle A(t)\rangle^2$ and $\operatorname{cov}\left[A(t)B(t)\right]=\langle A(t)B(t)\rangle-\langle A(t)\rangle\langle B(t)\rangle$. By squaring and averaging (3.1.2) and omitting higher powers of Δt we get

$$\left\langle x^2\left(t+\Delta t\right)\right\rangle=\left\langle x^2\left(t\right)\right\rangle+2\left\langle x\left(t\right)u\left(t\right)\right\rangle\Delta t \tag{3.2.13}$$

If we reverse the order of squaring and averaging we obtain

$$\langle x(t+\Delta t)\rangle^2 = \langle x(t)\rangle^2 + 2\langle x(t)\rangle\langle u(t)\rangle \Delta t \tag{3.2.14}$$

Equations (3.2.13) and (3.2.14) can be combined to give an ordinary differential equation for the evolution of the variance of position as $\Delta t \to 0$

$$\frac{d\sigma_x^2(t)}{dt} = 2\,\mathrm{cov}\{x(t)u(t)\} \tag{3.2.15}$$

In a similar way we can extract an o.d.e. for each variance and covariance. The final system for 1D motion under the influence of white noise also includes the equations

$$\frac{d\sigma_u^2(t)}{dt} = -2\gamma\sigma_u^2(t) + c^2 \tag{3.2.16}$$

$$\frac{d\,\mathrm{cov}\{x(t)u(t)\}}{dt} = -\gamma\,\mathrm{cov}\{x(t)u(t)\} + \sigma_u^2(t) \tag{3.2.17}$$

The initial values of all variances and covariances are assumed to be zero. Solving (3.2.15)-(3.2.17) yields the final expressions

$$\sigma_x^2(t) = \frac{c^2}{\gamma^3}\left[\gamma t - 2\left(1-e^{-\gamma t}\right) + \frac{1}{2}\left(1-e^{-2\gamma t}\right)\right] \tag{3.2.18}$$

$$\sigma_u^2(t) = \frac{c^2}{2\gamma}\left(1-e^{-2\gamma t}\right) \tag{3.2.19}$$

$$\mathrm{cov}\{x(t)u(t)\} = \frac{c^2}{2\gamma^2}\left(1-2e^{-\gamma t}+e^{-2\gamma t}\right) \tag{3.2.20}$$

The corresponding system in y, z already exists in the literature [7] and therefore is not repeated here. This procedure can be employed to simulate non-white noises, using equations (3.1.8) for the evolution of the noise term. The averages remain the same, while the covariance o.d.e's are presented in Tables 3.1-3.5. The one-dimensional problem leads to the equations of Table 3.1, while for the two-dimensional motion perpendicular to the magnetic field we must use equations (3.2.27)-(3.2.47), appearing in Tables 3.2-3.5. These were separated to indicate the discrete steps through which the solution is reached. Due to the symmetries of the problem, some expressions are shown to be equal (or opposite). The solution of the two systems is shown in Tables 3.6 and 3.7. In the following expressions, we have substituted $a = \varepsilon\gamma$ and $d = \varepsilon\Omega$. It has been confirmed that in the limit $\varepsilon \to 0$, the resulting equations are identical to the corresponding white noise equations.

Table 3.1: System of o.d.e's for the 1D problem.

$\frac{d\sigma_x^2(t)}{dt} = 2\,\mathrm{cov}\{x(t)u(t)\}$	(3.2.21)
$\frac{d\sigma_u^2(t)}{dt} = -2\gamma\sigma_u^2(t) + 2c\,\mathrm{cov}\{u(t)\xi_x(t)\}$	(3.2.22)
$\frac{d\sigma_{\xi_x}^2(t)}{dt} = -\frac{2\sigma_{\xi_x}^2(t)}{\varepsilon} + \frac{1}{\varepsilon^2}$	(3.2.23)
$\frac{d\,\mathrm{cov}\{x(t)u(t)\}}{dt} = -\gamma\,\mathrm{cov}\{x(t)u(t)\} + c\,\mathrm{cov}\{x(t)\xi_x(t)\} + \sigma_u^2(t)$	(3.2.24)
$\frac{d\,\mathrm{cov}\{u(t)\xi_x(t)\}}{dt} = -\left(\frac{1}{\varepsilon}+\gamma\right)\mathrm{cov}\{u(t)\xi_x(t)\} + c\sigma_\xi^2(t)$	(3.2.25)
$\frac{d\,\mathrm{cov}\{x(t)\xi_x(t)\}}{dt} = -\frac{\mathrm{cov}\{x(t)\xi_x(t)\}}{\varepsilon} + \mathrm{cov}\{u(t)\xi_x(t)\}$	(3.2.26)

Table 3.2: First system of o.d.e's for the 2D problem.

$\frac{d\,\mathrm{cov}\{y(t)\xi_z(t)\}}{dt} = -\frac{\mathrm{cov}\{y(t)\xi_z(t)\}}{\varepsilon} + \mathrm{cov}\{v(t)\xi_z(t)\}$	(3.2.27)
$\frac{d\,\mathrm{cov}\{z(t)\xi_z(t)\}}{dt} = -\frac{\mathrm{cov}\{z(t)\xi_z(t)\}}{\varepsilon} + \mathrm{cov}\{w(t)\xi_z(t)\}$	(3.2.28)
$\frac{d\,\mathrm{cov}\{y(t)\xi_y(t)\}}{dt} = -\frac{\mathrm{cov}\{y(t)\xi_y(t)\}}{\varepsilon} + \mathrm{cov}\{v(t)\xi_y(t)\}$	(3.2.29)
$\frac{d\,\mathrm{cov}\{z(t)\xi_y(t)\}}{dt} = -\frac{\mathrm{cov}\{z(t)\xi_y(t)\}}{\varepsilon} + \mathrm{cov}\{w(t)\xi_y(t)\}$	(3.2.30)

Table 3.3: Second system of o.d.e's for the 2D problem.

$\frac{d\sigma_{\xi_y}^2(t)}{dt} = -\frac{2\sigma_{\xi_y}^2(t)}{\varepsilon} + \frac{1}{\varepsilon^2}$	(3.2.31)
$\frac{d\sigma_{\xi_z}^2(t)}{dt} = -\frac{2\sigma_{\xi_z}^2(t)}{\varepsilon} + \frac{1}{\varepsilon^2}$	(3.2.32)
$\frac{d\,\mathrm{cov}\{v(t)\xi_y(t)\}}{dt} = -\left(\gamma+\frac{1}{\varepsilon}\right)\mathrm{cov}\{v(t)\xi_y(t)\} + \Omega\,\mathrm{cov}\{w(t)\xi_y(t)\} + c\sigma_{\xi_y}^2(t)$	(3.2.33)
$\frac{d\,\mathrm{cov}\{w(t)\xi_z(t)\}}{dt} = -\left(\gamma+\frac{1}{\varepsilon}\right)\mathrm{cov}\{w(t)\xi_z(t)\} - \Omega\,\mathrm{cov}\{v(t)\xi_z(t)\} + c\sigma_{\xi_z}^2(t)$	(3.2.34)
$\frac{d\,\mathrm{cov}\{w(t)\xi_y(t)\}}{dt} = -\left(\gamma+\frac{1}{\varepsilon}\right)\mathrm{cov}\{w(t)\xi_y(t)\} - \Omega\,\mathrm{cov}\{v(t)\xi_y(t)\} + c\,\mathrm{cov}\{\xi_y(t)\xi_z(t)\}$	(3.2.35)
$\frac{d\,\mathrm{cov}\{v(t)\xi_z(t)\}}{dt} = -\left(\gamma+\frac{1}{\varepsilon}\right)\mathrm{cov}\{v(t)\xi_z(t)\} + \Omega\,\mathrm{cov}\{w(t)\xi_z(t)\} + c\,\mathrm{cov}\{\xi_y(t)\xi_z(t)\}$	(3.2.36)
$\frac{d\,\mathrm{cov}\{\xi_y(t)\xi_z(t)\}}{dt} = -\frac{2\,\mathrm{cov}\{\xi_y(t)\xi_z(t)\}}{\varepsilon}$	(3.2.37)

Table 3.4: Third system of o.d.e's for the 2D problem.

$\frac{d\,\mathrm{cov}\{y(t)v(t)\}}{dt} = -\gamma\,\mathrm{cov}\{y(t)v(t)\} + \Omega\,\mathrm{cov}\{y(t)v(t)\} + c\,\mathrm{cov}\{y(t)\xi_y(t)\} + \sigma_v^2(t)$	(3.2.38)
$\frac{d\,\mathrm{cov}\{y(t)w(t)\}}{dt} = -\gamma\,\mathrm{cov}\{y(t)w(t)\} - \Omega\,\mathrm{cov}\{y(t)v(t)\} + c\,\mathrm{cov}\{y(t)\xi_z(t)\} + \mathrm{cov}\{v(t)w(t)\}$	(3.2.39)
$\frac{d\,\mathrm{cov}\{z(t)v(t)\}}{dt} = -\gamma\,\mathrm{cov}\{z(t)v(t)\} + \Omega\,\mathrm{cov}\{z(t)w(t)\} + c\,\mathrm{cov}\{z(t)\xi_y(t)\} + \mathrm{cov}\{v(t)w(t)\}$	(3.2.40)
$\frac{d\,\mathrm{cov}\{z(t)w(t)\}}{dt} = -\gamma\,\mathrm{cov}\{z(t)w(t)\} - \Omega\,\mathrm{cov}\{z(t)v(t)\} + c\,\mathrm{cov}\{z(t),\xi_z(t)\} + \sigma_w^2(t)$	(3.2.41)
$\frac{d\sigma_v^2(t)}{dt} = -2\gamma\sigma_v^2(t) + 2\Omega\,\mathrm{cov}\{v(t)w(t)\} + 2c\,\mathrm{cov}\{v(t)\xi_y(t)\}$	(3.2.42)
$\frac{d\sigma_w^2(t)}{dt} = -2\gamma\sigma_w^2(t) - 2\Omega\,\mathrm{cov}\{v(t)w(t)\} + 2c\,\mathrm{cov}\{w(t)\xi_z(t)\}$	(3.2.43)
$\frac{d\,\mathrm{cov}\{v(t)w(t)\}}{dt} = -2\gamma\,\mathrm{cov}\{v(t)w(t)\} + \Omega\left(\sigma_w^2(t) - \sigma_v^2(t)\right) + c\,\mathrm{cov}\{w(t)\xi_y(t)\} + c\,\mathrm{cov}\{v(t)\xi_z(t)\}$	(3.2.44)

Table 3.5: Final system of o.d.e's for the 2D problem.

$\frac{d\sigma_y^2(t)}{dt} = 2\,\mathrm{cov}\{y(t)v(t)\}$	(3.2.45)
$\frac{d\sigma_z^2(t)}{dt} = 2\,\mathrm{cov}\{z(t)w(t)\}$	(3.2.46)
$\frac{d\,\mathrm{cov}\{y(t)z(t)\}}{dt} = \mathrm{cov}\{y(t)w(t)\} + \mathrm{cov}\{z(t)v(t)\}$	(3.2.47)

Table 3.6: Solution of the 1D problem.

$\sigma_x^2(t) = c^2\left\{4a^2e^{-(1/\varepsilon+\gamma)t} - \left(e^{-2\gamma t} + a^3e^{-2t/\varepsilon}\right)(a+1) - 4\left(e^{-\gamma t} - a^2e^{-t/\varepsilon}\right)\left(a^2-1\right)\right.$ $\left.-(a-1)^2\left[3 + a(5+3a) - 2\gamma(1+a)t\right]\right\} / \left[2\gamma^3(a-1)\left(a^2-1\right)\right]$	(3.2.48)
$\sigma_u^2(t) = c^2\,\frac{-(1+a)e^{-2\gamma t} + 4ae^{-(1/\varepsilon+\gamma)t} + (a-1)^2 - ae^{-2t/\varepsilon}(1+a)}{2\gamma(a-1)\left(a^2-1\right)}$	(3.2.49)
$\sigma_{\xi_x}^2(t) = \frac{1}{2\varepsilon}\left(1 - e^{-2t/\varepsilon}\right)$	(3.2.50)
$\mathrm{cov}\{x(t)u(t)\} = c^2\left[e^{-\gamma t} - ae^{-t/\varepsilon} + (a-1)\right]^2 / \left[2\gamma^2(a-1)^2\right]$	(3.2.51)
$\mathrm{cov}\{u(t)\xi_x(t)\} = \frac{c}{2}\left[1 - 2e^{-(1/\varepsilon+\gamma)t} - a + e^{-2t/\varepsilon}(a+1)\right] / \left(1-a^2\right)$	(3.2.52)
$\mathrm{cov}\{x(t)\xi_x(t)\} = c\left[a(a-1) + a(1+a)e^{-2t/\varepsilon} + 2e^{-t/\varepsilon}\left(1-a^2\right) - 2e^{-(1/\varepsilon+\gamma)t}\right] / \left[2\gamma\left(a^2-1\right)\right]$	(3.2.53)

Table 3.7: Solution of the 2D problem.

$\sigma_y^2(t)=\sigma_z^2(t)=-c^2\left\{e^{-2\gamma t}\left[\gamma^2+\Omega^2\right]\left[(1+a)^2+d^2\right]+ae^{-2t/\varepsilon}\left[a\gamma+d\Omega\right]^2\left[(1+a)^2+d^2\right]\right.$ $-4ae^{-t/\varepsilon}\left[a\gamma+d\Omega\right]\left[\gamma(a-1)+d\Omega\right]\left[(1+a)^2+d^2\right]+\left[(a-1)^2+d^2\right]\left[-\Omega^2+\gamma^2\left(3+8a+8a^2+3a^3\right)\right.$ $\left.+\Omega\gamma\left(8ad+6a^2d+3d^3\right)-2\gamma\left(\gamma^2+\Omega^2\right)\left((1+a)^2+d^2\right)t\right]+4\gamma\left[e^{-\gamma t}\left[(1+a)^2+d^2\right]\right.$ $\left[(\gamma(a-1)-d\Omega)\cos(\Omega t)+(1-2a)\Omega\sin(\Omega t)\right]+e^{-(1/\varepsilon+\gamma)t}\left(a^2+d^2\right)$ $\left.\left.\left[-(\gamma+a\gamma-d\Omega)\cos(\Omega t)+(1+2a)\Omega\sin(\Omega t)\right]\right]\right\}/\left\{2\gamma\left[\gamma^2+\Omega^2\right]^2\left[1+2\left(d^2-a^2\right)+\left(a^2+d^2\right)^2\right]\right\}$	(3.2.54)
$\sigma_v^2(t)=\sigma_w^2(t)=c^2\left\{(1+a)\left[(a-1)^2+d^2\right]-\left(e^{-2\gamma t}+ae^{-2t/\varepsilon}\right)\left[(1+a)^2+d^2\right]\right.$ $\left.+4ae^{-(1/\varepsilon+\gamma)t}\left[(1+a)\cos(\Omega t)-d\sin(\Omega t)\right]\right\}/\left\{2\gamma\left[1+2\left(d^2-a^2\right)+\left(a^2+d^2\right)^2\right]\right\}$	(3.2.55)
$\sigma_{\xi_y}^2(t)=\sigma_{\xi_z}^2(t)=\frac{1}{2\varepsilon}\left(1-e^{-2t/\varepsilon}\right)$	(3.2.56)
$\operatorname{cov}\{v(t)w(t)\}=\operatorname{cov}\{y(t)z(t)\}=\operatorname{cov}\{\xi_y(t)\xi_z(t)\}=0$	(3.2.57)
$\operatorname{cov}\{v(t)\xi_y(t)\}=\operatorname{cov}\{w(t)\xi_z(t)\}=c\left\{(1+a)\left[(a-1)^2+d^2\right]-e^{-2t/\varepsilon}(a-1)\left[(1+a)^2+d^2\right]\right.$ $\left.+2e^{-(1/\varepsilon+\gamma)t}\left[\left(a^2-d^2-1\right)\cos(\Omega t)-2ad\sin(\Omega t)\right]\right\}/\left\{2+4\left(d^2-a^2\right)+2\left(a^2+d^2\right)^2\right\}$	(3.2.58)
$\operatorname{cov}\{v(t)\xi_z(t)\}=-\operatorname{cov}\{w(t)\xi_y(t)\}=c\left\{d\left[\left[(a-1)^2+d^2\right]-\left[(1+a)^2+d^2\right]e^{-2t/\varepsilon}\right]\right.$ $\left.+2e^{-(1/\varepsilon+\gamma)t}\left[2ad\cos(\Omega t)+\left(a^2-d^2-1\right)\sin(\Omega t)\right]\right\}/\left\{2+4\left(d^2-a^2\right)+2\left(a^2+d^2\right)^2\right\}$	(3.2.59)
$\operatorname{cov}\{y(t)\xi_y(t)\}=\operatorname{cov}\{z(t)\xi_z(t)\}=c\left\{\varepsilon(1+a)\left(\gamma^2+\Omega^2\right)\left[(a-1)^2+d^2\right]+\varepsilon e^{-2t/\varepsilon}(a-1)\left(\gamma^2+\Omega^2\right)\right.$ $\left[(1+a)^2+d^2\right]-2e^{-t/\varepsilon}\gamma\left[1+2\left(d^2-a^2\right)+\left(a^2+d^2\right)^2\right]-2e^{-(1/\varepsilon+\gamma)t}$ $\left.\left[\gamma\left(a^2-3d^2-1\right)\cos(\Omega t)+\Omega\left(1-3a^2+d^2\right)\sin(\Omega t)\right]\right\}/\left\{2\left[\gamma^2+\Omega^2\right]\left[1+2\left(d^2-a^2\right)+\left(a^2+d^2\right)^2\right]\right\}$	(3.2.60)
$\operatorname{cov}\{y(t)\xi_z(t)\}=-\operatorname{cov}\{z(t)\xi_y(t)\}=c\left\{\Omega\left(a^2+d^2\right)\left[(a-1)^2+d^2\right]+e^{-2t/\varepsilon}\Omega\left(a^2+d^2\right)\right.$ $\left[(1+a)^2+d^2\right]-2e^{-t/\varepsilon}\Omega\left[1+2\left(d^2-a^2\right)+\left(a^2+d^2\right)^2\right]+2e^{-(1/\varepsilon+\gamma)t}$ $\left.\left[\Omega\left(1-3a^2+d^2\right)\cos(\Omega t)+\gamma\left(1-a^2+3d^2\right)\sin(\Omega t)\right]\right\}/\left\{2\left[\gamma^2+\Omega^2\right]\left[1+2\left(d^2-a^2\right)+\left(a^2+d^2\right)^2\right]\right\}$	(3.2.61)
$\operatorname{cov}\{y(t)v(t)\}=\operatorname{cov}\{z(t)w(t)\}=c^2\left\{e^{-2\gamma t}+e^{-2t/\varepsilon}\left(a^2+d^2\right)-2e^{-t/\varepsilon}\left[a(a-1)+d^2\right]+\left[(a-1)^2+d^2\right]\right.$ $\left.+2\left[\left(-ae^{-(1/\varepsilon+\gamma)t}+e^{-\gamma t}(a-1)\right)\cos(\Omega t)-d\left(-e^{-(1/\varepsilon+\gamma)t}+e^{-\gamma t}\right)\sin(\Omega t)\right]\right\}/\left\{2\left[\gamma^2+\Omega^2\right]\left[(a-1)^2+d^2\right]\right\}$	(3.2.62)
$\operatorname{cov}\{y(t)w(t)\}=-\operatorname{cov}\{z(t)v(t)\}=c^2\left\{-\Omega(1+2a)\left[(a-1)^2+d^2\right]+\Omega\left(e^{-2\gamma t}+2ae^{-t/\varepsilon}\right)\left[(1+a)^2+d^2\right]\right.$ $-2\gamma\left[d\left(e^{-(1/\varepsilon+\gamma)t}\left[1+2a-\left(a^2+d^2\right)\right]+e^{-\gamma t}\left[(1+a)^2+d^2\right]\right)\cos(\Omega t)+\left(ae^{-(1/\varepsilon+\gamma)t}+e^{-\gamma t}(a-1)\left[(1+a)^2+d^2\right]\right.$ $\left.\left.\left.-e^{-(1/\varepsilon+\gamma)t}\left[a^3+(2+a)d^2\right]\right)\sin(\Omega t)\right]\right\}/\left\{2\gamma\left[\gamma^2+\Omega^2\right]\left[1+2\left(d^2-a^2\right)+\left(a^2+d^2\right)^2\right]\right\}$	(3.2.63)

3.3 Numerical implementation

The time interval $(0,t)$ can be replaced with $(t,t+\Delta t)$ in the analytic solutions of section 3.2, provided that analytical expressions for the mean value and variance exist. Then, the exact updating formulas can be used (only written for the x-component here)

$$u(t+dt)=\langle u(t)\rangle+\sigma_u^2(t)N_1(t) \tag{3.2.1}$$

$$x(t+dt)=\langle x(t)\rangle+\frac{\mathrm{cov}\{x(t)u(t)\}}{\sigma_u^2(t)}N_1(t)+\sqrt{\left[\sigma_x^2(t)\right]^2-\frac{\left[\mathrm{cov}\{x(t)u(t)\}\right]^2}{\left[\sigma_u^2(t)\right]^2}}N_2(t) \tag{3.2.2}$$

where $N_1(t)$ and $N_2(t)$ are independent normal random variables with the properties mentioned in Section 3.1, are used to obtain numerical values for $x(t+\Delta t)$ and $u(t+\Delta t)$ and progress in time, step by step [6, 7]. A proof of the relations shown above is straightforward and may be found in [6]. The main shortcoming of this approach is that the analytical expressions must already be available and therefore has little practical value since it can only be used to obtain individual trajectories.

Alternatively, the discretized equations (3.1.2)-(3.1.8) can be directly used to simulate the motion step by step in time (In this work, this technique will be called Direct Simulation, DS). This is a first order approximation and corresponds to a set of Euler integration steps. After realizing several hundreds of simulations, the values of position, velocity and force and their squares are averaged for every time instant in order to obtain the mean values and standard deviation. In one-dimensional problems, where only one random number is needed in every iteration, the second number generated by the Box-Mueller method is stored and used in the next step. This is the main numerical algorithm used in this chapter.

The numerical parameters are the time step Δt and the number of simulations N_R. In order to determine the impact of the time step, a series of tests was performed concerning the auto-correlation function of the stochastic force $\xi_x(t)$ in the case of non-white noise. The numerical values were benchmarked with the analytical ones, while the time step ranged from 10^{-2} down to 10^{-6} and 10^3 simulations were executed ($N_R=10^3$).

Some results are shown in Table 3.8. It is seen that for smaller time intervals the comparison is very good, while for larger Δt it is not possible to obtain some correlations and others are not estimated correctly. This is especially true for smaller values of correlation times ε because in this case white noise is approached and $\phi(\tau)$ is closer to Dirac delta function. The time step also plays an important role due to the fact that the numerical procedure consists of a set of three Euler type integration steps and therefore the results are strongly dependent on the time step. Furthermore, exceedingly large file sizes (about 1.5 Gb for a set of five simulations, their averages and standard deviations) occur when the quantities of interest are stored in every time step. More advanced schemes, such as stochastic Runge-Kutta integration, may be applied in the future.

Table 3.8: Estimation of $\phi(\tau)$ correlation using a variable time step, with $c=1$, $\gamma=1$, $N_R=10^3$.

	Δt	τ 0.0002	0.0005	0.002	0.005	0.02	0.05	0.2	0.5
$\varepsilon=10^{-3}$	10^{-3}	-	-	0.50	-0.26	-0.24	-0.13	-0.02	-0.09
	10^{-4}	426.35	310.84	64.40	2.78	0.11	-0.21	0.29	-0.21
	10^{-5}	411.16	304.15	67.30	3.44	0.18	0.15	-0.34	0.14
	Analytical	409.37	303.27	67.67	3.37	0.00	0.00	0.00	0.00

	Δt	τ 0.0002	0.0005	0.002	0.005	0.02	0.05	0.2	0.5
$\varepsilon=10^{-2}$	10^{-3}	-	-	42.46	30.94	6.39	0.27	-0.04	-0.06
	10^{-4}	49.23	47.76	41.08	30.39	6.80	0.40	-0.04	0.02
	10^{-5}	49.04	47.59	40.96	30.34	6.74	0.35	0.10	0.01
	Analytical	49.01	47.56	40.94	30.33	6.77	0.34	0.00	0.00

	Δt	τ 0.0002	0.0005	0.002	0.005	0.02	0.05	0.2	0.5
$\varepsilon=10^{-1}$	10^{-3}	-	-	4.89	4.74	4.08	3.02	0.67	0.02
	10^{-4}	4.96	4.94	4.87	4.72	4.07	3.01	0.66	0.03
	10^{-5}	4.94	4.93	4.85	4.71	4.05	2.99	0.66	0.07
	Analytical	4.99	4.98	4.90	4.76	4.09	3.03	0.68	0.03

The influence of the number of simulations was also investigated. The mean and variance of position and velocity in the x-direction was calculated with Direct Simulation and compared with the analytic expressions. It is observed in Figured 3.1 that the numerical curves fluctuate around the analytical ones. This characteristic behaviour is inherent in every numerical method for stochastic differential equations and disappears if a larger number of realizations is taken into account. It is seen that, for 10^4 simulations, the analytical and numerical curves eventually coincide. More calculations were performed for this parameter and some results are shown in Figure 3.2. The value of three correlation functions was calculated and the number of simulations didn't seem to affect them significantly after about 1000 realizations. However, since the computational cost for this method is not very high, we have used 10000 realizations for the calculations of this chapter $\left(N_R = 10^4\right)$.

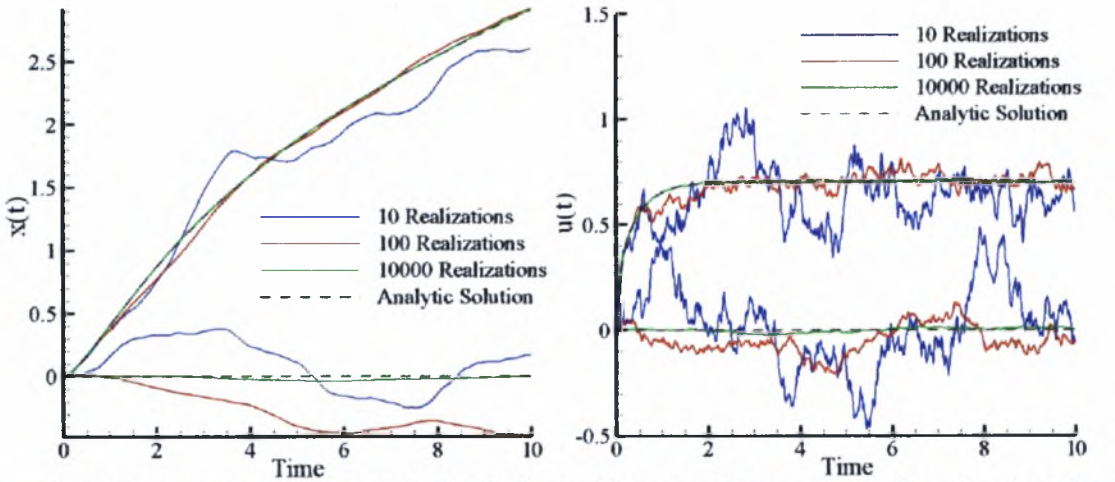

Figure 3.1: Convergence of numerical solution with increasing number of realizations ($c = 1$, $\gamma = 1$, $\varepsilon = 10^{-2}$, $\Delta t = 10^{-3}$).

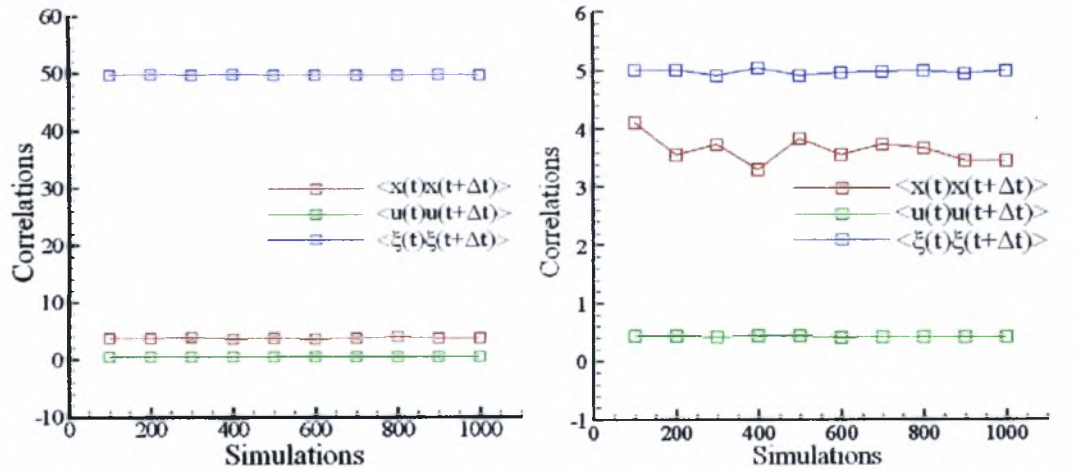

Figure 3.2: Convergence of typical correlation functions with increasing number of simulations ($c = 1$, $\gamma = 1$, $\varepsilon = 10^{-2}$ (left) and $\varepsilon = 10^{-1}$ (right), $\Delta t = 10^{-4}$).

Finally, it was assumed that satisfying accuracy can be achieved faster with single precision simulations. It has been found that it can be used for individual realizations but is inappropriate for the calculation of the standard deviation because the accumulation of round-off errors results in comparable values of $\langle X \rangle^2$ and $\langle X^2 \rangle$. Therefore the standard deviation can not be estimated in some cases and double precision becomes necessary.

Summarizing, the parameters shown in Table 3.9 have been used in the calculations of Section 3.4, unless otherwise stated. These values have also been used for the two dimensional y-z problem.

Table 3.9: Final choice of numerical parameters for extensive Direct Simulation runs.

DS	ε		
	10^{-3}	10^{-2}	10^{-1}
N_R	10000	10000	10000
Δt	10^{-5}	10^{-4}	10^{-4}

3.4 Numerical results

The mean value and standard deviation of the two most important quantities, position and velocity, were calculated numerically and analytically for non-white noise and the results are displayed in Figures 3.3-3.8. Due to the large number of simulations performed, the agreement between analytical and numerical curves is very good in every case examined (maximum relative error is less than 5%). It can be observed that for the time interval examined, the long term behaviour, i.e. $\sigma_x^2(t) \sim t, \sigma_u^2(t) = \text{constant}$, is reached in most cases.

In Figures 3.3-3.5, the effect of the three physical parameters, c, ε and γ, is investigated. It is shown in Figure 3.3 that, for the values of ε examined here, the differences in the estimation of the mean and variance were very small. Therefore, we deduce that this parameter does not play an important role when it takes values on the specific interval and for non-white noise.

In Figure 3.4, it is observed that a change in the noise strength c does not change the results qualitatively. The magnitude of the standard deviation depends proportionally to c, as can be seen from taking the square root of (3.2.48) and (3.2.49). Finally, the

value of γ strongly affects the standard deviation curve, as seen in Figure 3.5. The curvature of the standard deviation curve changes significantly since the maximum velocity is reached in a larger amount of time. This leads to higher velocities and larger position variances.

A representative two-dimensional case is also shown in Figure 3.6. It is seen that the variation of c changes the standard deviation curves similarly to the one dimensional case. It must be noted that the presence of oscillations in this case is due to the transversal magnetic field. The influence of these parameters will be commented again in Chapter 4, where results obtained by a different method will be presented.

Several simulations are also plotted in Figures 3.7-3.8. In Figure 3.7 the exact updating formulas with a fixed sequence of random numbers are used to simulate several instances for different values of ε. The mean ± one standard deviation curves are also drawn. It is seen that, as the correlation time becomes smaller, the curves retain the same form but with a lower magnitude. Finally, the discretized equations have been used in Figure 3.8 to track the trajectory of the particle in each time step when $c=1, \varepsilon=10^{-2}$ and γ takes the values $10^{-2}, 10^{-1}, 1$. It is seen that the displacement and velocity become larger as the friction parameter decreases.

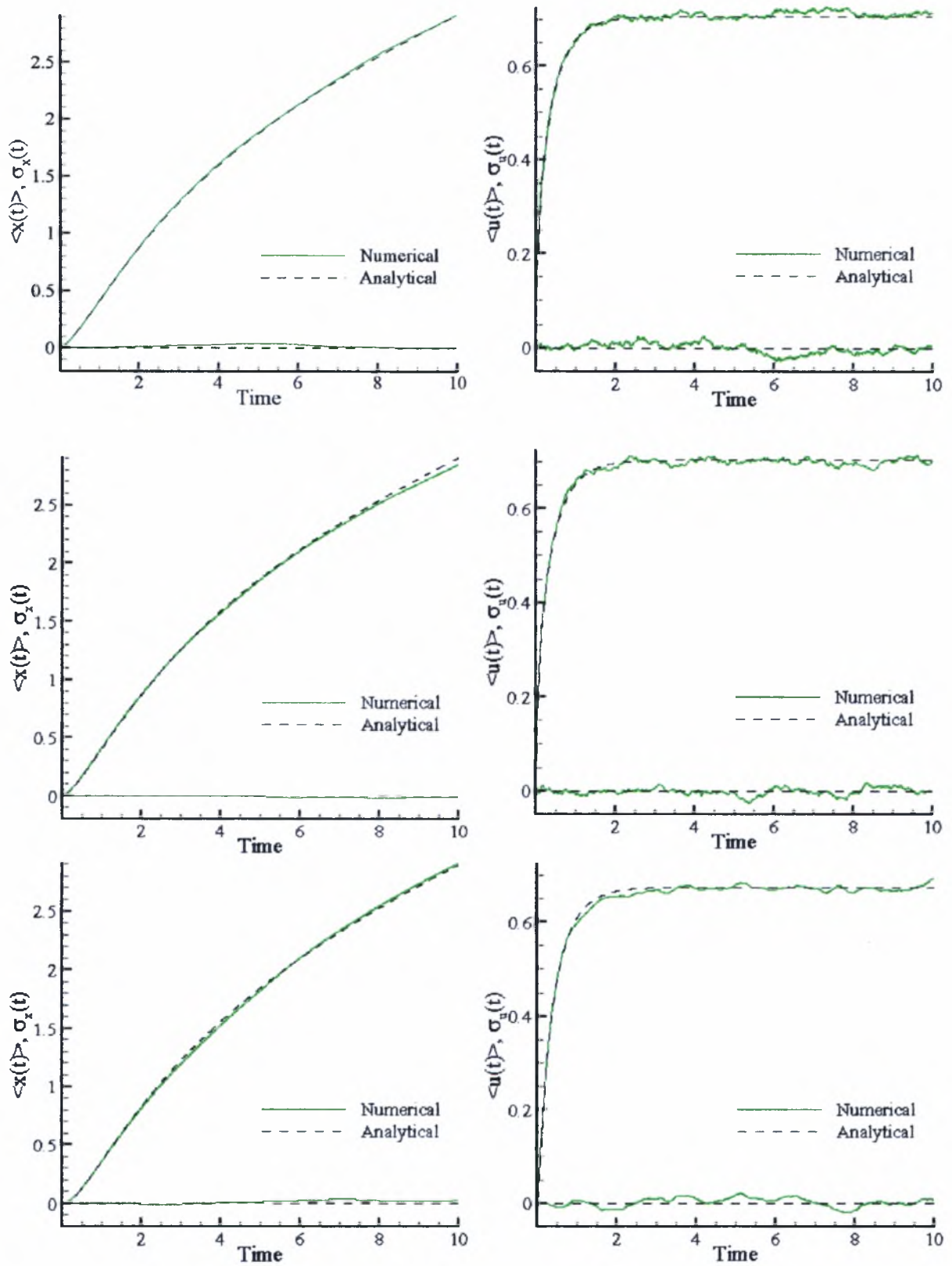

Figure 3.3: Mean and standard deviation of position and velocity for the 1D problem, with $c=1, \gamma=1$, $\varepsilon=10^{-3}$ (up), $\varepsilon=10^{-2}$ (middle), $\varepsilon=10^{-1}$ (down).

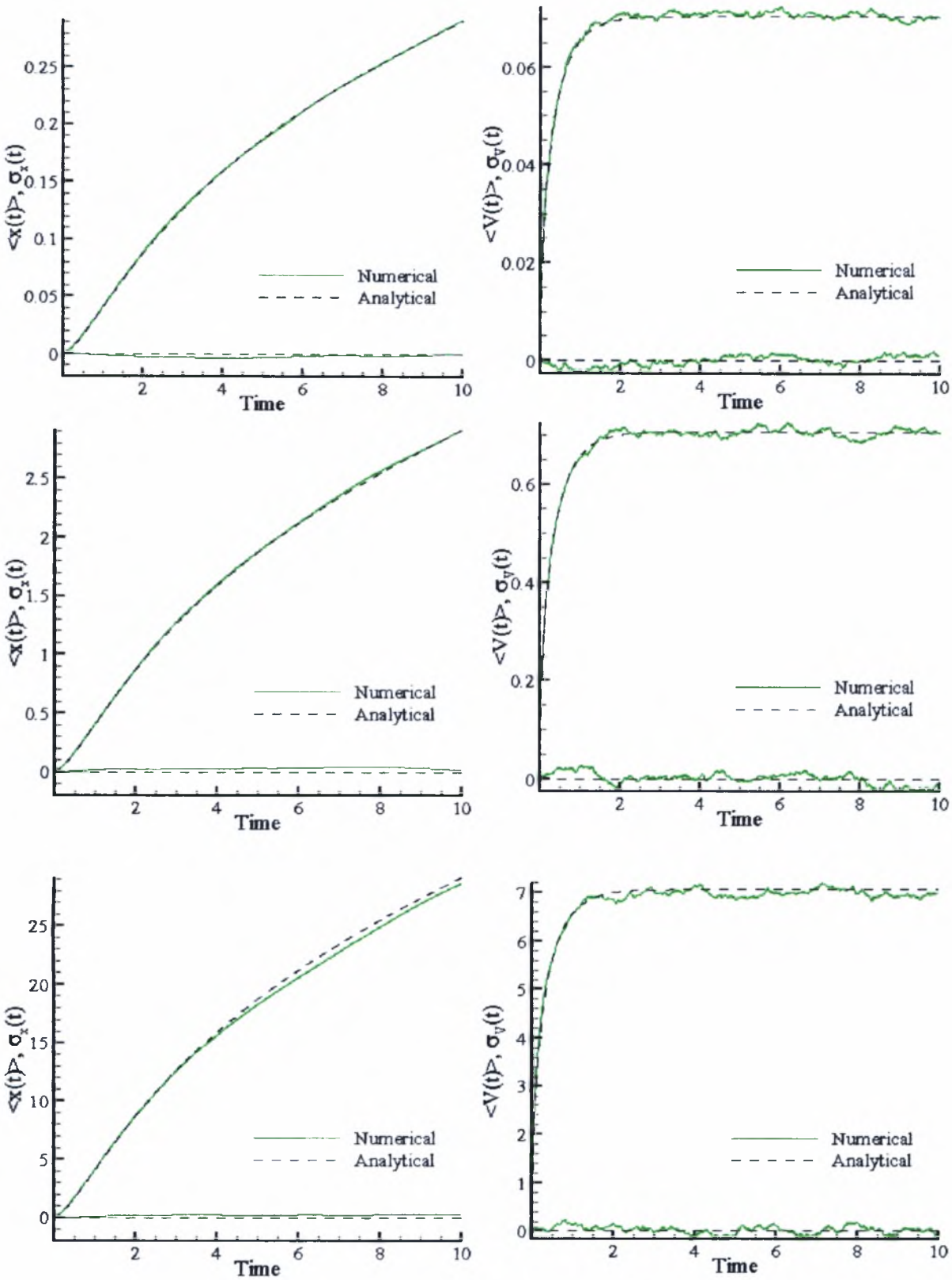

Figure 3.4: Mean and standard deviation of position and velocity for the 1D problem, with $\varepsilon = 10^{-3}, \gamma = 1$, $c = 0.1$ (up), $c = 1$ (middle), $c = 10$ (down).

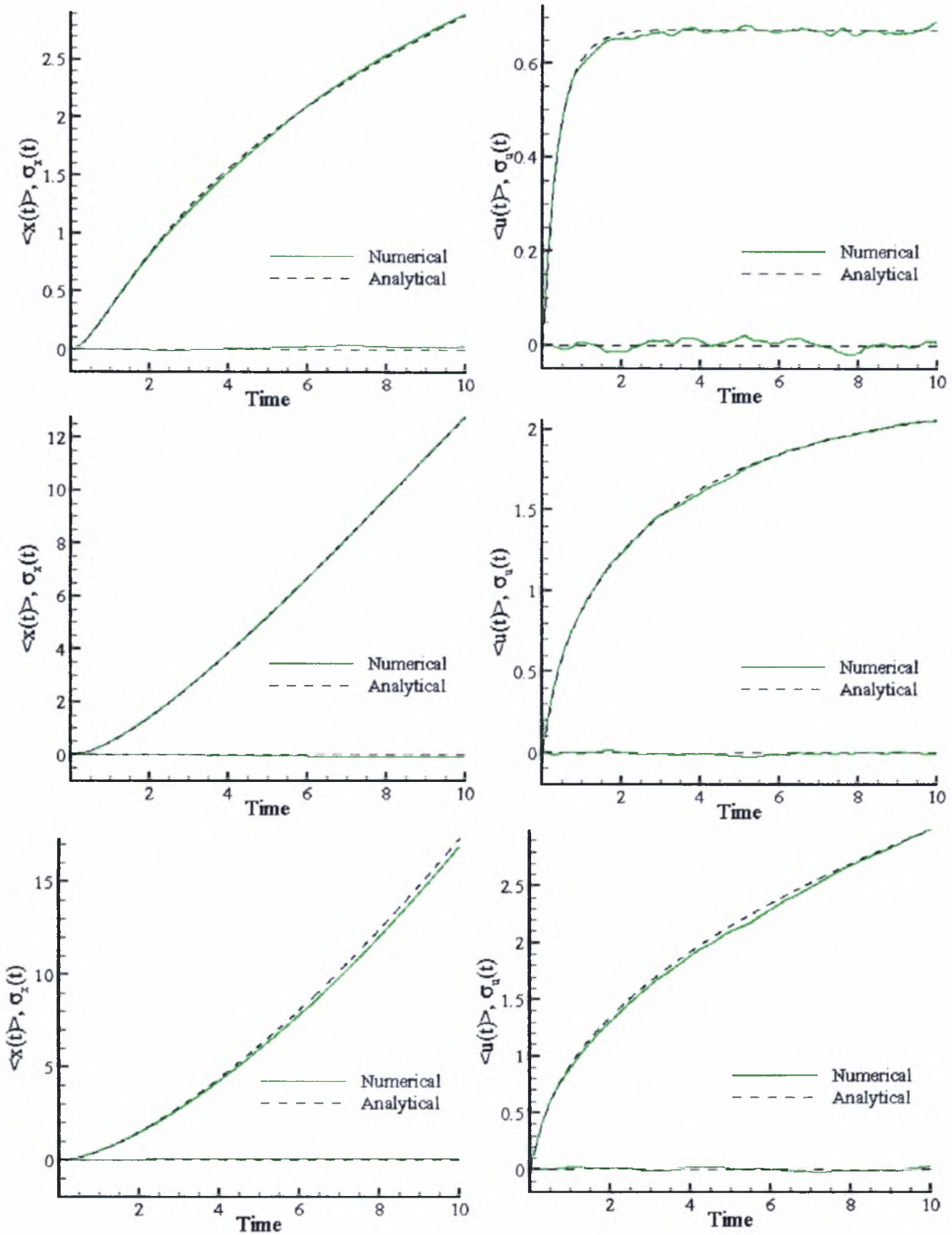

Figure 3.5: Mean and standard deviation of position and velocity for the 1D problem, with $c=1$, $\varepsilon=10^{-1}$, $\gamma=1$ (up), $\gamma=0.1$ (middle), $\gamma=0.01$ (down).

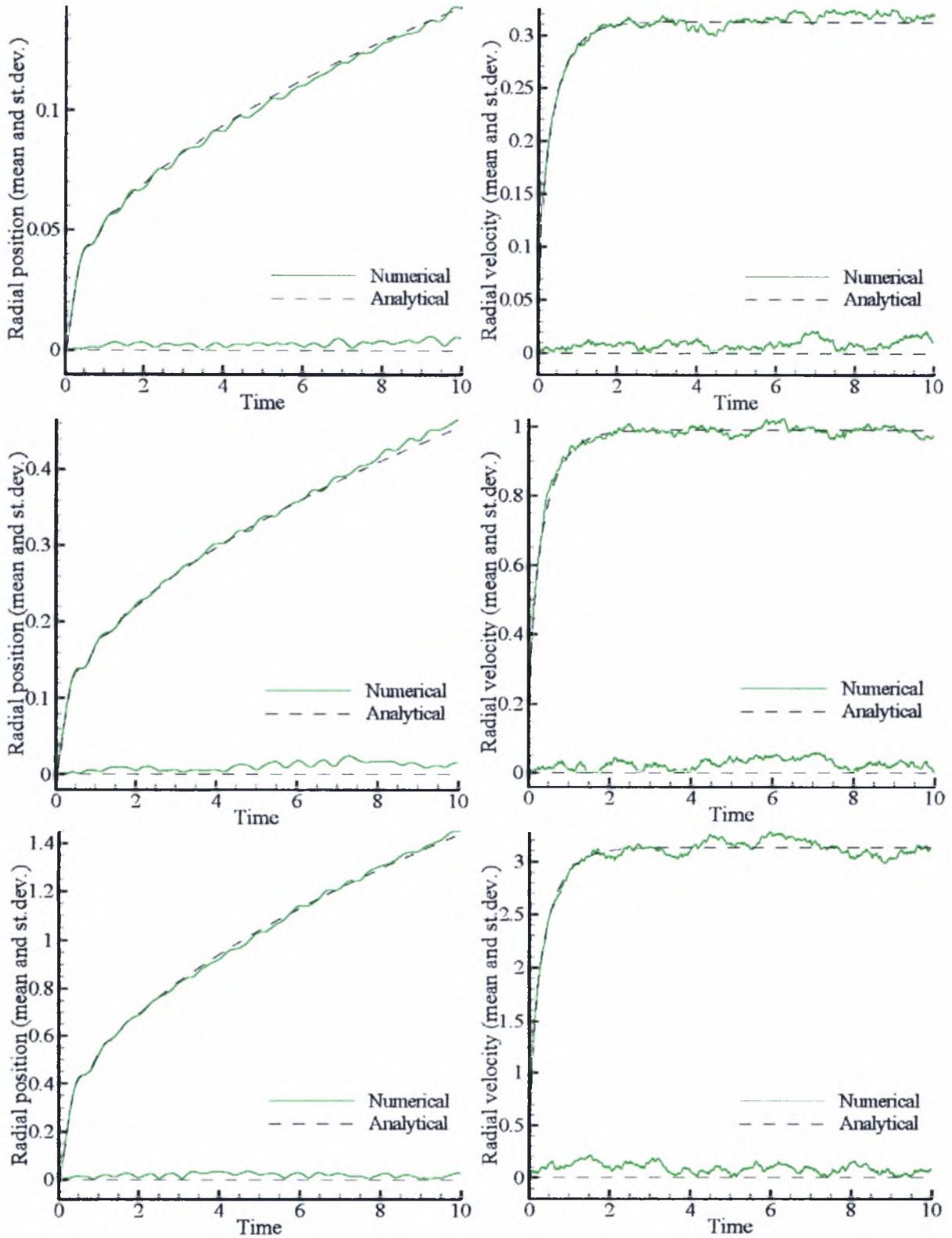

Figure 3.6: Mean and standard deviation of position and velocity for the 2D problem, with $\varepsilon = 10^{-2}$, $\gamma = 1$, $\Omega = 10$, $c = 0.1$ (up), $c = 1$ (middle), $c = 10$ (down).

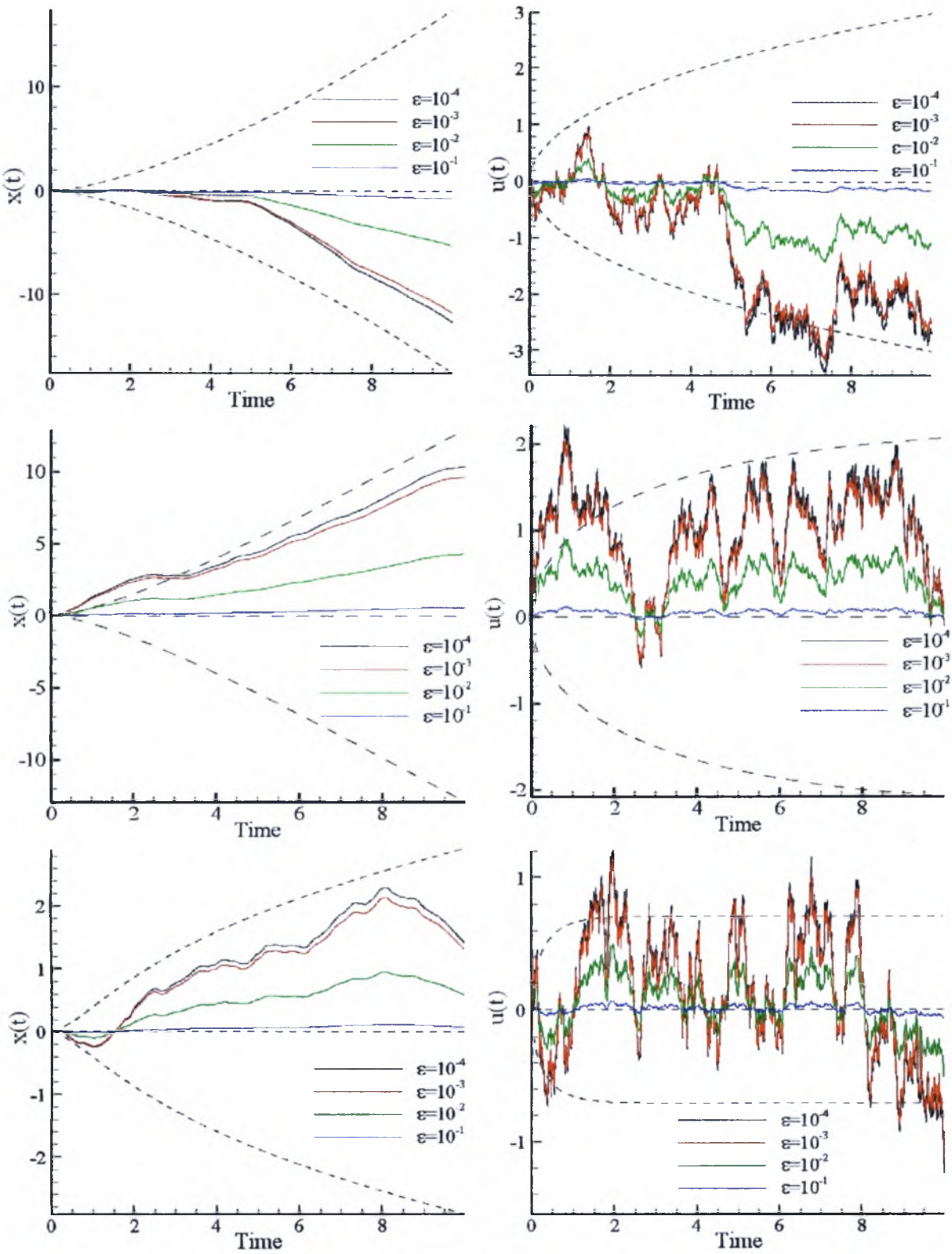

Figure 3.7: Realizations using the exact updating formulas, with $c=1$, $\gamma=10^{-2}$ (up), $\gamma=10^{-1}$ (middle), $\gamma=1$ (down).

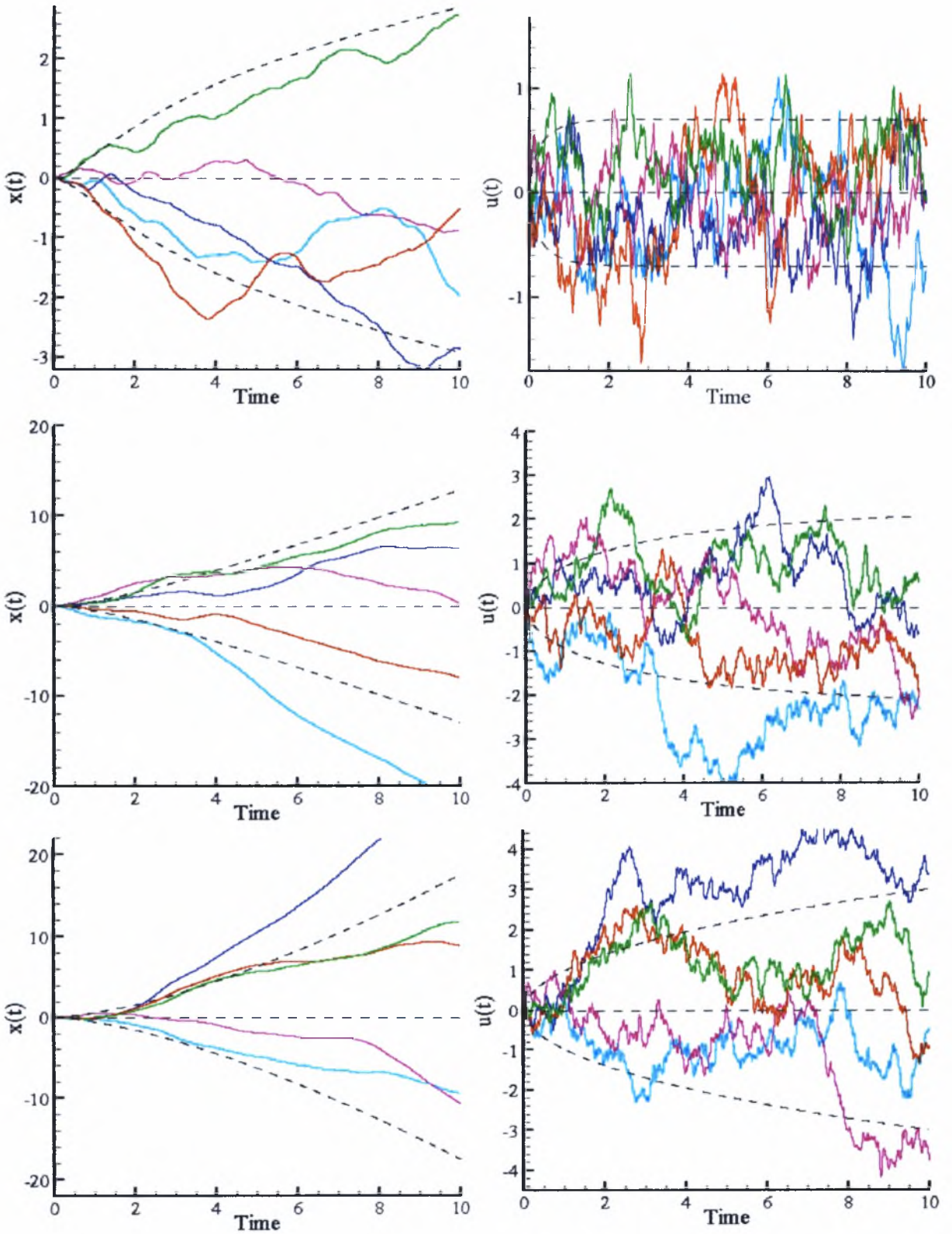

Figure 3.8: Realizations using the discretized form of equations, with $c=1$, $\varepsilon=10^{-2}$, $\gamma=1$ (up), $\gamma=10^{-1}$ (middle) and $\gamma=10^{-2}$ (down).

Chapter 4 – Fourier series expansion

4.1 Introduction

The stochastic force term can also be obtained in a different way. It is approximated by a Fourier cosine series which depends on the noise's spectral energy density (SED) and the discretization of the frequency space. This approach has been used for a long time [27] and is known to have many advantages [23]. Any type of noise (including white, coloured, Gaussian and Lorentzian) can be simulated by substituting the appropriate SED, without the need for an explicit equation for the time evolution of the force. The result is an ergodic, Gaussian process and a substantial portion of the "tail" is reproduced, a characteristic which is missing when the Box-Mueller algorithm is used. This was the case in the calculations of Chapter 3. The time step can also be at least one order of magnitude larger than in previous methods.

4.2 Series expansion of the force term

The noise term, following Billah and Shinozuka [23], is approximated by the Fourier series

$$\xi(t) = \sqrt{2}\sum_{n=1}^{N} \sqrt{2S_{\xi}(\omega_n)\Delta\omega}\cos(\omega_n t + \Phi_n). \qquad (4.2.1)$$

Each value of frequency is $\omega_n = n\Delta\omega$, where $\Delta\omega$ is the frequency step. The step depends on the maximum frequency considered $\omega_{\max}$ and the number of series terms N according to the equation

$$\Delta\omega = \omega_{\max} / N \qquad (4.2.2)$$

The $\omega_{\max}$ frequency parameter is chosen according to

$$\omega_{\max}\varepsilon = K \qquad (4.2.3)$$

where the value of the constant K determines the included percentage of the spectral energy density (SED) of the noise $S_{\xi}(\omega_n)$, which in turn depends on its correlation function. Finally, the Φ_n angles are random, mutually independent and uniformly

distributed in $[0, 2\pi]$. This is a special case of the general expression appearing elsewhere [46, 47], also containg random coefficients.

The definition of spectral energy density (SED) is

$$S(\omega) = \frac{1}{\pi} \int_0^{\infty} \phi(\tau) \cos(\omega\tau) d\tau \tag{4.2.4}$$

where the correlations $\phi(|\tau|)$ are chosen according to expressions (1.8)-(1.11). Thus, the following expressions are derived

$$S_{white}(\omega) = \frac{1}{2\pi} \tag{4.2.5}$$

$$S_{coloured}(\omega) = \frac{1}{2\pi} \frac{1}{1+\varepsilon^2\omega^2} \tag{4.2.6}$$

$$S_{Gaussian}(\omega) = \frac{1}{2\pi} e^{-(\varepsilon\omega)^2/4} \tag{4.2.7}$$

$$S_{Lorentzian}(\omega) = \frac{1}{2\pi} e^{-\varepsilon\omega}. \tag{4.2.8}$$

The SED curves are plotted in Figure 4.1. It is seen that as the correlation time ε approaches zero, all noise spectra approach the white noise spectrum which is constant for any frequency.

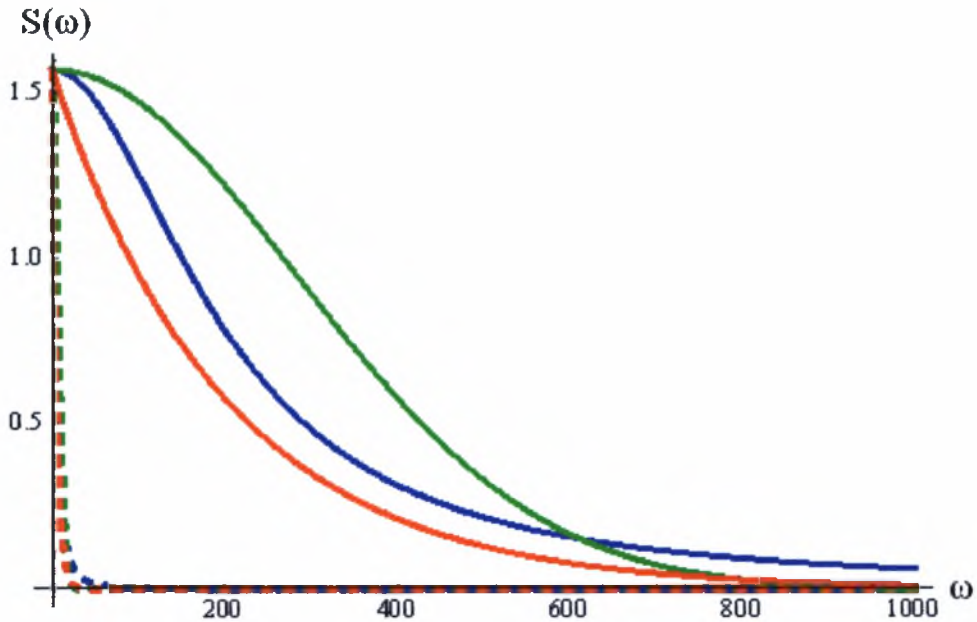

Figure 4.1: SED of three noises (coloured: blue, Gaussian: green, Lorentzian: red) and two correlation times (dashed: $\varepsilon = 0.2$, continuous: $\varepsilon = 0.005$).

4.3 Numerical simulation

To perform simulations with this approach, equations (3.1.2)-(3.1.7) are used again for the estimation of position and velocity and the force component is calculated by (4.2.1). The results depend on the selection of the numerical parameters.

The number of series terms N and the maximum frequency parameter ω_{max} are two parameters which did not exist in previous methods. The main disadvantage of the Fourier Series method is that it demonstrates a periodic behaviour in fixed intervals of duration $T = 2\pi / \Delta\omega$. Therefore, $\Delta\omega$ must be significantly low (N must be high enough) in order to simulate non-periodic motion. To calculate the required number of terms, we take into account (4.2.2) and (4.2.3) and obtain

$$N = 2T / (K\pi\varepsilon) \qquad (4.2.9)$$

If N is smaller, the periodic trend is apparent in the simulations, as shown in Figure 4.2. This feature causes crucial difficulties for very small ε (e.g. 10^{-4}) since a prohibitively large number of terms is required (~$1.7\text{x}10^5$ for a time interval of 10 time units). Furthermore, numerical tests have indicated that to calculate correctly the standard deviation, the actual number required is at least ten times the value of N obtained by (4.2.9). Using a smaller amount of terms leads to a discrepancy in the numerical standard deviation curve (Figure 4.3). In [24] it is argued that since the SED is almost constant over a wide range of frequencies for small ε, i.e. nearly white noise conditions, a small number of terms is adequate to obtain reasonably accurate results. However, this is not the case in our calculations, where as it pointed before a large number of terms is required.

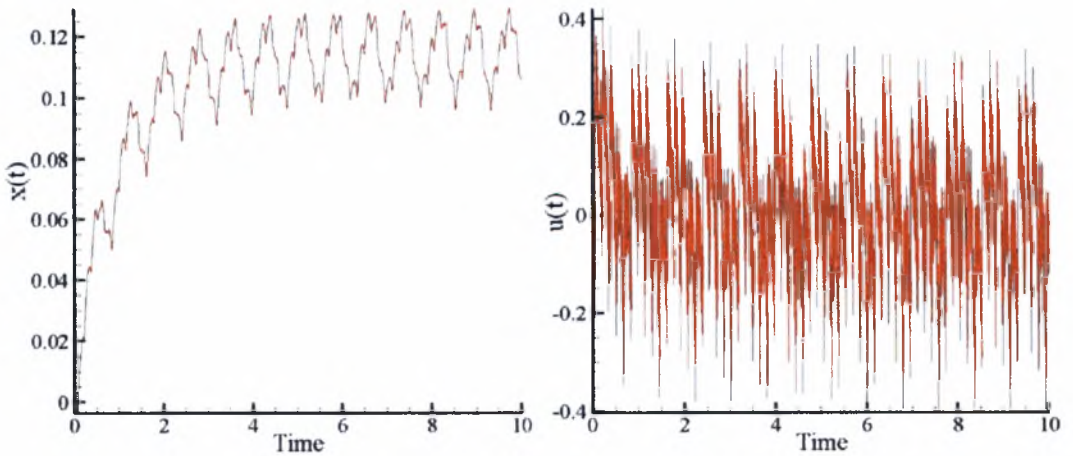

Figure 4.2: Periodic behaviour in position(left) and velocity(right), with $c = 1$, $\gamma = 1$, $N = 5000$ and $\varepsilon = 10^{-4}$

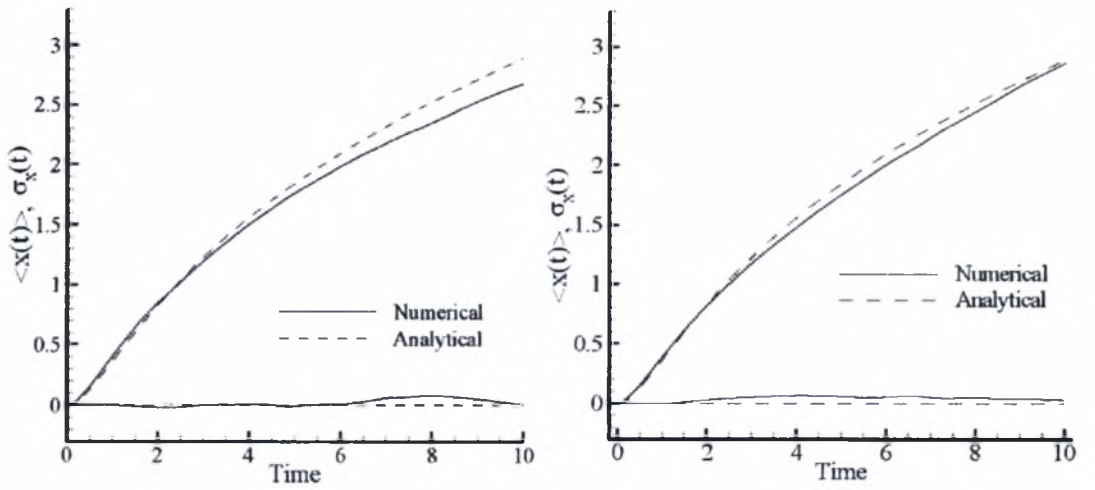

Figure 4.3: Discrepancy in the standard deviation of position (left: $N = 12 \cdot 10^3$) and better agreement with more terms (right: $N = 18 \cdot 10^3$) ($c = 1$, $\gamma = 1$ and $\varepsilon = 10^{-1}$).

Additionally, the time step and number of realizations are also important parameters of our computational scheme. The earlier comments regarding the number of simulations are also valid here. However, the computational cost is much larger in this case since, instead of determining the force by generating a random number, a large number of series terms must be added together in every time step. Therefore, by taking into consideration the computational effort, we deduce that $N_R = 1000$ leads to satisfying accuracy with reasonable computational times.

The behaviour of the scheme relative to the time step is also similar to other methods, except that larger values of Δt could be used. This happens because only two Euler integration steps take place for the position and velocity through equations (3.1.2)-(3.1.7), while the force is modelled by the Fourier series, which is independent of Δt. Time interval related discrepancies occur mostly for small values of γ and manifest as an overestimated standard deviation. In Figure 4.4, it is observed that the numerically predicted standard deviation of position largely diverges from the analytically calculated curve. The divergence in this case is due to the large time step in conjunction with a small value of the correlation parameter ε. The combination of sparse time discretization with a small friction parameter produces similar results, as seen in Figure 4.5, because even a small error in the estimation of the force may cause a significant displacement of the particle. The oscillating behaviour in this case is due to the fact that in this case, two-dimensional motion in a magnetic field is described.

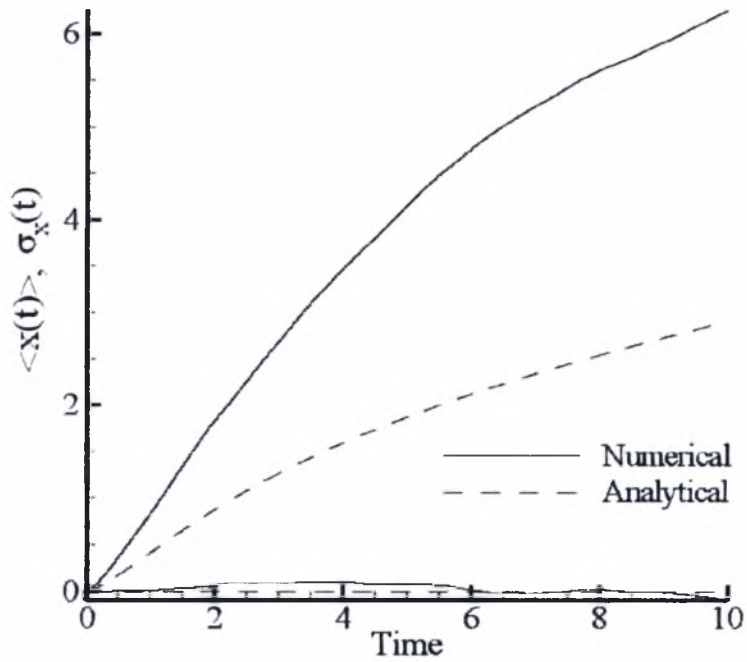

Figure 4.4: Discrepancy in the estimation of the standard deviation of position due to large time step and small ε (1D, $c=1$, $\gamma=1$, $N=1.8\cdot10^{6}$, $\varepsilon=10^{-4}$, $\Delta t=10^{-3}$).

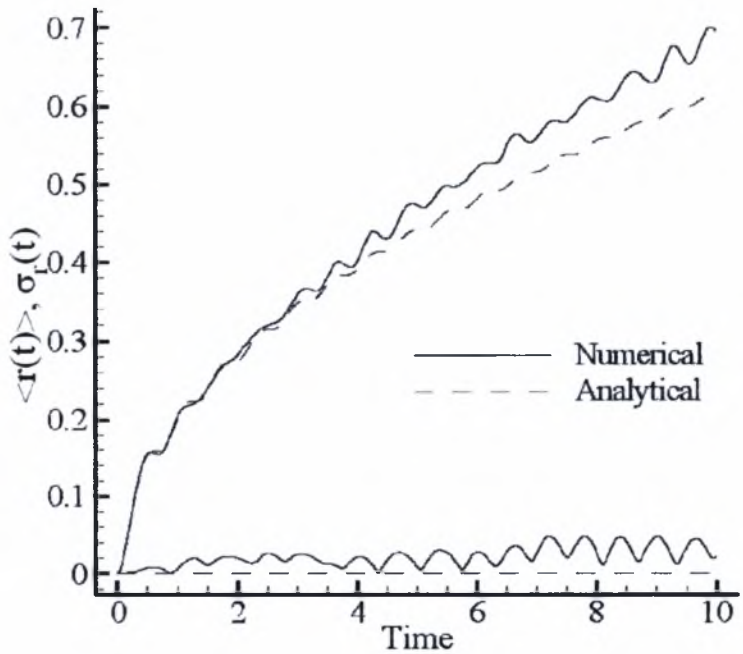

Figure 4.5: Discrepancy in the estimation of the standard deviation of position due to large time step and small γ (2D, $c=1$, $\gamma=10^{-2}$, $\Omega=10$, $N=1.8\cdot10^{5}$, $\varepsilon=10^{-3}$, $\Delta t=10^{-3}$).

The set of parameters providing accurate results has been chosen based on numerical experiments and is shown in Table 4.1. These values have been used in the calculations in the following Figures. The maximum frequency ω_{max} was selected according to (4.2.3), with $K = 10$. This value establishes that about 94% of the total spectral energy density curve is included.

Table 4.1: Final choice of numerical parameters for Fourier Series simulation

FS	ε		
	10^{-3}	10^{-2}	10^{-1}
N	180000	18000	18000
N_R	1000	1000	1000
ω_{max}	10000	1000	100
Δt	10^{-4}	10^{-3}	10^{-3}

These parameters have been used to calculate the correlation function $\phi(|\tau|)$ of coloured noise numerically and the results are shown in Figure 4.6. The continuous line corresponds to the analytical expression (1.9) and the dots represent the numerical approximation. It is seen that the agreement is very good for the parameters used here.

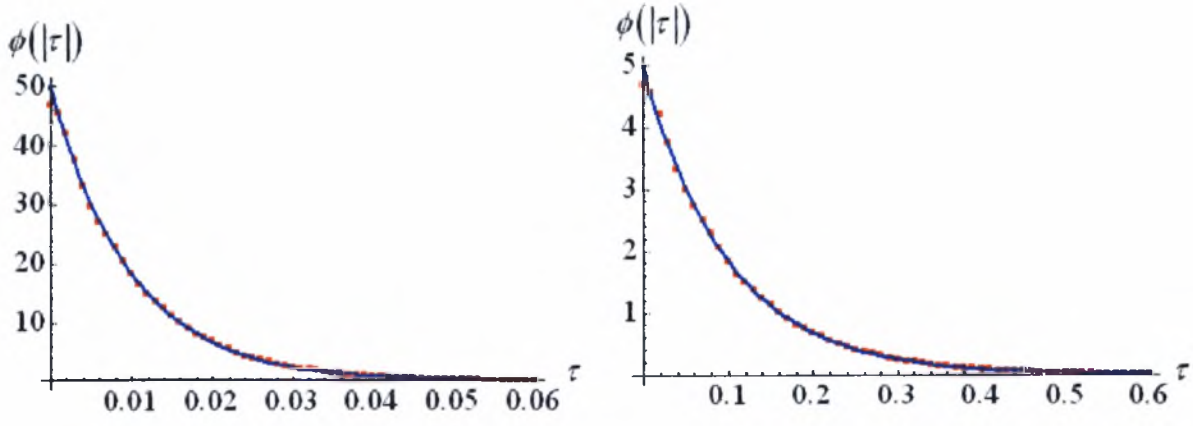

Figure 4.6: Correlation function $\phi(|\tau|)$ of coloured noise. Analytical curve (continuous line) and numerical approximation (dots) for $\varepsilon = 10^{-2}$ (left) and $\varepsilon = 10^{-1}$ (right).

A complete comparison between numerical results, obtained by the present analysis, and analytical results, obtained in Chapter 2, has been performed to benchmark the accuracy of the computational codes. The average and standard deviation of position

and velocity were estimated analytically and numerically and, taking into account the moderate number of simulations, the agreement is considered good in most cases. It is also observed that by increasing N, N_R and $\omega_{\max}$ and reducing the time interval the error is monotonically reduced. The maximum value of the relative error is about 10%.

It should be noted that the agreement depends significantly on the particular set of simulations. It is possible to repeat the calculations with a different random seed and obtain better (or worse) agreement. These conclusions are also valid for the two-dimensional motion.

4.4 Results and discussion

The results on the influence of every physical parameter on the mean and standard deviation of the particle's position and velocity are shown here. All previously mentioned noises for one-dimensional and two-dimensional motion have been considered. Concerning the stochastic term, the most usual choice in previous works was white noise. However, this hypothesis may not always be appropriate for the description of particle motion. Therefore, in order to have an idea about how appropriate this assumption is, the analytical white noise curves have also been added in the Figures. The symbol $\sigma_A = \sqrt{R_{AA}}$ has been used below to denote the standard deviation of the quantity A, with A being the one dimensional position x or velocity u, or the two dimensional position $r = \sqrt{y^2 + z^2}$ or radial velocity $V = \sqrt{v^2 + w^2}$.

The parameter c^2 is equal to 0.1, 1 and 10, the friction factor γ equal to $10^{-2}, 10^{-1}, 1$ and ε equal to $10^{-3}, 10^{-2}, 10^{-1}$. The values of γ are selected to be low because we are interested in the behaviour of the motion of charged particles in low-friction mediums, like fusion plasma. Results with such values of γ have not previously appeared in the literature.

The behaviour of the system in a variation of the value of c is examined in Figure 4.7. It is observed that the results do not change qualitatively but are only amplified or reduced accordingly. In fact, the quantities of interest seem to grow or diminish

proportionally to c. All curves are in good agreement due to the small value of correlation time.

On the contrary, the influence of γ is very apparent in Figure 4.8, where the standard deviation curve changes significantly, that is, the curvature is reversed. The curves also come closer to the white noise curve as the friction parameter is reduced. The magnitude of velocity is also increased because of the decreased amount of friction and larger times are required to obtain the long term behaviour, as predicted by the analytical results of Chapter 2.

In Figure 4.9, the influence of ε is examined while keeping other parameters constant. It is seen that for the values of correlation times studied here and for coloured noise, the results do not differ significantly. The curves remain qualitatively the same and also very close to each other. This is in agreement with Figures 2.2 and 2.3. This is not the case for the Lorentzian noise, as seen in Figure 4.10. We can see that if we examine a small time interval the divergence from white noise results is apparent and also in agreement with previous results.

The two-dimensional results and in particular the variance of radial position are of larger practical interest because of their application in nuclear fusion. It is attempted to determine how fast do plasma particles and/or impurities that travel along with them diffuse perpendicularly to the magnetic lines. As it is seen in Figure 4.11, the strength of the noise does not affect the curves qualitatively. On the other hand, a change of the friction factor γ did not have the same effect as in the one-dimensional problem, that is, the curvature of the standard deviation did not reverse, as it is seen in Figure 4.12. An important observation is that for smaller friction factors the effect of the oscillations due to the magnetic field become more apparent on the standard deviation curve.

In Figure 4.13, the mean and standard deviation of the radial position is also plotted against time as ε is varied. The oscillations owe their presence to the magnetic field and diminish as we increase the value of ε. Finally, the influence of the magnetic field through the Ω parameter is seen in Figure 4.14. For weak magnetic fields the oscillations occur with a low frequency and can be clearly observed. As the magnetic field becomes stronger and $\Omega = 100$, the oscillations are repeated so frequently that they

can not be easily distinguished (they do exist in the average in the two bottom pictures of Figure 4.14 but they are too small to see).

Some individual trajectories are shown in Figures 4.15 and 4.16. For large correlation times the particle moves in a smaller range and the trajectory nearly diminishes to zero displacement. The low γ, high ε curves tend to be smoother than the rest, in the case of both velocity and position. In Figure 4.16 some trajectories in two dimensions are shown. The circular motion is due to the magnetic field and is more noticeable for small values of the friction term γ. The trajectory is also longer in this case due to the larger velocity magnitude.

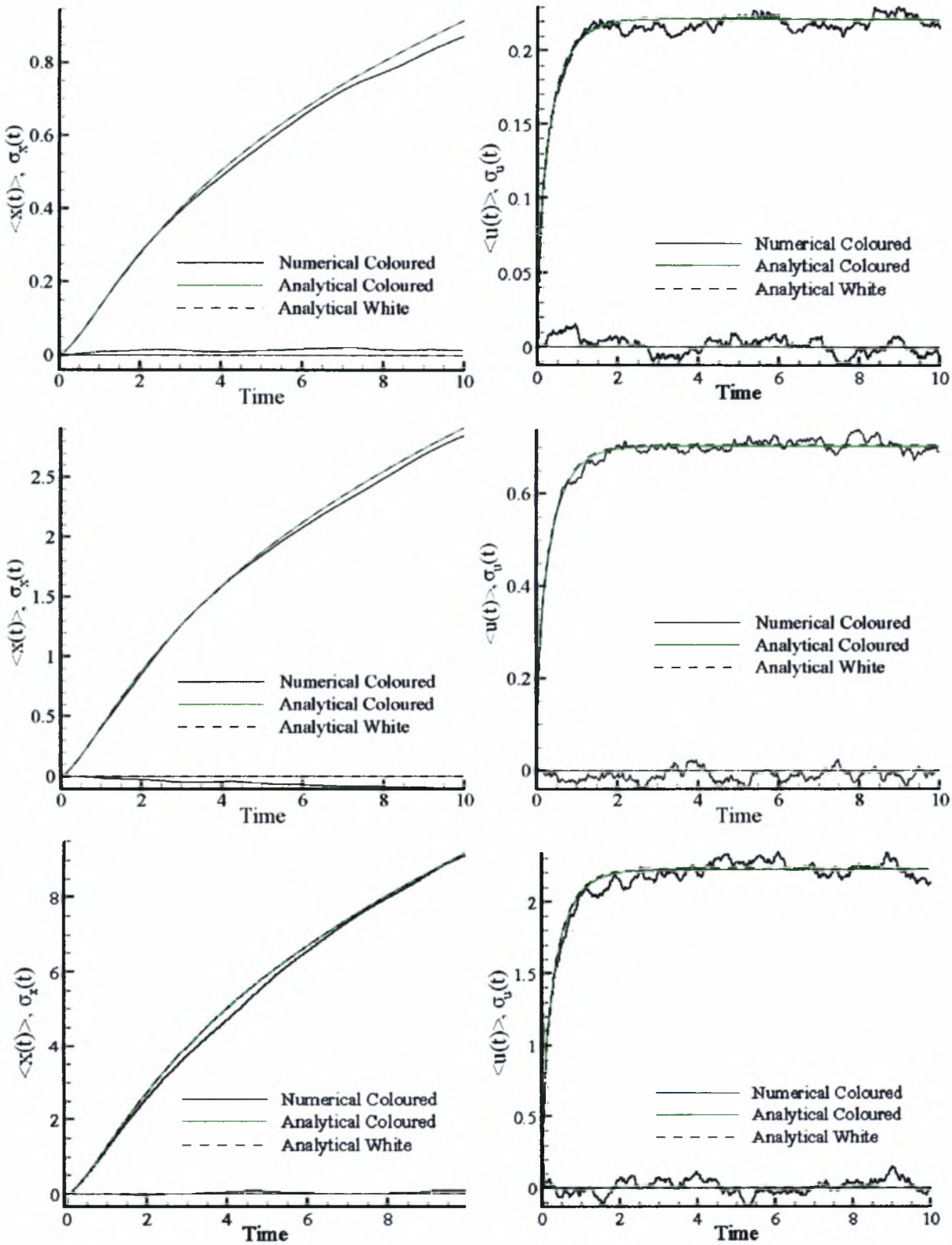

Figure 4.7: Mean and standard deviation of position and velocity for the 1D coloured noise problem, with $\gamma = 1$, $\varepsilon = 10^{-3}$, $c^2 = 10^{-1}$ (up), $c^2 = 1$ (middle), $c^2 = 10$ (down).

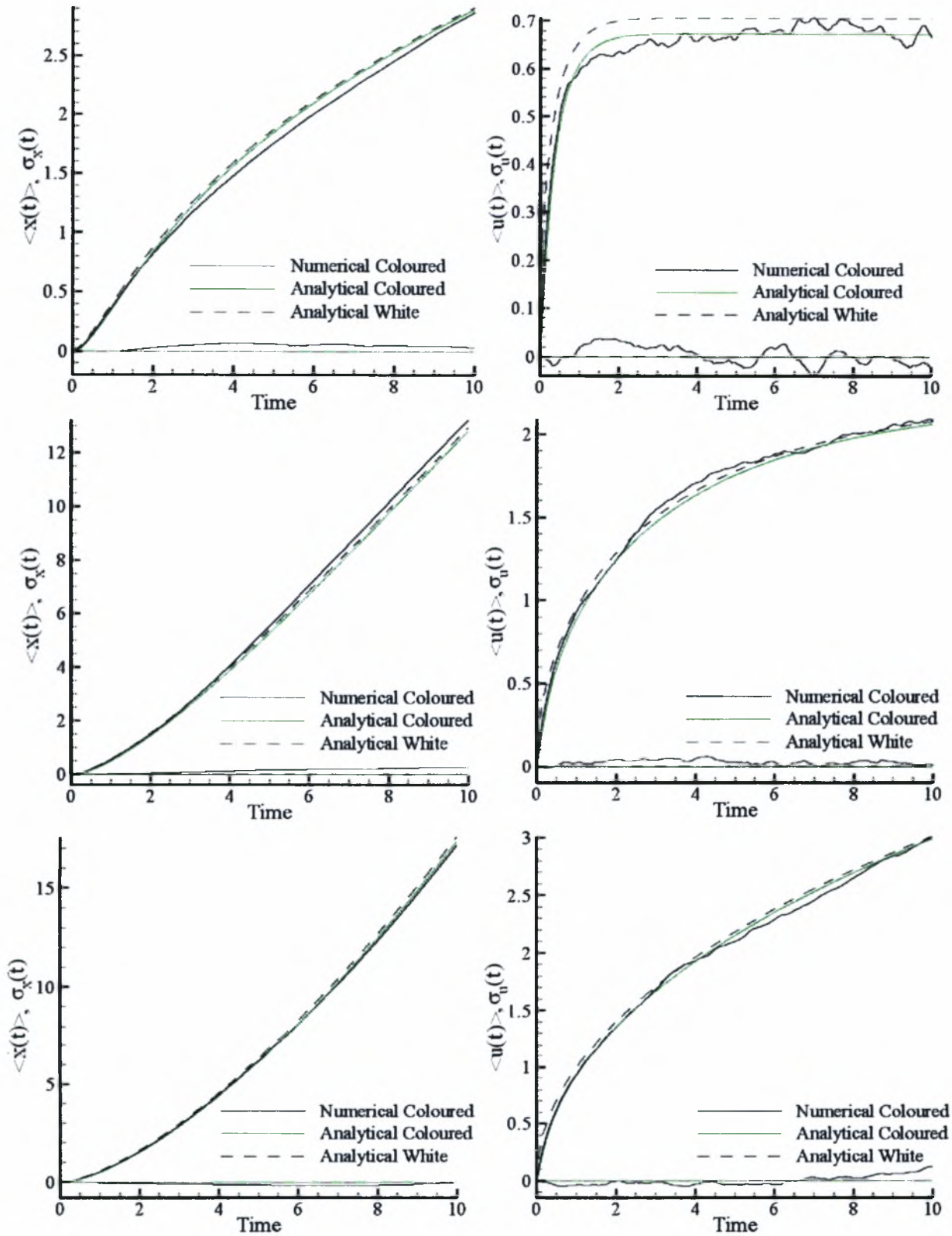

Figure 4.8: Mean and standard deviation of position and velocity for the 1D coloured noise problem, with $c^2 = 1$, $\varepsilon = 10^{-1}, \gamma = 1$ (up), $\gamma = 10^{-1}$ (middle), $\gamma = 10^{-2}$ (down).

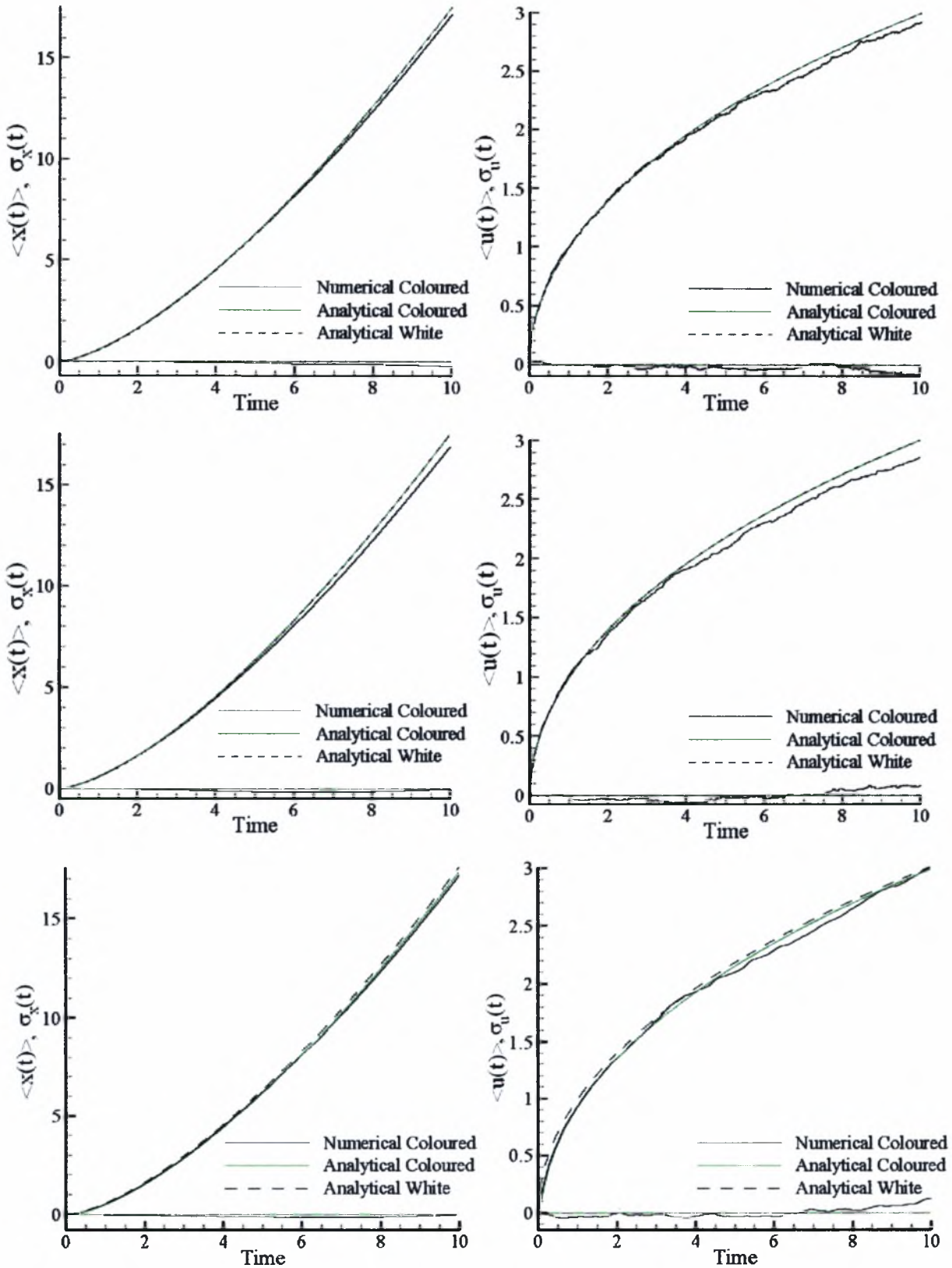

Figure 4.9: Mean and standard deviation of position and velocity for the 1D coloured noise problem, with $c^2 = 1$, $\gamma = 10^{-2}$, $\varepsilon = 10^{-3}$(up), $\varepsilon = 10^{-2}$ (middle), $\varepsilon = 10^{-1}$ (down).

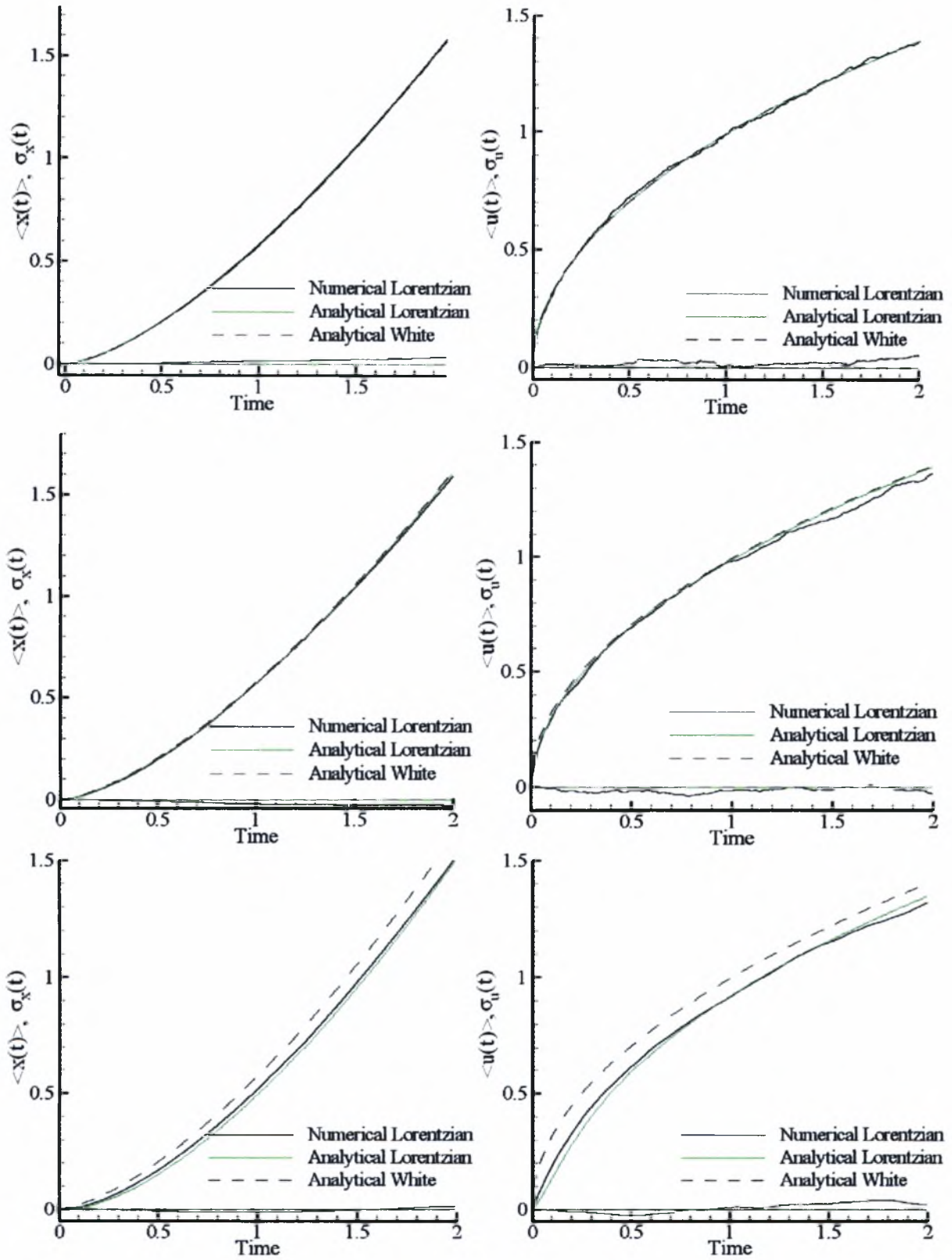

Figure 4.10: Mean and standard deviation of position and velocity for 1D Lorentzian noise and a small time interval, with $c^2 = 1$, $\gamma = 10^{-2}$, $\varepsilon = 10^{-3}$ (up), $\varepsilon = 10^{-2}$ (middle), $\varepsilon = 10^{-1}$ (down).

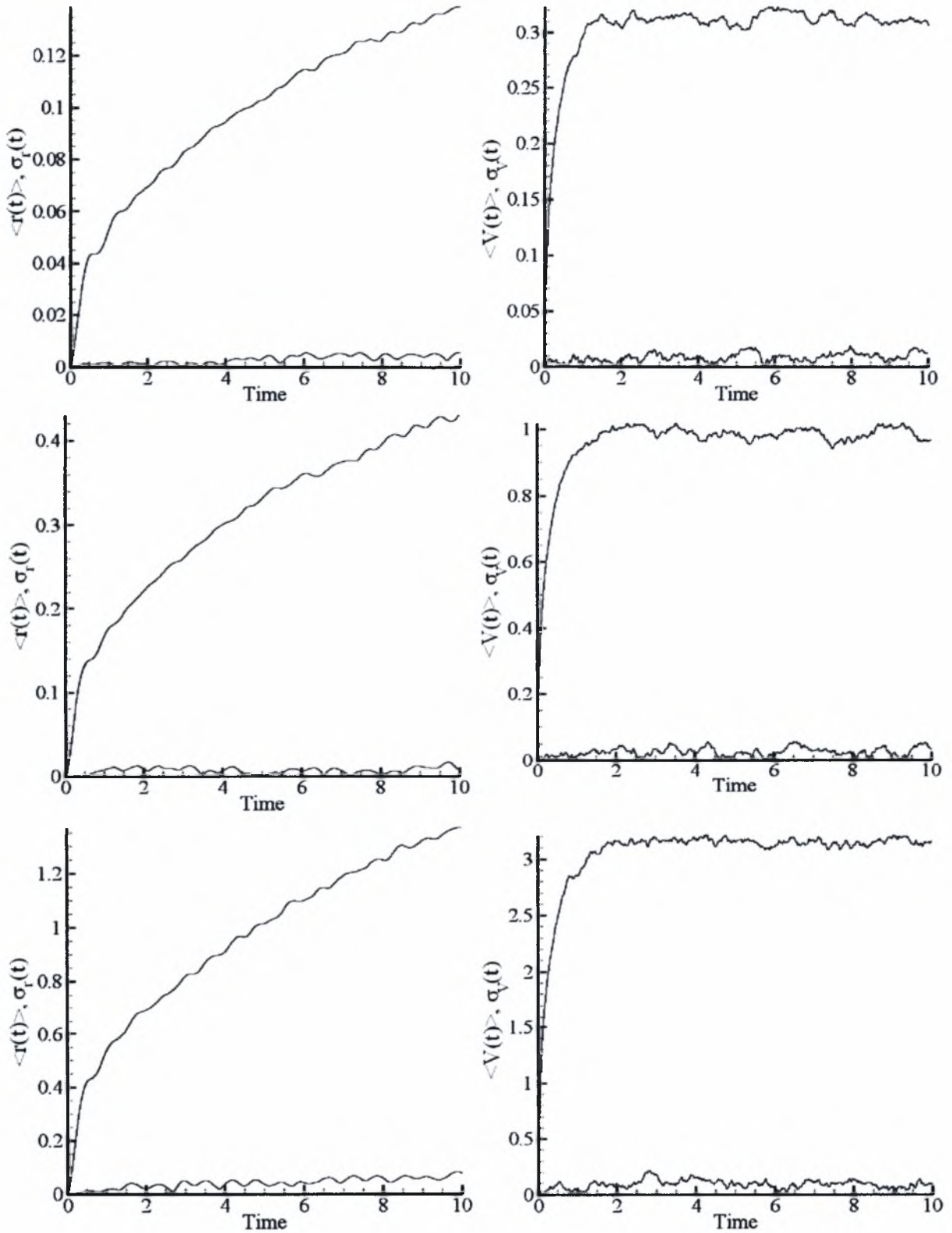

Figure 4.11: Mean and standard deviation of position and velocity for 2D coloured noise, with $\gamma = 10^{-1}$, $\varepsilon = 10^{-2}$, $\Omega = 10$, $c^2 = 10^{-1}$ (up), $c^2 = 1$ (middle), $c^2 = 10$ (down).

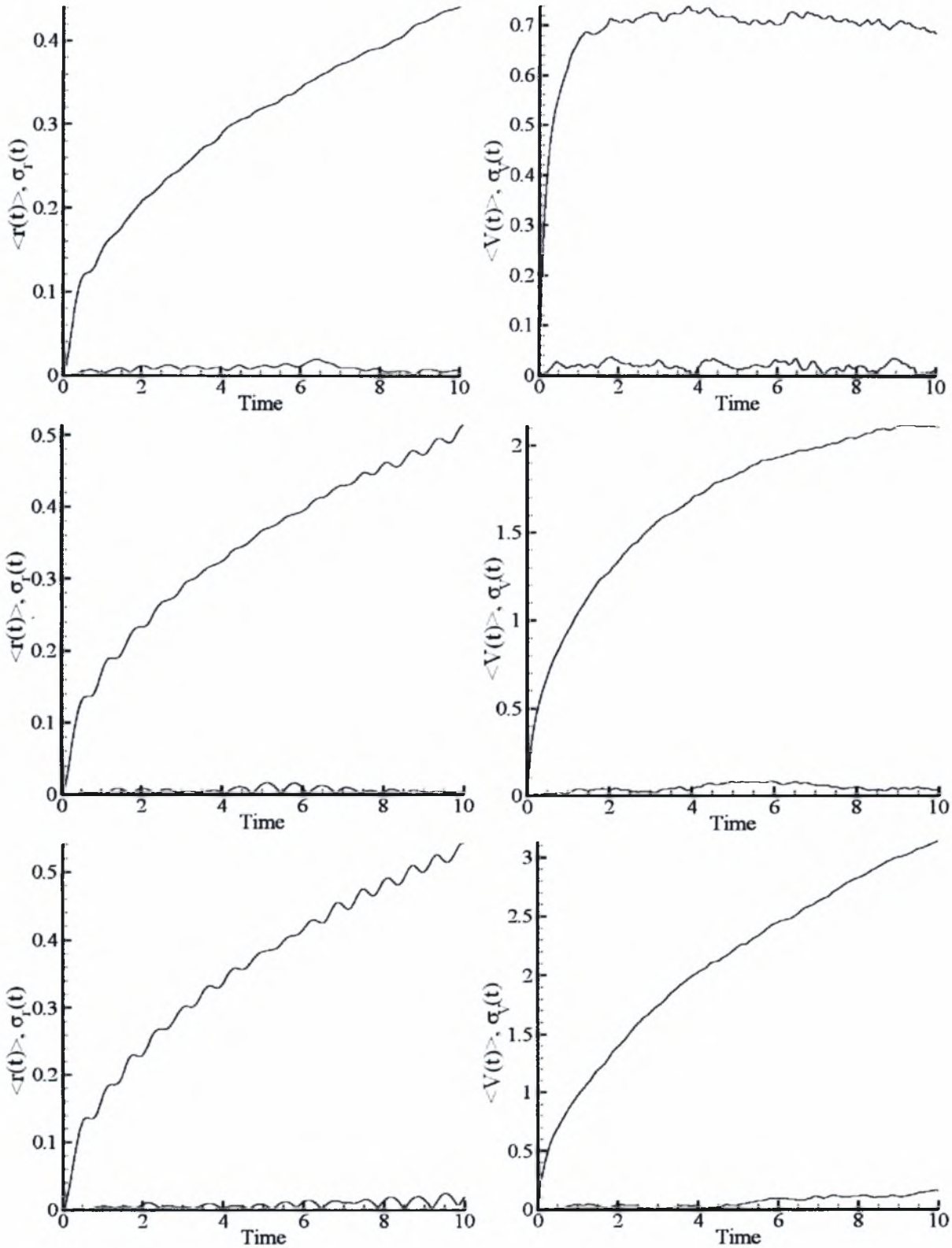

Figure 4.12: Mean and standard deviation of position and velocity for 2D coloured noise, with $c^2 = 1$, $\varepsilon = 10^{-1}$, $\Omega = 10$, $\gamma = 1$ (up), $\gamma = 10^{-1}$ (middle), $\gamma = 10^{-2}$ (down).

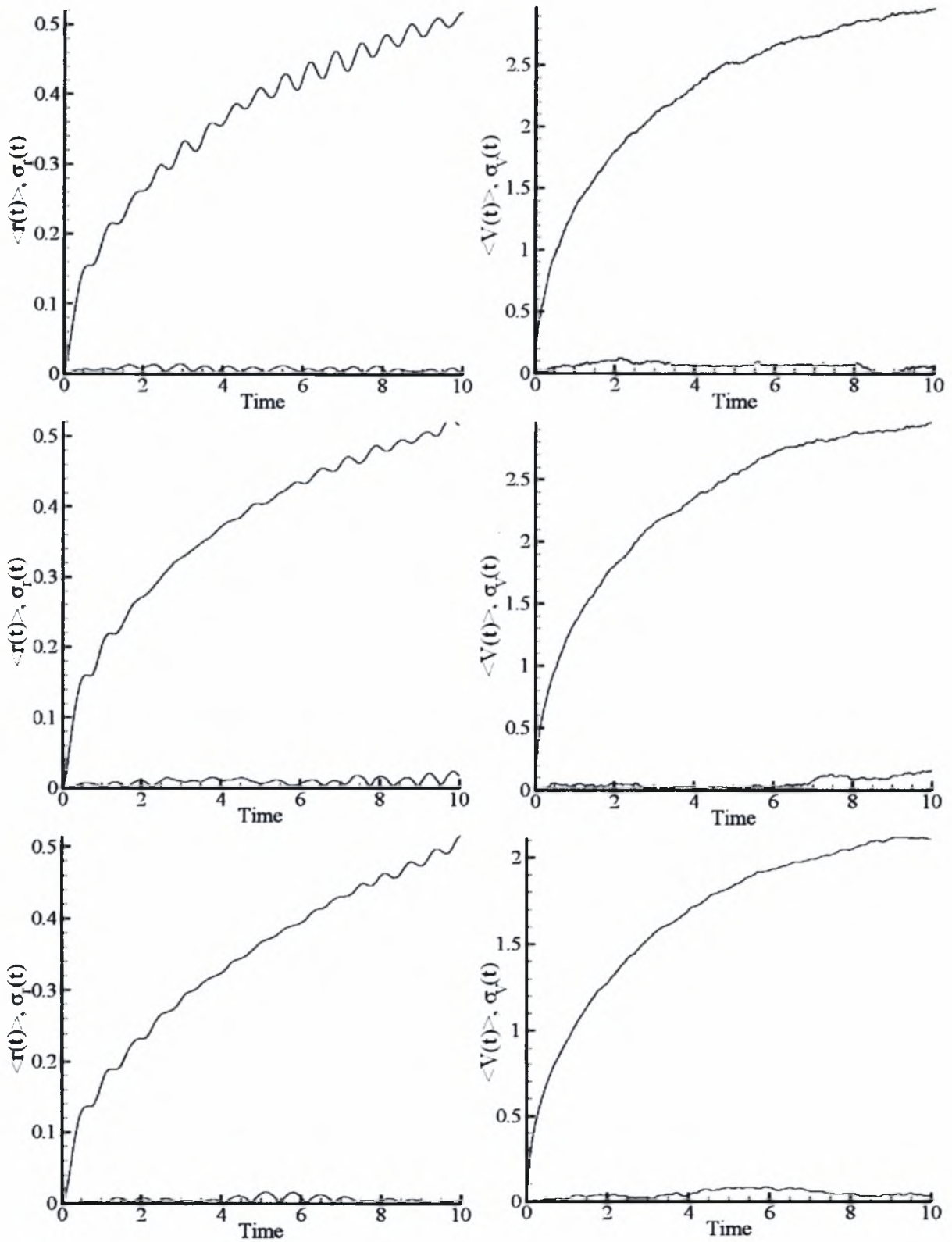

Figure 4.13: Mean and standard deviation of position and velocity for 2D coloured noise, with $c^2 = 1$, $\gamma = 10^{-1}$, $\Omega = 10$, $\varepsilon = 10^{-3}$ (up), $\varepsilon = 10^{-2}$ (middle), $\varepsilon = 10^{-1}$ (down).

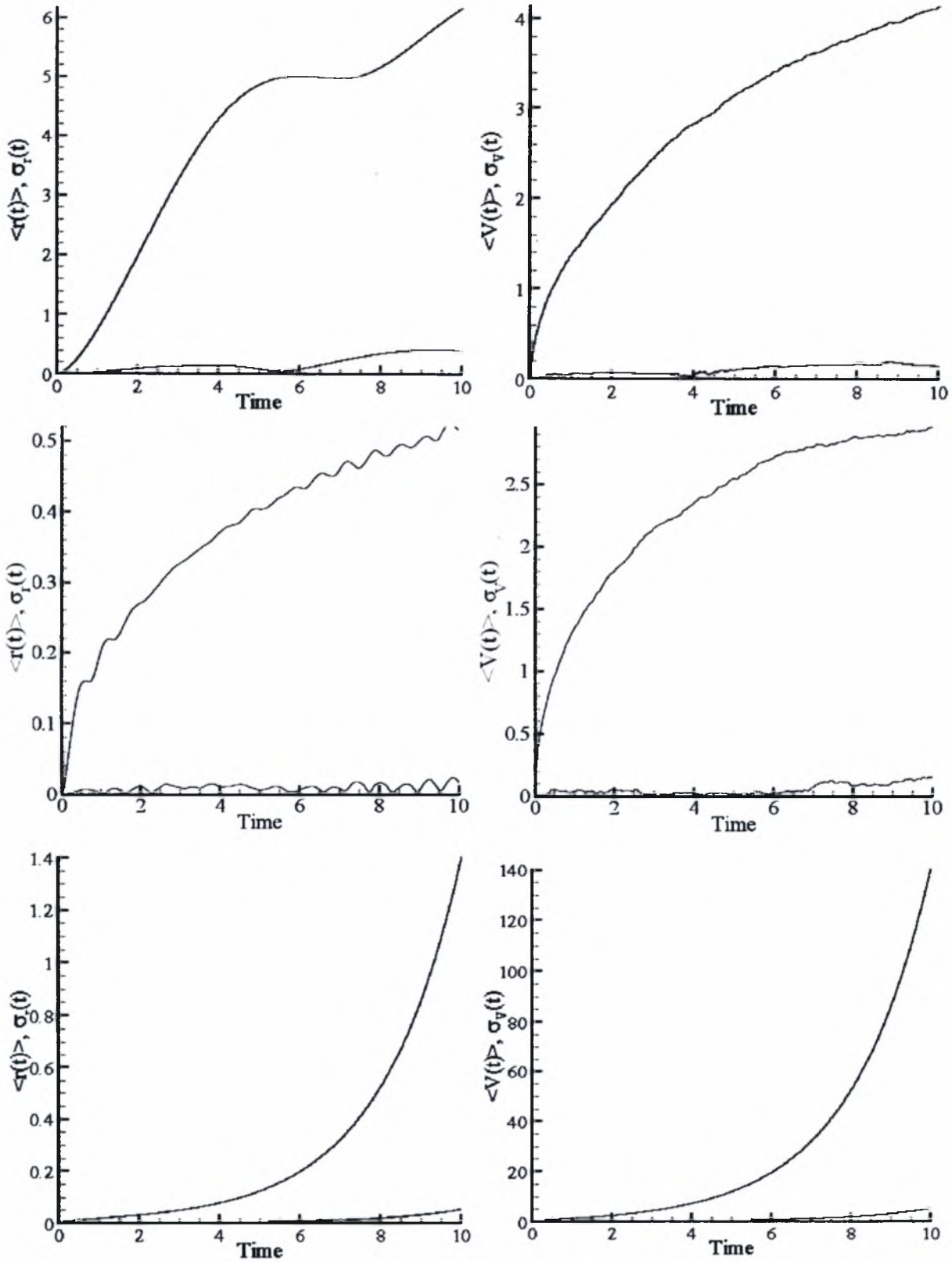

Figure 4.14: Mean and standard deviation of position and velocity for 2D coloured noise, with $c^2 = 1$, $\gamma = 10^{-2}$, $\varepsilon = 10^{-2}$, $\Omega = 1$ (up), $\Omega = 10$ (middle), $\Omega = 10^2$ (down).

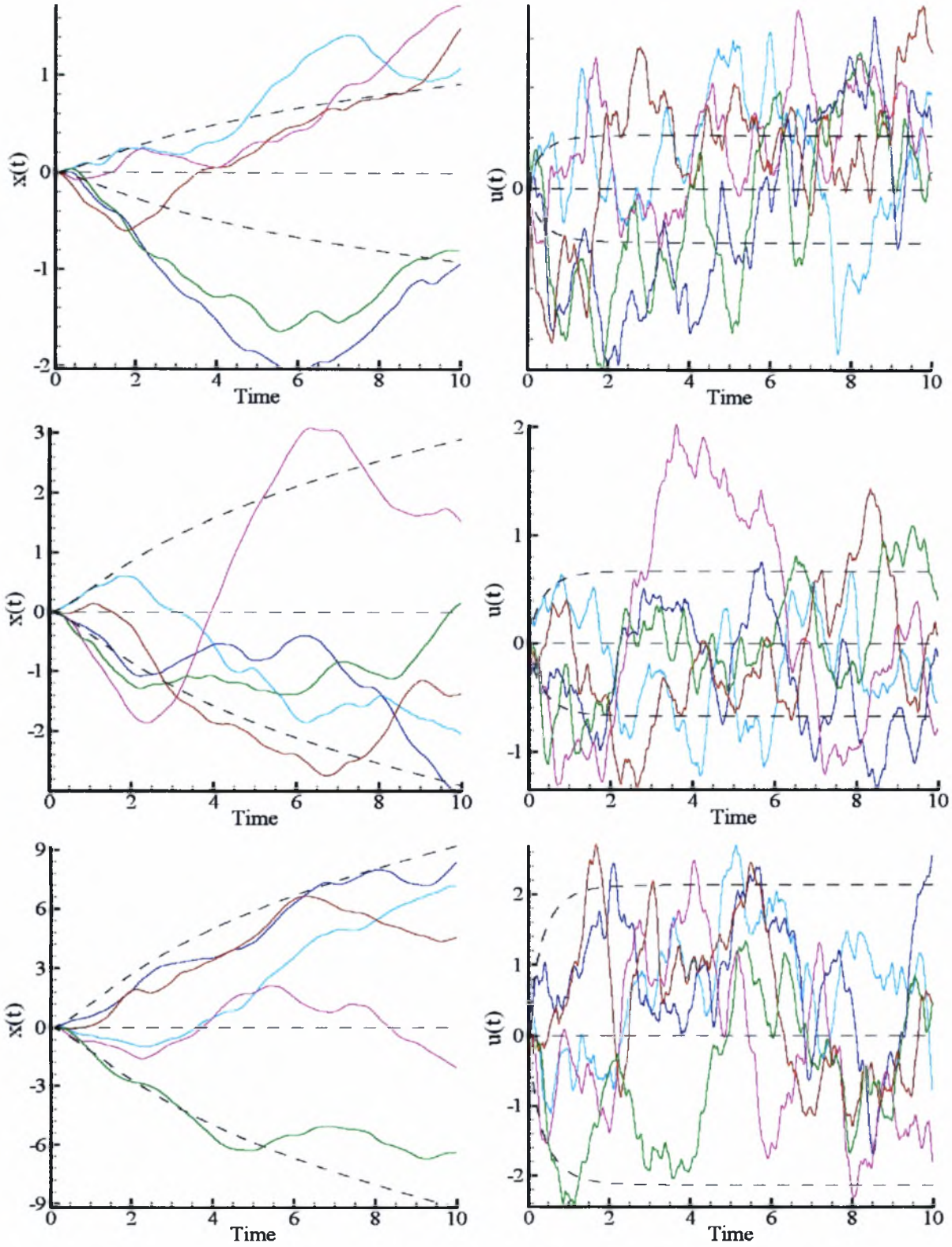

Figure 4.15: Simulations in 1D, with $\gamma = 1$, $\varepsilon = 10^{-1}$, $c^2 = 10^{-1}$ (up), $c^2 = 1$ (middle), $c^2 = 10$ (down).

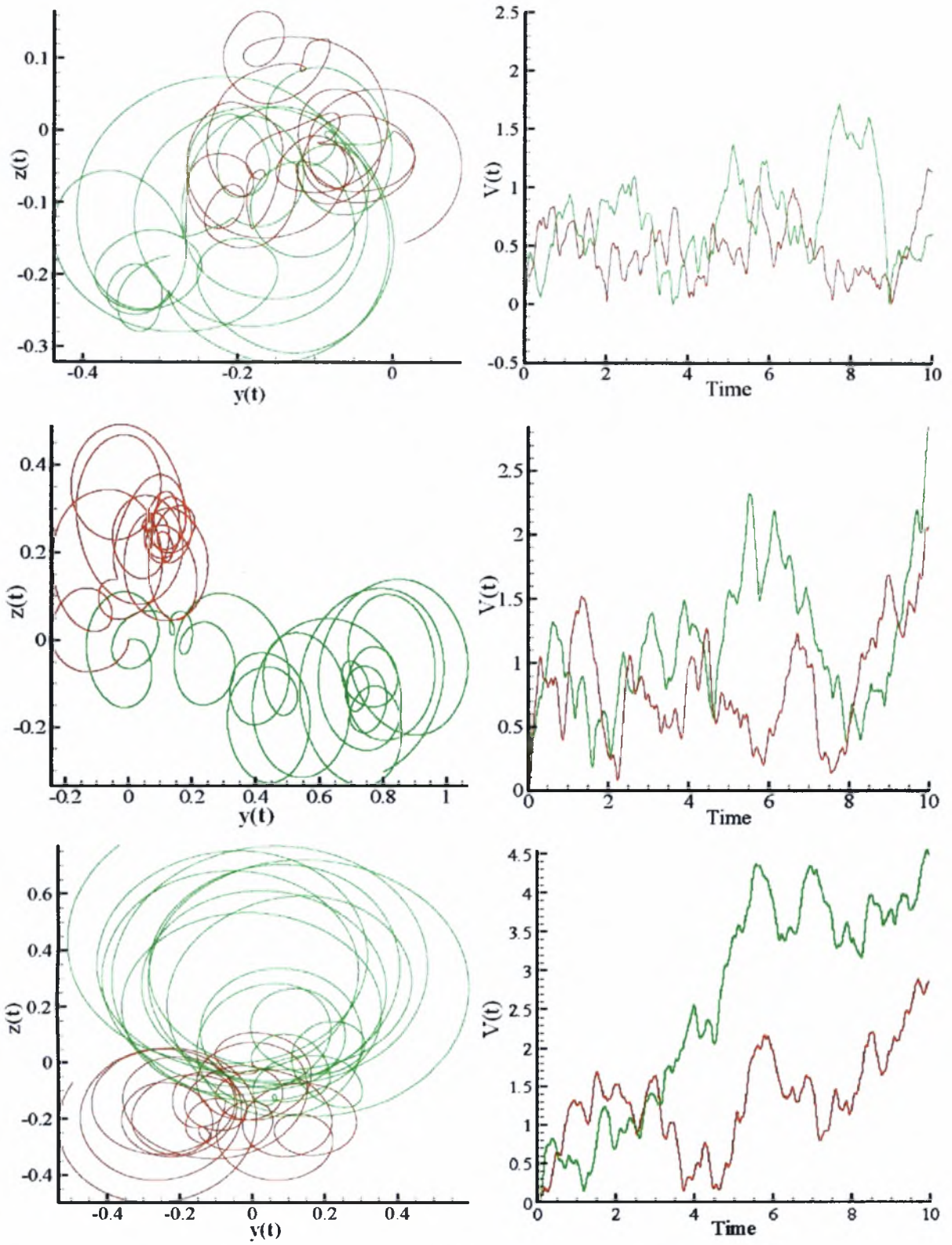

Figure 4.16: Simulations in 2D, with $c^2 = 1$, $\varepsilon = 10^{-1}$, $\gamma = 1$ (up), $\gamma = 10^{-1}$ (middle), $\gamma = 10^{-2}$ (down).

Chapter 5 – Motion in a stochastic electric field

5.1 Formulation

The random motion can also occur due to the presence of a stochastic field. The difference here is that the field is spatially dependent. The governing equations are

$$\frac{dx(t)}{dt} = u(t) \tag{5.1.1}$$

$$\frac{du(t)}{dt} = p^2 E(x) \tag{5.1.2}$$

and our goal is to study the motion of the charged particle in a field with the properties

$$\langle E(x) \rangle = 0 \tag{5.1.3}$$

$$\langle E(x) E(x+x') \rangle = \frac{1}{\lambda\sqrt{\pi}} e^{-\frac{x^2}{\lambda^2}}. \tag{5.1.4}$$

This can be performed numerically by approximating the field distribution with a Fourier cosine series with random phases (from equation 4.2.1)

$$E(x) = \sqrt{2} \sum_{n=1}^{N} \sqrt{2 S_E(\omega_n) \Delta\omega} \cos(\omega_n x + \Phi_n) \tag{5.1.5}$$

A benchmark problem, susceptible to analytical solution, is also investigated here. A charged particle is moving in a stationary electric field, expressed by a cosine function with a random, uniformly distributed phase $\Phi \in [0, 2\pi]$

$$E(x) = p^2 \cos(x + \Phi). \tag{5.1.6}$$

This simple problem will be used to become acquainted with electric fields of cosine form.

5.2 Analytical solution of the benchmark problem

We define $U(x)$ so that

$$E(x) = -\frac{dU(x)}{dx} \tag{5.2.1}$$

and therefore

$$\frac{du(t)}{dt} = -p^2 \frac{dU(x)}{dx} \tag{5.2.2}$$

It follows that

$$\frac{du(t)}{dt}u(t) = -p^2 \frac{dU(x)}{dx}u(t) \tag{5.2.3}$$

and

$$\frac{d}{dt}\left[\frac{1}{2}u^2(t) + p^2 U(x)\right] = 0 \tag{5.2.4}$$

Thus the quantity

$$C = \frac{1}{2}u^2(t) + p^2 U(x)$$

is constant and expresses the energy. The solution can be found by further integration

$$\frac{dx}{dt} = \sqrt{2\left[C - Au(x)\right]}$$

$$t = \frac{1}{\sqrt{2}}\int_0^x \frac{1}{\sqrt{C - Au(y)}}dy \tag{5.2.5}$$

It must be noted that the expression in brackets must be non-negative.

In the specific case of (5.1.6)

$$U(x) = -\sin(x + \Phi) \tag{5.2.6}$$

Consequently, assuming $p^2 = 1$ for simplicity, the initial conditions lead to the expression

$$C(\Phi) = \frac{1}{2}u_0^2 - \sin(x_0 + \Phi)$$

and

$$F(x) = C - U(x) = \frac{1}{2}u_0^2 - \sin(x_0 + \Phi) + \sin(x(t) + \Phi) \tag{5.2.7}$$

The initial position x_0 can be omitted if we introduce the displaced position $x' = x - x_0$ with initial condition $x_0' = 0$ and random phase $\Phi' = \Phi + x_0$, uniformly distributed in the same angle interval.

It is observed in (5.2.7) that the initial condition of velocity plays an important role. For $|u_0| \geq 2$, $F(x) \geq 0$ and the particle velocity does not change its sign. For $u_0 = 0$ and $x_0 = 0$, $F(x)$ vanishes when

$$\sin(\Phi) = \sin(x + \Phi) \qquad \rightarrow x = k(2\pi)\ ,\ k = 0,1... \qquad (5.2.8)$$

or

$$x + \Phi = \pi - \Phi + k(2\pi) \qquad \rightarrow x = \pi - 2\Phi + k(2\pi),\ k = 0,1... \qquad (5.2.9)$$

The instant that the motion stops may be expressed by an elliptic integral

$$t_*(\Phi) = \frac{1}{\sqrt{2}} \int_0^{\pi - 2\Phi + k(2\pi)} \frac{dx}{\sqrt{\sin(x+\Phi) - \sin\Phi}} = \frac{1}{\sqrt{2}} \int_0^{\pi - \Phi + k(2\pi)} \frac{dy}{\sqrt{\sin y - \sin\Phi}} \qquad (5.2.10)$$

In the case that the field is time dependent

$$E(x,t) = p^2 \cos(x - t + \Phi), \qquad (5.2.11)$$

the problem reduces to the previous one by substituting $x' = x - t$ and $u' = u - 1$ with appropriate boundary conditions.

5.3 Results

The verification is performed on the simpler case where the electric field is of the explicit form (5.1.6). Since the force is given, the numerical solution of the problem can be realized using the discretized form of equations (5.1.1), (5.1.2) and (5.1.6). Furthermore, due to the fact that each phase has the same probability, we can choose to simulate a number of equidistant angles.

The easiest way to benchmark our numerical results would be to test if $u = 0$ when $x = k(2\pi)$ and $x = \pi - 2\Phi + k(2\pi)$, $k = 0,1...$, where the expressions (5.2.8) and (5.2.9) hold. It can be observed in the position-velocity plot of Figure 5.1 (up) for $u_0 = 0$ that this is true for angles distributed in the whole 2π.

It is observed that the particle engages in an infinite motion in many occasions when the initial velocity is not zero (Figure 5.1). It is also interesting to note that the oscillations in the standard deviation curve are much more evident for small initial

velocities (Figure 5.2). The examination of this simple case offers important insights for the more complex case where only the properties of the field (5.1.4) is known, because this kind of problems can only be solved using the Fourier Series method. Therefore, through this example, an intuitive estimation of the behaviour of each cosine term was sought to be gained.

When the field of the form (5.1.4) is examined, it is seen that several properties are shared with the benchmark case, such as the periodicity of the simulation curves and the zero mean values for $u_0 = 0$ (Figure 5.3). It has been confirmed through numerical experiments that this periodicity is not due to a small number of series terms. The mean and standard deviation of position and velocity are also shown in Figure 5.4. Again, the particle moves endlessly for some initial velocities. However, the velocity has a decreasing tendency for $u_0 = 1$. This is in agreement with the corresponding case for the cosine-formed electric field where, as shown in Figure 5.2 (middle), the velocity does not remain constant and equal to the initial value but is reduced instead. The parameters appearing in Table 4.1 were also used in this problem, substituting ε with λ. The only modification was that, due to the non-linear nature of the problem, the time step had to be further decreased by one order of magnitude.

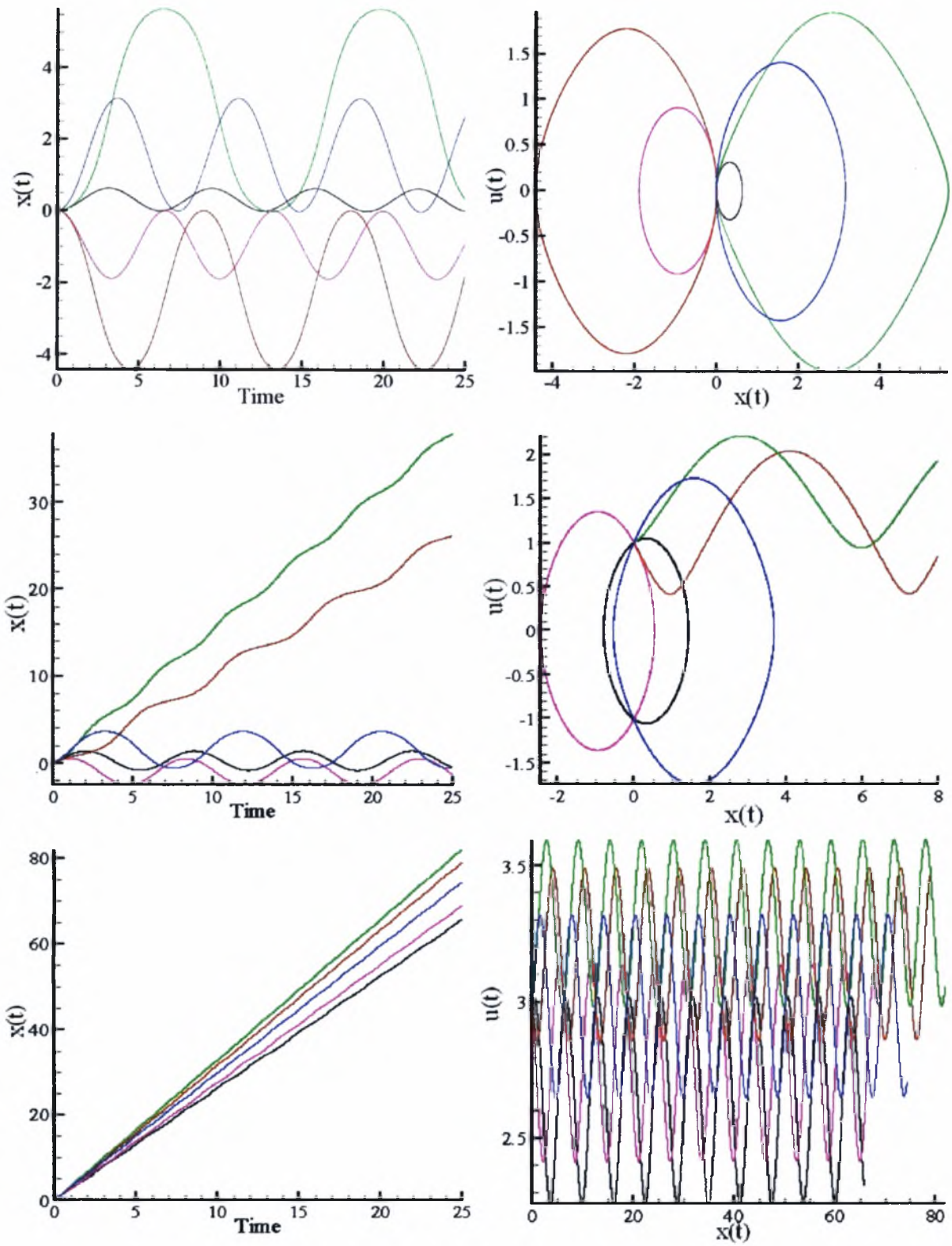

Figure 5.1: Simulations and x-u plot for 5 equidistant angles for the cosine-formed electric field problem, with $p^2 = 1$, $u_0 = 0$ (up), $u_0 = 1$ (middle), $u_0 = 3$ (down).

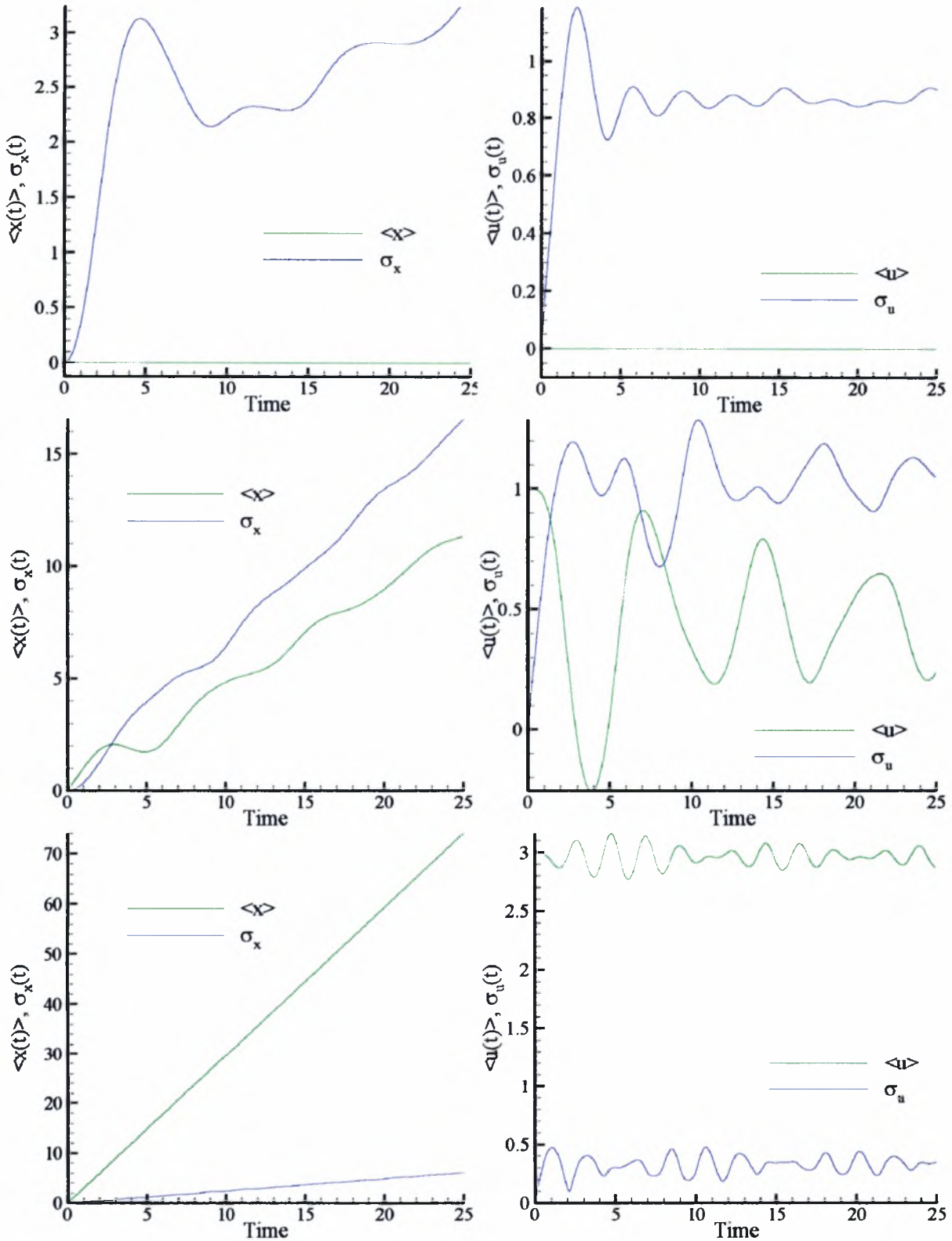

Figure 5.2: Mean and standard deviation of position and velocity for the cosine-formed electric field problem, with $p^2 = 1$, $u_0 = 0$ (up), $u_0 = 1$ (middle), $u_0 = 3$ (down).

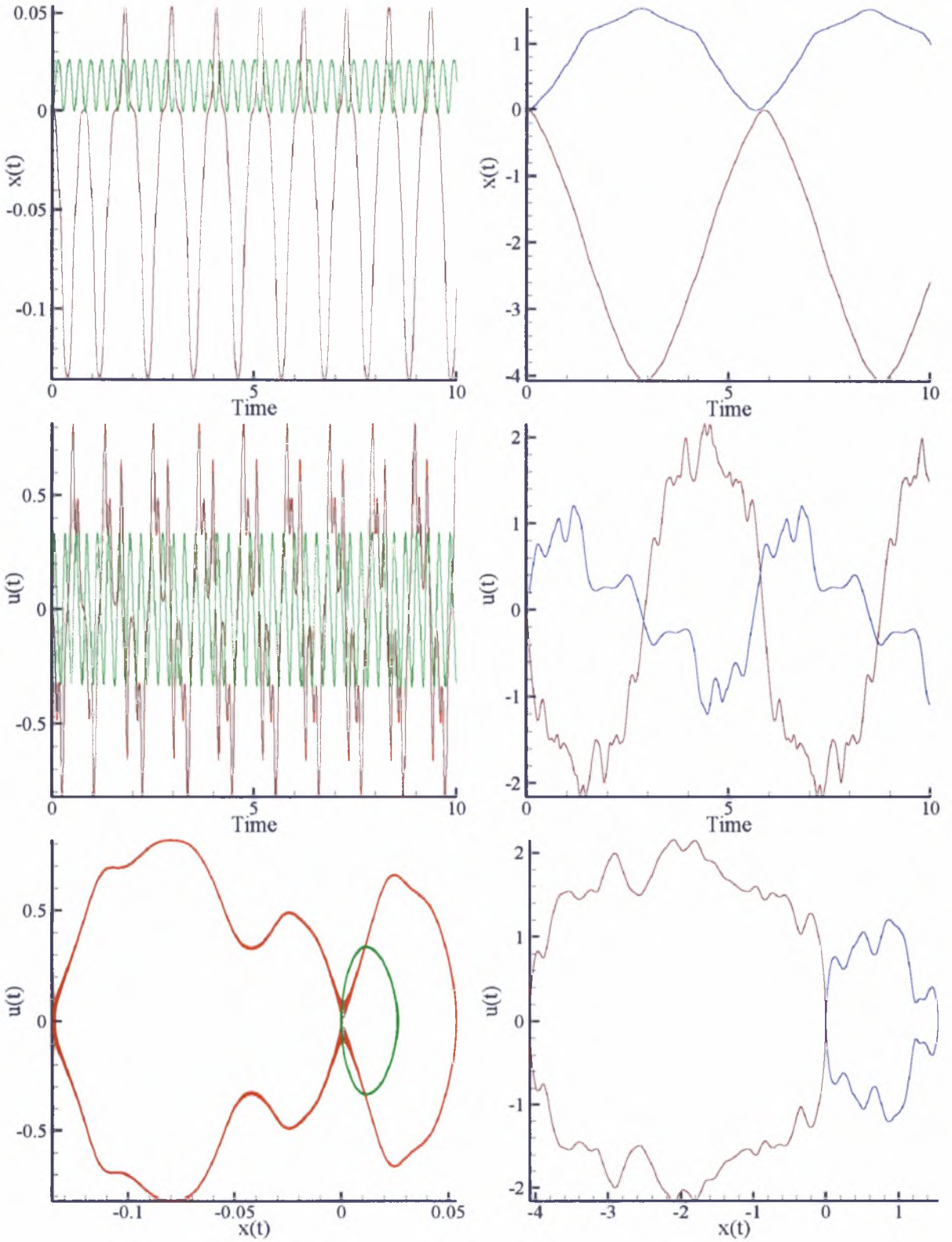

Figure 5.3: Simulations of motion in a stochastic electric field with Gaussian correlation, with $p^2 = 1$, $u_0 = 0$, $\lambda = 10^{-2}$ (left) and $\lambda = 10^{-1}$ (right).

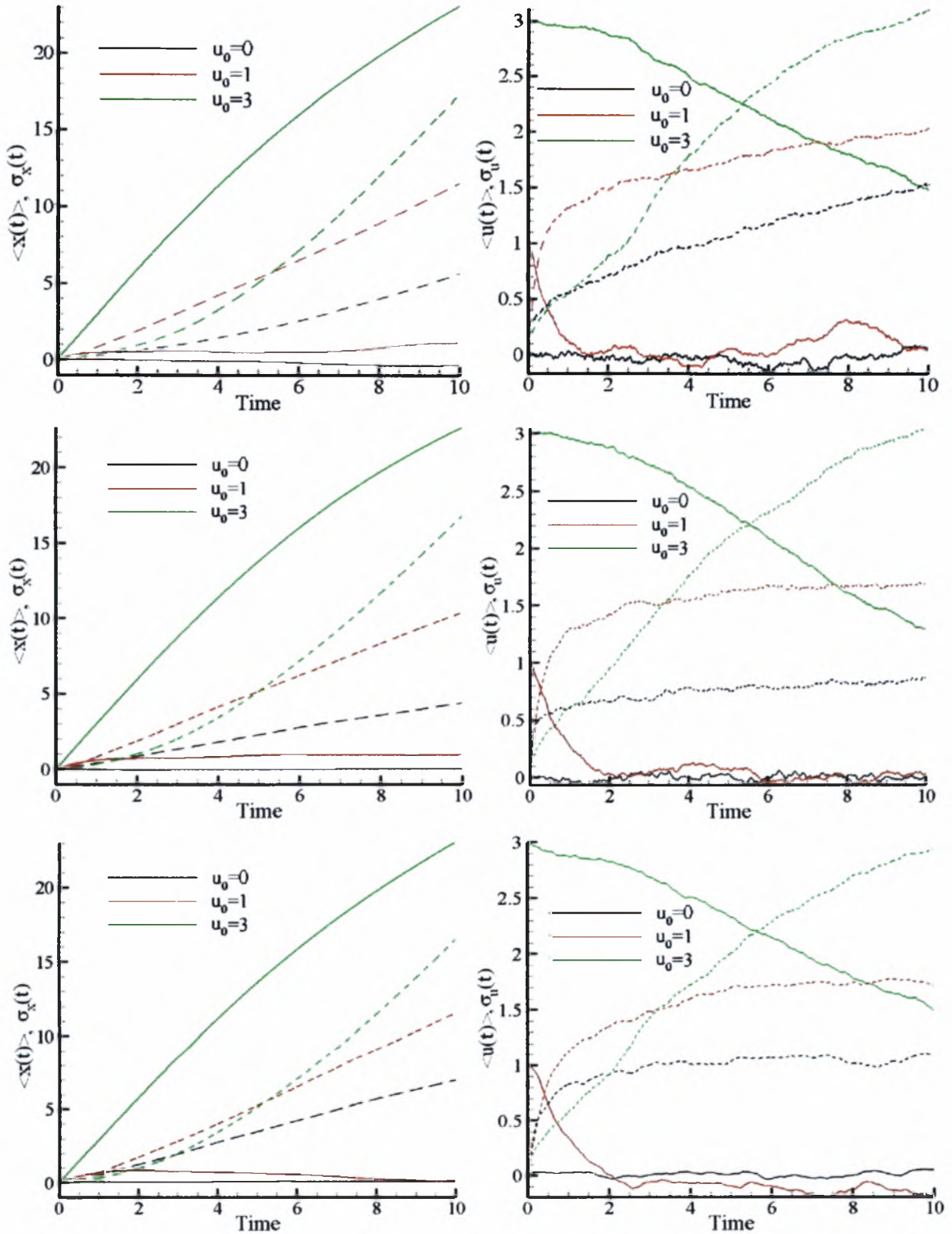

Figure 5.4: Mean (continuous line) and standard deviation (dashed line) for various initial conditions of velocity, with $p^2 = 1$, $\lambda = 10^{-3}$ (up), $\lambda = 10^{-2}$ (middle) and $\lambda = 10^{-1}$ (down).

Concluding Remarks

Analytical and computational solutions of stochastic differential equations have been presented and applied to the problem of motion of a charged particle inside a homogeneous magnetic field under the influence of an additive random force. This problem is related to the anomalous transport phenomenon and is of main interest for plasma confinement in fusion reactors. Following Langevin, the force is taken to be the sum of a friction term, proportional to the velocity, and a fluctuating component referred to as "noise". Four different types of noise, namely the cases of white, coloured, Gaussian and Lorentzian have been investigated. The problem has been decomposed in two systems of equations, one for the longitudinal motion along the direction of the field and another for the two dimensional transverse motion. These two systems have been studied independently due to the linearity of the problem. Correlations of position and velocity have been obtained and plotted for several types of noise.

In addition two different simulation methodologies have been applied. The first is based on an additional expression for the evolution of noise, while the second one on a stochastic Fourier series expansion of the random force. The latter approach has been applied successfully to several engineering fields but not in the area of fusion plasma technology. Extensive parametric investigation has been carried out and the influence of the strength of the noise c, the friction factor γ and the correlation time ε has been observed and commented. It has been found that the noise strength produces qualitatively similar behaviour while all correlations increase proportionally to the second power of c. The effect of the friction factor is more significant, changing in many cases the curvature of the standard deviation. Also, as γ is increased, the velocity of the particles is increased as well. It is noted that small values of γ are particularly important within the scope of this work because it can be used to model fusion plasma conditions. The correlation time does not affect the results significantly because for the range of parameters tested all types of noise are close to the classical white noise.

The above results have been verified by both methodologies of noise numerical simulation. In both cases the computational effort is modest and the results are in good

agreement with the corresponding analytical ones. However, the potential of the Fourier series expansion is more promising since it can be used to tackle non-linear problems with arbitrary noise. This is an important advantage since it allows more complete and reliable modelling of transport phenomena.

As a first step in that direction the Fourier expansion methodology has been used to study a stochastic, space dependent electric field. This is a non-linear problem and has been solved in an efficient manner. Such problems are highly dependent on the imposed initial conditions. Therefore, three different initial conditions for the velocity have been applied deducing different results for particle trajectories, velocities and the corresponding correlations. The overall performance of the scheme has been evaluated positively through benchmarking. The fact that the Fourier series expansion approach has proven to be very efficient is very encouraging for its implementation in other physical systems.

Based on the above, other non-linear problems such as random motion in inhomogeneous magnetic fields and electromagnetic fields occurring from a cylindrical approximation will be investigated. Further efforts for the improvement of computational accuracy and time will be made with the modification of the numerical codes in order to work in a parallel computer environment.

References

[1] Einstein, A. 1905 *Über die von der molekularkinetischen Theorie der Wärme geforderte Bewegung von in ruhenden Flüssigkeiten suspendierten Teilchen* (*On the movement of small particles suspended in a stationary liquid demanded by the molecular kinetic theory of heat*), Ann. Phys., 17, pp. 549-560. Translated by A. D. Cowper (Methuen, London, 1926 – Reprinted by Dover, New York, 1956).

[2] Einstein, A. 1906 *Zur Theorie der Brownschen Bewegung* (*On the theory of Brownian movement*), Ann. Phys., 19, pp. 371-381. Translated by A. D. Cowper (Methuen, London, 1926 – Reprinted by Dover, New York, 1956).

[3] Perrin, J.B. 1909 *Mouvement brownien et réalité moléculaire*, Annales de Chimie et de Physique 18, pp. 1-114. Translation by Frederick Soddy (London: Taylor and Francis, 1910)

[4] Von Smoluchowski, M. 1906 *Zur kinetischen Theorie der Brownschen Molekularbewegung und der Suspensionen*, Ann. Phys., 21, 326, pp. 756-780.

[5] Langevin, P. 1908 *Sur la théorie du mouvement brownien*, Comptes Rendues, 146, 530-533. Translation by Gythiel A. and introduced by Lemons, D.S. in Am. J. Phys. 65, 11, 1997.

[6] Gillespie, D.T 1996 *Exact numerical simulation of the Ornstein-Uhlenbeck process and its integral*, Physical Review E, 54, 2, pp. 2084-2091.

[7] Lemons, D.S. and Kaufman, D.L. 1999 *Brownian motion of a charged particle in a magnetic field*, IEEE Transactions on plasma science, 27, 5, pp. 1288-1296.

[8] Zhu, S., Yu, A.W. and Roy, R. 1986 *Statistical fluctuations in laser transients*, Physical Review A, 34, 5, pp. 4333-4347.

[9] Hänggi, P., Marchesoni, F. and Grigolini, P. 1984 *Bistable flow driven by coloured Gaussian noise: A critical study*, Z. Phys. B – Condensed Matter, 56, pp. 333-339.

[10] Sancho, J.M., Miguel, M.S, Katz, S.L. and Gunton, J,D. 1982 *Analytical and numerical studies of multiplicative noise*, Physical Review A, 26, 3, pp. 1589-1609.

[11] Zhu, P. 2007 *Associated relaxation time and intensity correlation function of a bistable system driven by cross-correlation additive and multiplicative coloured noise sources*, Eur. Phys. J. B, 55, pp. 447-452.

[12] Goswami, G., Majeee, P., Barik, D. and Bag, B.C. 2006 *Role of colored cross-correlation in additive and multiplicative white noises on upper bound of time derivative of information entropy*, Acta Physica Polonica B, 37, 9, pp. 2433-2444.

[13] Vlahos, L., Isliker, H., Kominis, Y. and Hizanidis, K. 2008 *Normal and Anomalous Diffusion: A tutorial*, http://arxiv.org/PS_cache/arxiv/pdf/0805/0805.0419v1.pdf

[14] Risken, H. 1989 *The Fokker-Planck Equation – Methods of Solution and Applications*, 2nd edition, Springer-Verlag, Berlin.

[15] Milshtein, G.N. and Tret'yakov, M.V. 1994 *Numerical Solution of differential equations with colored noise*, Journal of Statistical Physics, 77, 3-4, pp. 691-715.

[16] Kloeden, P.E. and Platen E. 1992 *Numerical solution of stochastic differential equations*, Springer-Verlag Berlin Heidelberg.

[17] Gillespie, D.T. 1995 *The mathematics of Brownian motion and Johnson noise*, Am. J. Phys., 64, 3, pp. 225-240.

[18] Drummond, I.T., Hoch, A. and Horgan, R.R. 1986 *Numerical integration of stochastic differential equations with variable diffusivity*, J. Phys. A: Math. Gen., 19, pp. 3871-3881.

[19] Roessler, A. 2006 *Runge-Kutta methods for Itô stochastic differential equations with scalar noise*, BIT Numerical Mathematics, 46, pp. 97-110

[20] Ruemelin, W. 1982 *Numerical treatment of stochastic differential equations*, SIAM J. Numer. Anal., 19, 3, pp. 604-613.

[21] Fox, R.F., Gatland, I.R., Roy, R. and Vemuri, G. 1988 *Fast, accurate algorithm for numerical simulation of exponentially correlated colored noise*, Physical Review A, 38, 11, pp. 5938-5940.

[22] Schimansky-Geier, L. and Zülicke, C. 1990 *Harmonic noise:Effect on bistable systems*, Z. Phys. B – Condensed Matter, 79, pp. 451-460.

[23] Billah, K.Y.R and Shinozuka, M. 1990 *Numerical method for colored-noise generation and its application to a bistable system*, Physical Review A, 42, 12, pp. 7492-7495

[24] Billah, K.Y.R and Shinozuka, M. 1992 *Reply to the "Comment on 'Numerical method for colored-noise generation and its application to a bistable system' "*, Physical Review A, 46, 12, pp. 8031-8033

[25] Wu, M.M., Billah, K.Y.R and Shinozuka, M. 1995 *Systematic adiabatic analysis of a nonlinear oscillator with inertia driven by colored noise*, Physical Review E, 52, 4, pp. 3377-3380.

[26] Basios, V., Bountis, T. and Nicolis, G. 1999 *Controlling the onset of homoclinic chaos due to parametric noise*, Physics Letters A, 251, pp. 250-258.

[27] Shinozuka, M. 1970 *Simulation of multivariate and multidimensional random processes*, Journal of Accoustic Society of America, pp. 357-368.

[28] Lesnik, D., Gordienko, S., Neuer, M. and Spatschek, K.-H. 2008 *Diffusion in a stochastic magnetic field*, http://arxiv.org/abs/nlin/0404056v3.

[29] Coronado, M., Vitela, J.E. and Akcasu, A.Z. 1992 *Diffusion of charged particles in tokamak-like stochastic magnetic and electric fields*, Phys. Fluids B, 4, 12, pp. 3935-3951.

[30] Kourakis, I. and Grecos, A. 2003 *Plasma diffusion and relaxation in a magnetic field*, Communications in Nonlinear Science and Numerical Simulation, 8, pp. 547-551.

[31] Unterberg, B., Busch, C., Bock, M.d., Coenen, J.W., Finken, K.H., Jachmich, St., Jakubowski, M.W., Kikuchi, Y., Krämer-Flecken, A., Lehnen, M., Samm, U., Schmitz, O., Soldatov, S., Tokar, M.Z., Hellermann, M.v., Wolf, R.C., Xu, Y. and TEXTOR-team 2007 *Impact of stochastic magnetic fields on plasma rotation and radial electric fields in the plasma edge of the tokamak TEXTOR*, Journal of Nuclear Materials, 363-365, pp. 698-702.

[32] Biewer, T.M., Forest, C.B., Anderson, J.K., Fiksel, G., Hudson, B., Prager, S.C., Sarff, J.S., Wright, J.C., Brower, D.L., Ding, W.X. and Terry, S.D. 2003 *Electron Heat Transport Measured in a Stochastic Magnetic Field*, Physical Review Letters, 91, 4, pp. 045004-1 – 045004-4.

[33] Dumbrajs, O., Igochine, V., Zohm, H. and the ASDEX Upgrade Team 2008 *Diffusion in a stochastic magnetic field in ASDEX Upgrade*, Nuclear Fusion 48, 024011.

[34] Fischer, O. and Cooper, W.A. 1998 *Mapping of a stochastic magnetic field in toroidal systems*, http://infoscience.epfl.ch/record/121152/files/lrp_598_98_hq.pdf

[35] Strumberger, E. 1998 *Stochastic Magnetic Field Structure in the edge region of W7-X*, Contrib. Plasma Phys., 38, 1/2, pp. 106-111.

[36] Vanden Eijnden, E. 1997 *Some remarks on the quasilinear treatment of the stochastic acceleration problem*, Phys. Plasmas, 4, 5, pp. 1486-1488.

[37] Doveil, F. and Grésillon, D. 1982 *Statistics of charged particles in external random longitudinal electric fields*, Phys. Fluids, 25, 8, pp. 1396-1402.

[38] Ishihara, O., Xia, H. and Watanabe, S. 1993 *Long-time diffusion in plasma turbulence with broad uniform spectrum*, Phys. Fluids B, 5, 8, pp. 2786-2792.

[39] Xia, H., Ishihara, O. and Hirose, A. 1993 *Non-Markovian diffusion in plasma turbulence*, Phys. Fluids B, 5, 8, pp. 2892-2904.

[40] Ishihara, O. and Hirose, A. 1985 *Wave-particle resonance broadening in a Langmuir turbulence*, Phys. Fluids, 28, 7, pp. 2159-2161.

[41] Perotti, F. 1990 *Structural response to non-stationary multiple-support random excitation*, Earthquake engineering and structural dynamics, 19, pp. 513-527.

[42] Talay, D. 1996 *Probabilistic Numerical methods for partial differential equations: Elements of analysis*, published in "Probabilistic models for nonlinear partial differential equations", edited by Talay, D. and Tubaro, L., Lecture Notes in Mathematics, 1627.

[43] Vanden Eijnden, E. and Grecos, A. 1998 *Stochastic modelling of turbulence and anomalous transport in plasmas*, J. Plasma Physics, 59, pp. 683-694.

[44] De Grooth, B.G. 1999 *A simple model for Brownian motion leading to the Langevin equation*, Am. J. Phys., 67, 12, pp. 1248-1252.

[45] Bird, G.A. 1994 *Molecular Gas Dynamics and the Direct Simulation of Gas Flows*, Oxford University Press, Oxford, England, UK.

[46] Lindgren, G. 2006 *Lectures on Stationary Stochastic Processes*, Lecture Notes, Lund University, http://www.maths.lth.se/matstat/staff/georg/Publications/lecture2006.pdf.

[47] Gleeson, J. *Applied Stochastic Differential Equations*, Lecture Notes, University of Limerick, Ireland, http://www.ul.ie/gleesonj/Papers/SDEs/Applied_SDEs_notes.pdf.

Appendix A: Elements of Statistics

The symbol $\langle A(t)\rangle$ denotes the mean value of the quantity A at time t. This is obtained by taking a large number of particle trajectory simulations (or realizations) and averaging over the values of the quantity A

$$\langle A(t)\rangle = \frac{1}{N_R}\sum_{i=1}^{N_R} A_i(t)$$

In the text, the symbol $N(t)$ denotes random values, conforming to a normal distribution with zero mean value and standard deviation equal to unity $N(0,1)$. Its properties are

$$\langle N(t)\rangle = 0 \qquad \text{(A.1)}$$

$$\langle N^2(t)\rangle = 1 \qquad \text{(A.2)}$$

It can be generated with two ways: the acceptance-rejection method [45] and the Box-Mueller method [6].

Acceptance-Rejection method

We define the normalized position

$$x' = \frac{x-a}{b-a} \qquad \text{(A.3)}$$

and distribution

$$f'(x') = f(x')/f_{\max} \qquad \text{(A.4)}$$

where $f_{\max}$ is the maximum value of the distribution. The distribution function plot would fit this way in a unit square. We choose pairs of random numbers R_1, R_2 uniformly distributed in $[0,1]$ and check whether $R_2 \le f'(R_1)$. If this relation holds then x' is accepted and x is determined by equation B.1, otherwise another pair of random numbers is calculated and the process is repeated. The efficiency of this algorithm depends on the value of

$$I = \int_0^1 f'(x')\,dx' \tag{A.5}$$

The closer this integral is to unity, the least amount of random numbers will be rejected.

Box-Mueller method

Two uniform random numbers R_1, R_2 are generated and replaced in

$$s = \sqrt{2\ln(1/R_1)} \tag{A.6}$$

and

$$\theta = 2\pi R_2 . \tag{A.7}$$

These can be used to yield two statistically independent sample values of $N(0,1)$

$$n_1 = s\cos\theta \tag{A.8}$$

and

$$n_2 = s\sin\theta . \tag{A.9}$$

Both methods work well, as seen in Figure A.1. The Box-Mueller algorithm has been chosen because it's simple, it is widely used in the literature and for efficiency reasons, since R_1 and R_2 are guaranteed to provide two normally distributed random numbers.

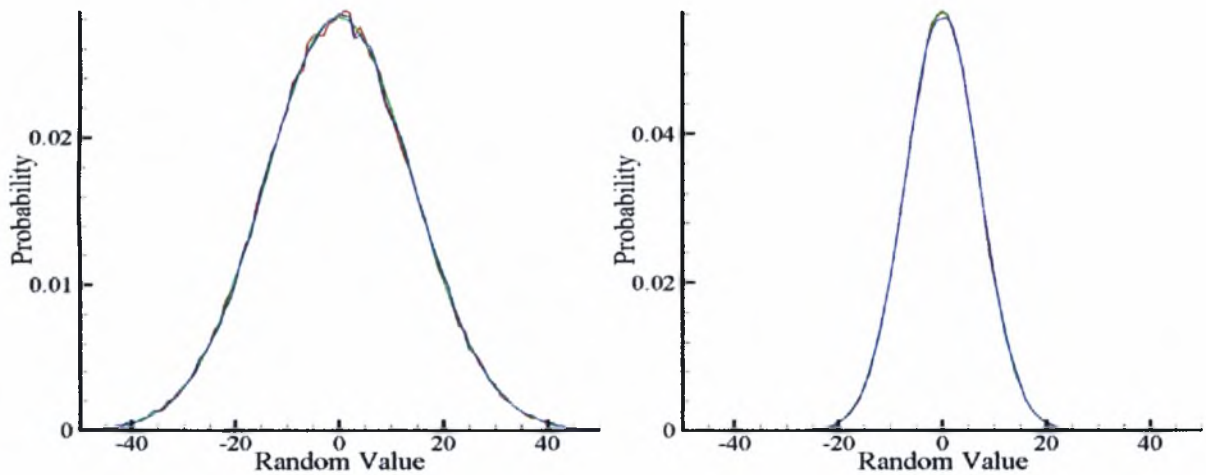

Figure A.1: Generation of normal distributions with two methods and comparison with analytical curves.

Appendix B: Analytical solution of the x-component correlations

Starting from expression (2.2.9)

$$R_{uu}(t,s)=c^2e^{-\gamma(t+s)}\int_0^t\int_0^s e^{\gamma(s'+t')}\phi\left(\left|t'-s'\right|\right)ds'dt'=c^2e^{-\gamma(t+s)}I \tag{B.1}$$

we can simplify the integral if we substitute $x=t'-s'$ and $y=t'+s'$. The Jacobian is equal to $1/2$ and the limits will also be transformed according to Figure B.1

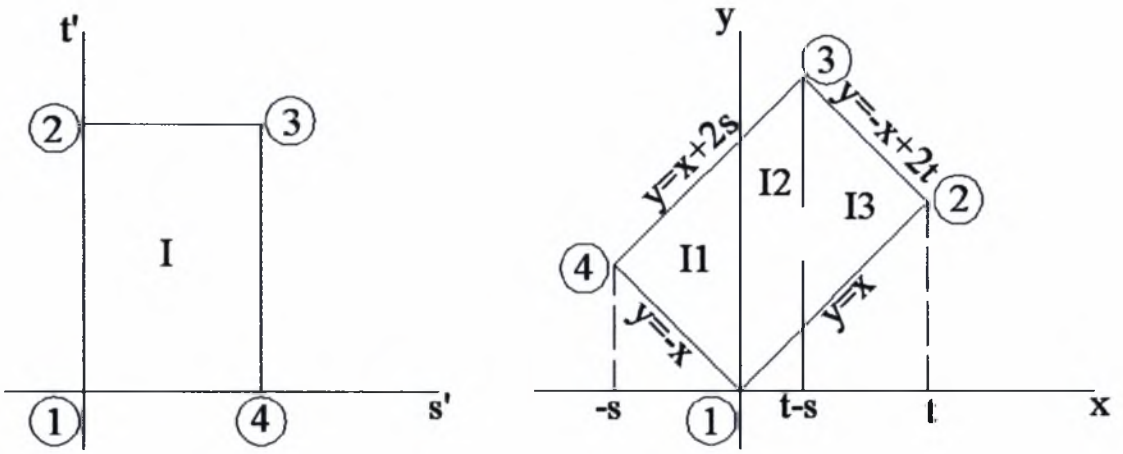

Figure B.1: Transformation of coordinates for the calculation of I.

Thus, the integral is split in three parts

$$I=\frac{1}{2}\left\{\int_{-s}^{0}\phi\left(|x|\right)\left[\int_{-x}^{x+2s}e^{\gamma y}dy\right]dx+\int_{0}^{t-s}\phi\left(|x|\right)\left[\int_{x}^{x+2s}e^{\gamma y}dy\right]dx+\int_{t-s}^{t}\phi\left(|x|\right)\left[\int_{x}^{-x+2t}e^{\gamma y}dy\right]dx\right\}=$$

$$=I_1+I_2+I_3$$

$$I_1=\frac{1}{2}\int_{-s}^{0}\phi\left(|x|\right)\left[\int_{-x}^{x+2s}e^{\gamma y}dy\right]dx=$$

$$=\frac{e^{2\gamma s}}{2\gamma}\int_{-s}^{0}e^{\gamma x}\phi\left(|x|\right)dx-\frac{1}{2\gamma}\int_{-s}^{0}e^{-\gamma x}\phi\left(|x|\right)dx \tag{B.2}$$

$$I_2=\frac{1}{2}\int_{0}^{t-s}\phi\left(|x|\right)\left[\int_{x}^{x+2s}e^{\gamma y}dy\right]dx=$$

$$=\frac{e^{2\gamma s}}{2\gamma}\int_{0}^{t-s}e^{\gamma x}\phi\left(|x|\right)dx-\frac{1}{2\gamma}\int_{0}^{t-s}e^{\gamma x}\phi\left(|x|\right)dx \tag{B.3}$$

$$I_3 = \frac{1}{2}\int_{t-s}^{t} \phi(|x|)\left[\int_{x}^{-x+2t} e^{\gamma y}dy\right]dx =$$
$$= \frac{e^{2\gamma t}}{2\gamma}\int_{t-s}^{t} e^{-\gamma x}\phi(|x|)dx - \frac{1}{2\gamma}\int_{t-s}^{t} e^{\gamma x}\phi(|x|)dx \quad \text{(B.4)}$$

Combining the above expressions yields

$$I = \frac{1}{2\gamma}\left\{e^{2\gamma t}\int_{-t}^{s-t} e^{\gamma t'}\phi(|t'|)dt' + e^{2\gamma s}\int_{-s}^{t-s} e^{\gamma t'}\phi(|t'|)dt'\right.$$
$$\left. -\left[\int_{0}^{t} e^{\gamma t'}\phi(|t'|)dt' + \int_{0}^{s} e^{\gamma t'}\phi(|t'|)dt'\right]\right\} \quad \text{(B.5)}$$

and thus we obtain (2.2.10). The integral

$$J = \int_{0}^{t}\int_{0}^{s} e^{\gamma s'}\phi(|t' - s'|)ds'dt' \quad \text{(B.6)}$$

which is found in $R_{xu}(t,s)$ is calculated similarly. The transformation $t'' = t' - s'$ is needed for J and the integration limits are determined in Figure B.2.

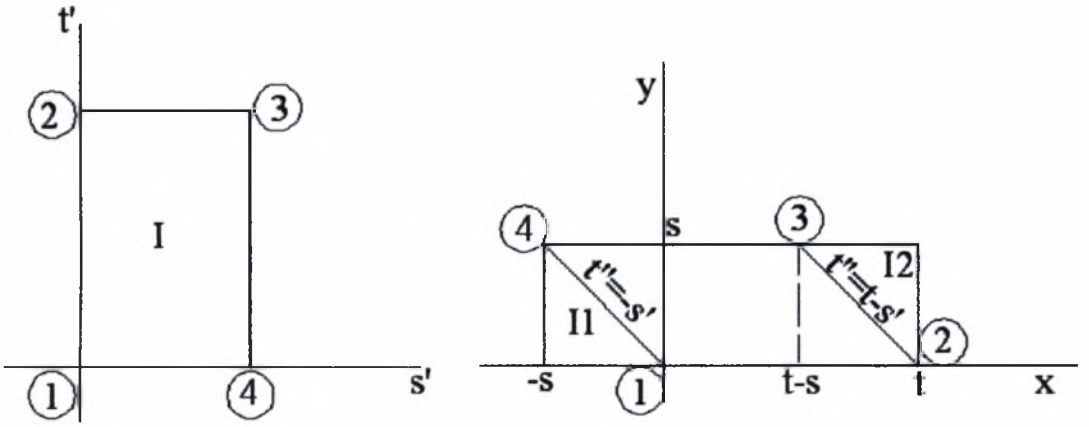

Figure B.2: Transformation of coordinates for the calculation of J.

Then, we have

$$J = \int_{0}^{s} e^{\gamma s'}\left[\int_{-s}^{t} \phi(|t''|)dt''\right]ds' - \int_{-s}^{0} \phi(|t''|)\left[\int_{0}^{-t''} e^{\gamma s'}ds'\right]dt'' - \int_{t-s}^{t} \phi(|t''|)\left[\int_{t-t''}^{s} e^{\gamma s'}ds'\right]dt'' \quad \text{(B.7)}$$

The integration in relation to s' can be carried out and we obtain

$$J = e^{\gamma s}\int_{t-s}^{t}\phi\left(\left|t'\right|\right)dt' - \int_{0}^{t}\phi\left(\left|t'\right|\right)dt' - \int_{-s}^{0}e^{-\gamma t'}\phi\left(\left|t'\right|\right)dt' + e^{\gamma t}\int_{t-s}^{t}e^{-\gamma t'}\phi\left(\left|t'\right|\right)dt' \tag{B.8}$$

Combining the above results, we have

$$R_{xu}(t,s) = \frac{c^2}{\gamma}\left(e^{-\gamma s}J - e^{-\gamma(t+s)}I\right) \tag{B.9}$$

and the calculations lead to (2.2.12).

Finally, the R_{xx} correlation function consists of integrals I and J, as well as

$$K = \int_{0}^{t}\int_{0}^{s}\phi\left(\left|t'-s'\right|\right)ds'dt' \tag{B.10}$$

$$L = \int_{0}^{t}\int_{0}^{s}e^{\gamma t'}\phi\left(\left|t'-s'\right|\right)ds'dt' \tag{B.11}$$

The transformation $t'' = t' - s'$ is used again and we obtain

$$K = s\int_{-s}^{t}\phi\left(\left|t'\right|\right)dt' + \int_{-s}^{0}t'\phi\left(\left|t'\right|\right)dt' - \int_{t-s}^{t}\left(s-t+t'\right)\phi\left(\left|t'\right|\right)dt' \tag{B.12}$$

$$L = \frac{e^{\gamma s}-1}{\gamma}\int_{-s}^{t}e^{\gamma t'}\phi\left(\left|t'\right|\right)dt' - \int_{-s}^{0}\frac{1-e^{\gamma t'}}{\gamma}\phi\left(\left|t'\right|\right)dt' - \int_{t-s}^{t}\frac{e^{\gamma\left(s+t'\right)}-e^{\gamma t}}{\gamma}\phi\left(\left|t'\right|\right)dt' \tag{B.13}$$

The final expression is

$$\begin{aligned}
R_{xx}(t,s) &= \frac{\lambda^2}{\gamma^2}\left(K - e^{-\gamma s}J - e^{-\gamma t}L + e^{-\gamma(t+s)}I\right) = \\
&= \frac{\lambda^2}{\gamma^3}\left\{(\gamma s-1)\int_{-s}^{t-s}\phi\left(\left|t'\right|\right)dt' + (\gamma t-1)\int_{t-s}^{t}\phi\left(\left|t'\right|\right)dt'\right. \\
&+ e^{-\gamma s}\int_{0}^{t}\phi\left(\left|t'\right|\right)dt' + e^{-\gamma t}\int_{0}^{s}\phi\left(\left|t'\right|\right)dt' - \gamma\int_{0}^{s}t'\phi\left(\left|t'\right|\right)dt' - \gamma\int_{t-s}^{t}t'\phi\left(\left|t'\right|\right)dt' \\
&+ e^{-\gamma s}\int_{0}^{s}e^{\gamma t'}\phi\left(\left|t'\right|\right)dt' - \left(e^{\gamma s}-1\right)e^{-\gamma t}\int_{-s}^{t}e^{\gamma t'}\phi\left(\left|t'\right|\right)dt' + e^{-\gamma(t-s)}\int_{t-s}^{t}e^{\gamma t'}\phi\left(\left|t'\right|\right)dt' \\
&+ \frac{e^{-\gamma(s-t)}}{2}\int_{-t}^{s-t}e^{\gamma t'}\phi\left(\left|t'\right|\right)dt' - \frac{e^{-\gamma(t+s)}}{2}\int_{0}^{t}e^{\gamma t'}\phi\left(\left|t'\right|\right)dt' + \frac{e^{-\gamma(t-s)}}{2}\int_{-s}^{t-s}e^{\gamma t'}\phi\left(\left|t'\right|\right)dt' \\
&\left. - \frac{e^{-\gamma(t+s)}}{2}\int_{0}^{s}e^{\gamma t'}\phi\left(\left|t'\right|\right)dt' - e^{\gamma(t-s)}\int_{t-s}^{t}e^{-\gamma t'}\phi\left(\left|t'\right|\right)dt' - e^{-\gamma t}\int_{0}^{s}e^{-\gamma t'}\phi\left(\left|t'\right|\right)dt'\right\}
\end{aligned} \tag{B.14}$$

and substituting $s = t$ leads to (2.2.15).